Universidade do Minho
Escola de Engenharia

Ana Catarina da Silva Castro

Replication of microstructures by compression, for self-cleaning surface applications

dezembro de 2021

Replication of microstructures by compression, for self-cleaning surface applications

Ana Catarina da Silva Castro

UMinho | 2021

Universidade do Minho
Escola de Engenharia

Ana Catarina da Silva Castro

Replication of microstructures by compression, for self-cleaning surface applications

Dissertação de Mestrado
Ciclo de Estudos Integrados Conducentes ao
Grau de Mestre em Engenharia de Polímeros

Trabalho efetuado sob a orientação do
Professor Doutor António Vilela Pontes

dezembro de 2021

DIREITOS DE AUTOR E CONDIÇÕES DE UTILIZAÇÃO DO TRABALHO POR TERCEIROS

Este é um trabalho académico que pode ser utilizado por terceiros desde que respeitadas as regras e boas práticas internacionalmente aceites, no que concerne aos direitos de autor e direitos conexos.

Assim, o presente trabalho pode ser utilizado nos termos previstos na licença abaixo indicada.

Caso o utilizador necessite de permissão para poder fazer um uso do trabalho em condições não previstas no licenciamento indicado, deverá contactar o autor, através do RepositóriUM da Universidade do Minho.

Atribuição-NãoComercial-SemDerivações
CC BY-NC-ND

https://creativecommons.org/licenses/by-nc-nd/4.0/

ACKNOWLEGMENTS

This Master Thesis is the culmination of 5 years of experiences, that contributed for my personal and professional growth, so I could not fail to thank all those who accompanied me along this journey. I would also like to show my gratitude to all the several people and institutions who provided the help and support for the development of the work presented in the master thesis.

To Professor António Pontes, my master thesis supervisor, for the opportunity and trust provided to work on this project.

To Ângela Rodrigues, who guide me and help me everyday through all the stages of this dissertation. There are no words to describe how thankful I am for everything you done, thank you for the transmitted knowledge, the patience, trust and all the disponibility provided during this project.

To the personnel at DEP and PIEP who always showed disponibility for the technical support during the experimental work and the help when problems arise.

To my amazing group of friends who accompany me from the first day of this experience, The Wallace, for all the support, laugh and adventures that we lived that made this journey unforgettable.

To my partner and best friend for all the patience, encouragement, affection, and companionship throughout this journey. Thank you for always being there for me and for always making me laugh.

Last, the most important thanks of all, to my parents, for the unconditional support in all stages of my life and for providing me the best of life. They are the ones who made all this possible, there will never be enough gratitude for everything they have done for me. The greatest thanks are for them and to all the pets I ever had, who are my family and light up my day.

This work is supported by European Structural and Investment Funds in the FEDER component, through the Operational Competitiveness and Internationalization Programme (COMPETE 2020) [Project no 037902; Funding Reference: POCI-01-0247-FEDER-037902].

STATEMENT OF INTEGRITY

I hereby declare having conducted this academic work with integrity. I confirm that I have not used plagiarism or any form of undue use of information or falsification of results along the process leading to its elaboration.

I further declare that I have fully acknowledged the Code of Ethical Conduct of the University of Minho.

RESUMO

A presente dissertação consiste no desenvolvimento de uma *protective optical window* (POW) com a propriedade de auto-limpeza, através do processo de *hot embossing*, para a protecção de um sensor LiDAR aplicado à condução autónoma. Para o bom funcionamento do sensor, a *protective optical window* deve ter uma excelente transmissão óptica no comprimento de onda operacional do sensor.

A primeira fase compreende a investigação de conceitos e o estado da arte relativo à propriedade de autolimpeza, a influência da rugosidade de uma superfície nas propriedades ópticas, as abordagens em biomimética destas superfícies artificialmente com materiais poliméricos e uma visão geral dos processos disponíveis para a replicação de microestruturas, com um enfoque específico no processo de *hot embossing* e na forma como as suas condições de processo influenciam a qualidade da peça.

O principal objetivo deste trabalho foi testar a funcionalidade de uma configuração previamente desenvolvida num inserto metálico na superfície de materiais poliméricos com boas propriedades ópticas, como o PC e o PMMA, através da simulação do processo de *hot embossing*. Por esta razão, foi estudado o efeito das condições de processamento no grau de replicação, e a influência do padrão replicado nas propriedades da superfície, através de testes de caracterização para avaliar as propriedades hidrofóbicas e as propriedades ópticas das peças produzidas. Além disso, foi também realizado um estudo adicional sobre o efeito da aplicação de um revestimento hidrofóbico em amostras microestruturadas, seguido da determinação da sua influência na molhabilidade da superfície e na transmitância óptica.

Os resultados dos estudos apresentados nesta dissertação demonstraram que o padrão microestruturado aumentava o ângulo de contacto com a água (WCA) das amostras produzidas apenas até ao regime hidrofóbico. Para as amostras de PC, a replicação por *hot embossing*, resultou no enchimento completo das cavidades, o que resultou num aumento do WCA em quase 50% em comparação com uma amostra não microestruturada. Embora, para o PMMA o enchimento completo não tenha sido alcançado, com as estruturas com uma média máxima de até 84% da altura desejada, ainda se verificou um aumento do WCA em 30°. No entanto, o padrão replicado na superfície também afetou negativamente o desempenho óptico das peças, invalidando a sua aplicação numa POW para um sensor LiDAR. A aplicação de um revestimento hidrofóbico numa superfície microestruturada, embora provocando repelência às gotas de água, também se revelou uma abordagem não válida devido à sua significativa influência negativa sobre a transmitância óptica.

Palavras-chave: Ângulo de Contacto, Auto-Limpante, Hot Embossing, Microestruturas, Transmitância

ABSTRACT

The present dissertation consists in the development of a protective optical window (POW) with the property of self-cleaning, through the process of hot embossing, for the protection of a LiDAR sensor applied in autonomous driving. For the proper functioning of the sensor, the optical window must have an excellent optical transmission in the sensor operational wavelength.

The first stage comprises the research of concepts and the state-of-the-art concerning the self-cleaning property, the influence of surface roughness on optical properties, the approaches in biomimetic these surfaces artificially with polymer materials and an overview of processes available for the replication of microstructures, with a specific focus on the hot embossing process and how its process conditions influence the part quality.

The main goal of this work was to test the functionality of a structure configuration previously developed in a metallic insert on the surface of polymeric materials with good optical properties, such as PC and PMMA, through the simulation of the hot embossing process. For this reason, it was studied the effect of the processing conditions of the hot embossing process in the replication degree, and the influence of the replicated microstructured pattern on the surface properties by performing characterization tests to evaluate the hydrophobic properties and optical properties of the produced parts. Furthermore, an additional study of the effect of the application of a hydrophobic coating on microstructured samples was also conducted, followed by the determination of its influence on the surface wettability and optical transmittance.

The results of the studies presented in this dissertation demonstrated that the microstructured pattern enhanced the water contact angle (WCA) of the produced samples only up to the hydrophobic regime. For the PC samples, the replication by hot embossing, resulted in the complete filling of the cavities, which resulted in an increase of the WCA by almost 50% in comparison with a non-microstructured sample. Although, for the PMMA the complete filling was not achieved, with the structures with a maximum average up to 84% of the desired height, it still resulted in an enhancement of the WCA in 30°. However, the pattern of the surface also negatively affected the optical performance of the parts, invalidating its application in a POW for a LiDAR sensor. The application of a coating on a microstructured surface, although causing water repellency of the water droplets, also showed to be an invalid approach due to its significative negative influence on the optical transmittance.

Keywords: Hot Embossing, Microstructures, Self-Cleaning, Transmittance, Water Contact Angle

TABLE OF CONTENTS

LIST OF ABBREVIATIONS AND ACRONYMS

3D – Three-dimensional
ADAS – Advanced Driver Assistance Systems
ANOVA – Analysis of Variance
CVD – Chemical Vapor Deposition
CA – Contact Angle
CAH – Contact Angle Hysteresis
COP – Cyclic Olefin Polymer
CBD – Electrochemical Deposition
DRIE – Deep Reactive Ion Etching
DEP – Departamento de Engenharia de Polímeros (Polymer Engineering Department)
DOE – Design of Experiments
FEP – Fluorinated Ethylene Propylene
LbL – Layer-by-layer
LiDAR – Light Detection and Ranging
LIGA – Lithographie, Galvanoformung, Abformung (Lithography, Electroplating, and Molding)
P2P – Plate to Plate
PIEP – Pólo de Investigação em Engenharia de Polímeros (Polymer Engineering Research Center)
PMMA – Poly(methyl methacrylate)
PC – Polycarbonate
PDMS – Polydimethylsiloxane
PP – Polypropylene
PTFE – Polytetrafluoroethylene
POW – Protective Optical Window
R2P – Roll to Plate
R2R – Roll to Roll
RMS – Root Mean Square (roughness)
SEM – Scanning Electron Microscopy
Si – Silicon
UV – Ultraviolet Radiation
WCA – Water Contact Angle

LIST OF FIGURES

LIST OF TABLES

CHAPTER 1 – INTRODUTION

This chapter provides an overview of this work and its organization. Firstly, the framework and motivations that led to the selection of the topics covered in this thesis are presented. Then, bearing in mind the work motivations, the main objectives are introduced, and finally, the organization/structure of the thesis is presented.

1.1. Framework and Motivation

In the last decades, the human being has been using nature as a source of inspiration for the development of new materials and/or systems, trying to mimic them. It is well-know that nature and natural processes are adaptable to changing environmental conditions, and with millions of years of evolution and natural selection, organisms have achieved sophisticated structures, patterns or textures with complex multifunctionality (Yılgör et al., 2016). Among all the fascinating characteristics observed in biosystems, self-cleaning ability is regarded as one of the most interesting topics in biomimicry because of its potential applications in various fields such as aerospace, automotive, textile, energy conversion, biomedical, environmental protection, beyond others (Xu et al., 2016).

Studies on self-cleaning surfaces were prompted by the understanding of phenomena existing in nature in more than 200 animals and vegetable species, such as the leaves of some plants, the feathers of birds, the wings of some insects, among others (Verplanck et al., 2007). Natural or biosurfaces principally maximize or minimize the contact angles of the droplets to facilitate free liquid droplet movement. The use of scanning electron microscopy (SEM) on studies with various types of organisms conducted decades ago has led to a clear understanding of the close relationship between the topography and wetting behavior of natural surfaces (Barthlott & Neinhuis, 1997). Investigations about these self-evolved structures has also led to intense progress that has allowed the development of products with hydrophobic and superhydrophobic properties, with high contact angles and low sliding angles, characteristic of self-cleaning surfaces.

Based on research about the natural superhydrophobic phenomenon, artificial superhydrophobic surfaces are more controllable under the combination of low surface energy materials or coatings and designed hierarchical roughness materials in both micro and nanoscales (Sun, Li, et al., 2019). Compared to metallic materials, polymers have a lower free surface energy. Hydrophobic or even superhydrophobic characteristics can be achieved as long as the hierarchical micro/nanostructures were fabricated on their surfaces. Due to several characteristics of polymers, such as excellent workability,

temperature resistance, low cost for high-volume fabrication, among others, it is very simple and diverse to manufacture micro/nanostructures on polymeric surfaces via injection molding, hot embossing, besides many others (J. Li et al., 2018; Khosrow Maghsoudi et al., 2020; Zhou et al., 2018).

Self-cleaning surfaces are highly important in several applications due to their potential in the durability and efficiency of products improvement, eliminating additional cleaning actions, and consequently reducing the use of water, energy and potentially hazardous substances that enter the environment through those actions. One of the applications where self-cleaning surfaces can demonstrate a significant importance is in optical sensors, especially for autonomous driving, if certain properties, such as optical transmittance at certain wavelengths is achieved.

Autonomous driving is one of the main development targets in the automotive industry today (Kutila et al., 2016). In addition to daily usage, autonomous vehicles can expand transportation options for the elderly and the disabled, facilitate navigation in unknown places and even reduce the number of traffic accidents through the extinction of the primary cause, human error. Autonomous vehicles rely on their perception systems to acquire information about their immediate surroundings. Safety concerns and the need for accurate estimations have led to the introduction of LiDAR systems to complement camera- or radar-based perception systems (Y. Li & Ibanez-Guzman, 2020).

LiDAR (Light Detection and Ranging) sensors are the key sensors for autonomous vehicles, using pulsed laser waves to map the distance of the surrounding objects, allowing to obtain a three-dimensional view of the environment around the car in real time. LiDAR systems emit pulsed light waves, in the infrared, to the surrounding environment, which reverberate on objects and return to the sensor. The distances of the objects are calculated based on the time it took for each pulse to return to the sensor. By transmitting and receiving data from hundreds of thousands of laser pulses every second, the on-board computer records each laser reflection point, producing a 3D point cloud that corresponds to the surrounding environment in real time.

Currently, automotive manufacturers have been integrating LiDAR into ADAS (Advanced Driver Assistance Systems) in order to visualize the constantly changing environments their vehicles are immersed in, from mapping the static environment to detecting and identifying moving vehicles, pedestrians and wild animals. The amount of data collected allows ADAS systems to make carefully considered and safe driving decisions. These devices have the same function in the context of autonomous driving, their outputs are used for object detection, classification, tracking and intention prediction, corresponding to various layers of information that allows safe driving (Y. Li & Ibanez-Guzman, 2020).

In this manner, the application of a protective optical window with self-cleaning properties for the sensor protection is extremely important, not allowing any deposition of particles that may obstruct and/or hinder the emission and reception of the laser pulses, leading to greater efficiency of this equipment and consequently safer and more efficient autonomous driving. However, it is challenging to develop a surface with self-cleaning properties and optimum optical transmittance of light at the same time. Since typical superhydrophobic property is usually achieved on a rough surface. Meanwhile, rough structured surfaces often suffer from strong scattering or diffraction effects, thus inducing large loss of light transmittance. Furthermore, research about surfaces with superhydrophobic properties and optical transmittance are rarely reported. In addition, for its viability it is also necessary to find manufacturing processes and operating conditions that allow its production in large quantities and with the required properties to enable the achievement of self-cleaning properties and the correct functioning of the sensor.

For this, compression processes, such as hot embossing, appear as effective procedures in the replication of structures on the micro and nano scale in polymeric materials, and can offer a solution for the production of this type of surfaces on a large scale and with the desired properties.

1.2. Objectives

The present dissertation consists in the development/production of a protective optical window with the property of self-cleaning, through the process of hot embossing, for the protection of a LiDAR sensor applied in autonomous driving. For the proper functioning of the sensor, the optical window must have an excellent optical transmission in the sensor wavelength.

The objectives and tasks of this dissertation (Figure 1) include the surface replication of a structure previously developed in a metallic insert on the surface of polymeric materials, such as PC and PMMA, through the simulation of the hot embossing process. Furthermore, it is intended to obtain the effect of the processing conditions of the hot embossing process in the replication degree, and the influence of the replicated microstructured pattern on the surface properties by performing characterization tests to evaluate the hydrophobic properties and optical properties of the produced parts. An additional study of the effect of the application of a hydrophobic coating on microstructured samples produced with conditions that allow the achievement of the higher replication degree should also be performed, followed by the determination of its influence on the surface wettability and optical transmittance.

The results obtained in the studies of this dissertation shall help to understand if microstructured pattern and the materials used for the production of the samples, as well as the application of a coating on a rough surface approach are valid options for the production of protective optical window with self-

cleaning properties for the protection of a LiDAR sensor.

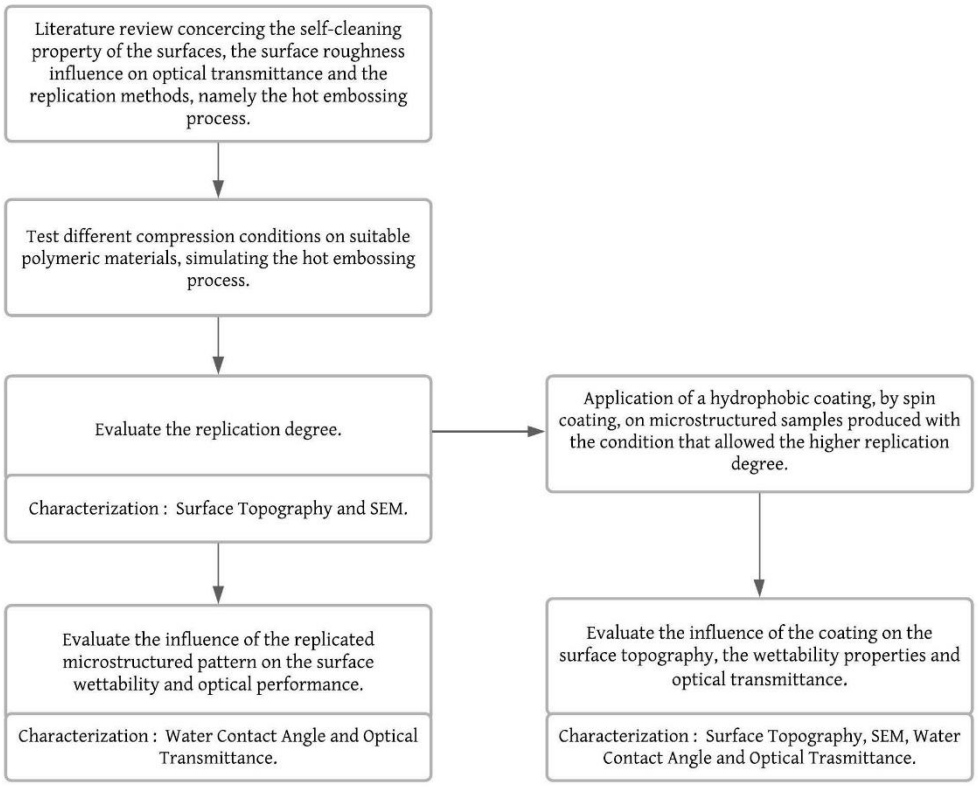

Figure 1 - Flowchart representing the tasks follow-up to fulfil the defined goals of the master thesis work.

1.3. Thesis Organization

The methodology and results obtained in this work are presented in 7 separate chapters.

In chapter 1, the framework of the theme, motivation and objectives of the work are enunciated.

The chapter 2 comprises the research of concepts and the state-of-art concerning the self-cleaning property, the influence of surface roughness on optical properties and an overview of processes available for the replication of microstructures, with a specific focus on the hot embossing process and how its process conditions influence the part quality.

Chapter 3 comprises the materials, procedures and methodologies used in the experimental work defined for this dissertation. The experimental planning is presented, followed by an overview of the production techniques, the materials and aspects related to the productive tools applied.

The descriptions of the tests performed for the characterization of the samples produced in the experimental work are given in Chapter 4.

The results of the experimental work performed are reported in Chapter 5.

Chapter 6 and Chapter 7 show an overall view of the results obtained and the main conclusions taken, and the given suggestions for further work within the framework of the project, respectively.

CHAPTER 2 – LITERATURE REVIEW

This chapter presents the theoretical foundations about the main fields covered in this thesis, especially in what concerns the wettability of polymers surfaces, the roughness influence on the optical transmittance of the surfaces and replica-based techniques to achieve self-cleaning surfaces, especially the hot embossing process.

2.1. Wettability and Surface Energy of Polymers

The self-cleaning ability of a surface depends on its wettability, which is a very important property of surfaces and is related to the tendency of a liquid to spread or not to spread on a given surface (K. Liu et al., 2013). It is the ability of a liquid to maintain contact with a solid surface as a result of intermolecular interactions (Fei et al., 2020).

Ideally, when a drop is deposited on a surface, it can spread out to form a thin liquid film, or remain on the surface in a spherical shape (K. Liu et al., 2013). The contact angle (CA) is a quantitative measure of the wettability of a solid surface by a liquid, and is dependent on the surface tension of the liquid involved, the solid surface, and the surrounding gas (Koch & Barthlott, 2009). This is the angle formed by the drop of liquid, in the three-phase liquid, gas and solid boundary, between the plane tangent to the surface of the liquid and the plane tangent to the surface of the solid (Figure 2) (K. Liu et al., 2013).

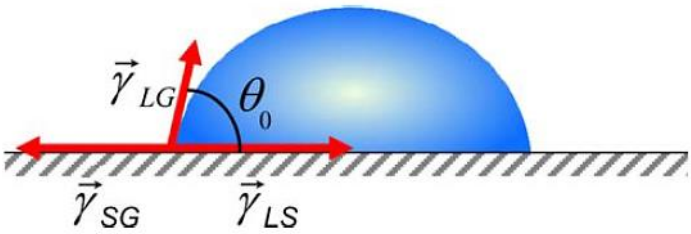

Figure 2 - Surface tensions acting on the three-phase contact line of a liquid droplet deposited on an ideal substrate. (Adapted from Verplanck et al., 2007).

A surface is regarded as wetting when the contact angle formed by the drop with it is lower than 90°. In the opposite case, where the contact angle is higher than 90°, the surface is nonwetting (Verplanck et al., 2007). The wettability of a smooth surface and the contact angle are directly related to the intensity of the liquid-liquid and liquid-solid intermolecular forces, referred to as cohesive and adhesive forces, respectively. If the cohesive forces are stronger than the adhesive forces, then the solid surface will not be wetted by the liquid and the CA will be greater than 90°. If the adhesive forces are stronger, the drop of liquid will interact very intensely with the solid surface, thus wetting of the solid will occur and the CA will be less than 90°(Yılgör et al., 2016). The wettability of a liquid on a given surface is inversely proportional to the contact angle, the smaller the contact angle, the higher the wettability.

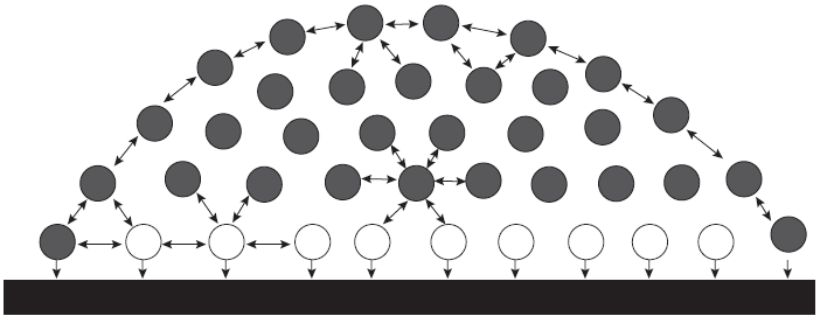

Figure 3 - Schematic of various cohesive and adhesive intermolecular forces in a droplet placed on an inert solid surface. (Adapted from Yılgör et al., 2016)

The wetting behavior of solid surfaces can be divided into four classes, defined by their static contact angle (Figure 4)(Figure 5). Surfaces are termed superhydrophilic when the contact angle is less than 10°. Surfaces with contact angles greater than 10° and less than 90° are referred to as hydrophilic. Hydrophobic surfaces have high contact angles, meaning that the liquid on the surface forms a spherical or semi-spherical droplet, and the contact angle is greater than 90° and less than 150°. For a surface to be considered superhydrophobic, the contact angle must be greater than 150° (Koch & Barthlott, 2009).

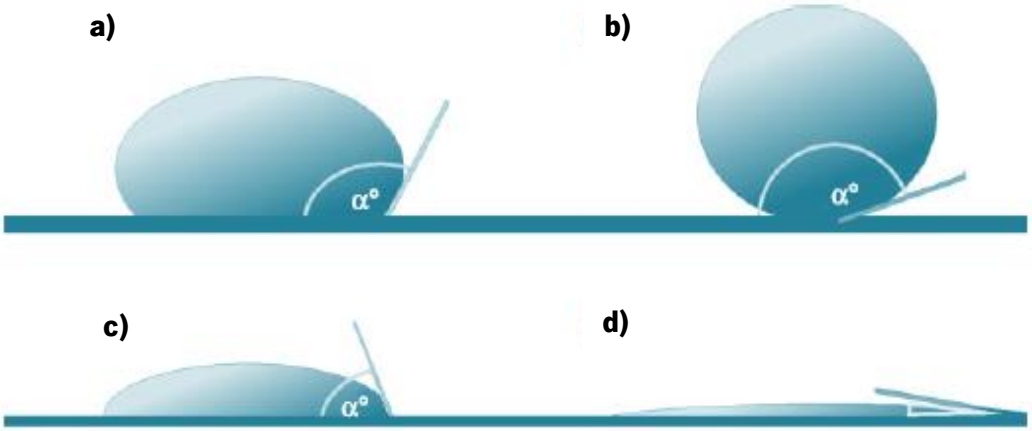

Figure 4 - Four classes of wettability of a surface and their respective contact angles. a) Hydrophobic surface. b) Superhydrophobic surface. c) Hydrophilic surface. d) Superhydrophilic surface. (Adapted from Koch & Barthllot, 2009)

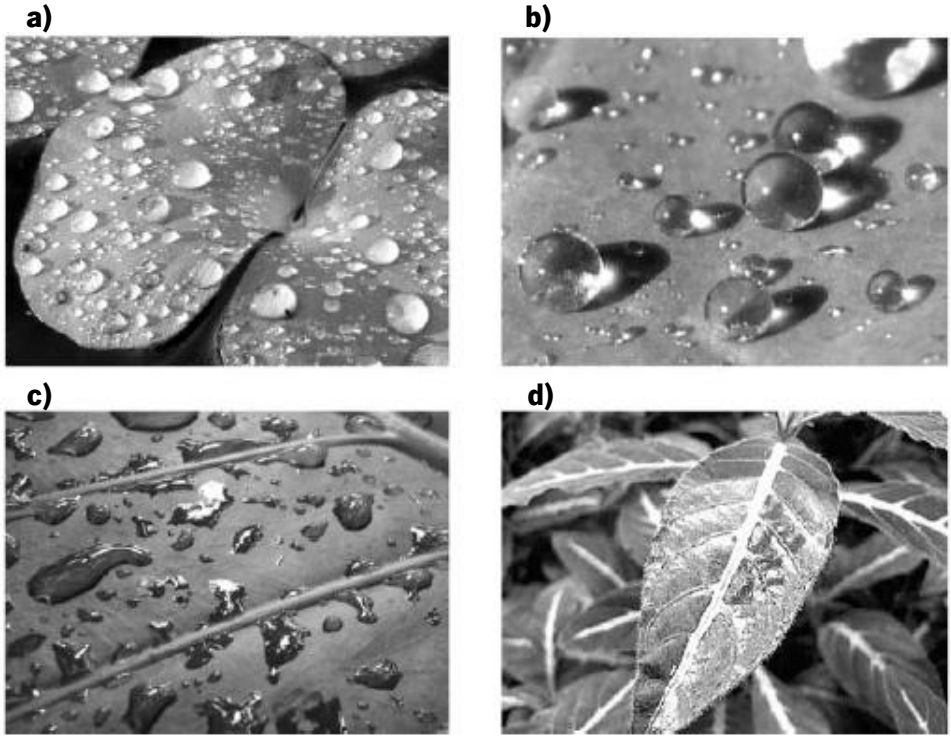

Figure 5 - Four classes of the wettability of a surface represented on leaves. a) The hydrophobic leaf of Regnellidium diphyllum (Marsileaceae). b) Superhydrophobic surface of a leaf of Brassica oleracea. c) The hydrophilic leaf of Alocasia odora. d) The superhydrophilic leaf of Ruellia devosiana. (Adapted from Koch & Barthllot, 2009)

In 1805, Young was the first to describe the equilibrium contact angle and wetting model (Young, 1805). For a drop of liquid on an ideal flat surface (Figure 2), the wettability is determined by the surface free energy of the solid surface, which is expressed through Young's equation:

$$\gamma_{SG} = \gamma_{SL} + \gamma_{LG} cos\theta_Y \qquad (2.1)$$

Where, γ represents the surface tension (or surface free energy), θ_Y is the contact angle of the liquid on the surface in the Young's model, γ_{SG}, γ_{SL} and γ_{LG} are the interfacial tensions involved in the solid-gas, solid-liquid and liquid-gas system, respectively. Young's equation can successfully predict the contact angle of a water droplet deposited on a flat surface with a homogeneous interface (Xu et al., 2016).

The chemical structure of a material defines the surface tension, which in return, partially determines the wettability and adhesion of materials. The magnitude of the surface energy of polymers is related to the intensity of the intermolecular forces between the polymer chains (van der Waals). If the polymer structure contains polar groups, then reasonably strong intermolecular forces result in high surface energy. For apolar polymers, in which only weak intermolecular interactions arising from dispersion or London forces are present, the surface energy is low. In general, polymer structures can contain both polar and non-polar groups, so the total surface energy of a polymer is considered to be the sum of the dispersive and polar components (Yılgör et al., 2016). In general, as the surface energy of the polymer increases, the surfaces become more polar and the water contact angle decreases. Therefore, a low surface energy results in hydrophobic properties while high surface energy leads to hydrophilic properties.

The contact angle of a water droplet (WCA) on the surface of various polymers, together with their surface energies are given in Table 1.

Table 1 - Surface energy and WCA of various polymers (Adapted from Yılgör et al., 2016).

Polymer	Surface Energy (mN/m)	WCA (°)
PVOH	37.0	51.0
PA-66	46.5	68.3
PMMA	41.1	70.9
PC	44.6	82.0
PVC	41.5	85.6
PS	40.6	87.4
PE	35.7	96.0
PP	30.1	102.1
PTFE	20.0	109.2

During the last decades, there has been a great deal of interest in the preparation and characterization of polymer surfaces that exhibit superhydrophilic and superhydrophobic properties. As noted in Table 1, none of the surfaces of the polymers mentioned exhibit a contact angle of a water droplet as low or as high as necessary. However, as will be discussed later, polymer surfaces with superhydrophilic or superhydrophobic characteristics can be obtained through various physical and chemical surface modification methods.

2.2. The Effect of Roughness on the Water Contact Angles

Young's equation is used to determine unique contact angle values for a drop of liquid deposited on an ideal solid surface, i.e., perfectly smooth, homogeneous, rigid, as well as chemically and physically inert with regards to the used fluid. However, in practice these properties are not all present on real solid surfaces. In particular, chemical variations of the surface and roughness are the most observed situations when dealing with real solid surfaces (Hejazi et al., 2014). Thus, the wettability of rough and/or chemically heterogeneous surfaces is characterized by the apparent contact angle, which is the macroscopically measured equilibrium contact angle (Bormashenko, 2015).

The wettability of a solid surface is essentially dependent on two factors, surface energy, as mentioned previously, and surface roughness (A. Nakajima et al., 2001). The roughness of a surface plays a critical role in determining the wettability of a solid surface (K. Liu et al., 2013). The Wenzel and Cassie-Bexter models provide expressions for the relationship between contact angle and solid surface roughness.

2.2.1. Wenzel Model

The effect of roughness on the apparent contact angle of a chemically homogeneous surface was first studied by Wenzel in 1936. Wenzel proposed a model to express the relationship between surface roughness and contact angle according to the following equation:

$$cos\theta_W = r\ cos\theta_Y \tag{2.2}$$

Where θ_W is the apparent contact angle in Wenzel's model, θ_Y is the contact angle in Young's model and r is the surface roughness factor, defined as the ratio between the real and apparent surface area (Wenzel, 1936). For ideal flat surfaces, r = 1, however, since all real surfaces are not smooth at molecular level, $r > 1$.

In Wenzel's theory it is assumed that the liquid contacts with the entire rough surface, filling all the micro geometries that characterize the roughness of the surface (Figure 6a). According to equation (2.2, roughness can further amplify the hydrophilic or hydrophobic character of a surface (Forbes, 2008). If the surface roughness of an inherently hydrophobic material (θ>90°) is increased, the static contact angle also increases ($\theta_W > \theta$). If the surface roughness of an inherently hydrophilic material (θ<90°) is increased, the static contact angle decreases ($\theta_W < \theta$).

2.2.2. Cassie-Bexter Model

In 1944, Cassie and Bexter derived an equation to describe the effect of chemical heterogeneities on the contact angle at solid surfaces (Cassie & Bexter, 1944). This model assumes that the liquid does not completely wet the rough surface, due to the existence of air between the depressions (Figure 6b).

This model assumes that the liquid only contacts the solid through the top of the protrusions and that there are pockets of air trapped beneath the liquid, which gives a composite surface (Figure 6b). In this case, the liquid surface interface consists of two phases, a liquid-solid interface and a liquid-gas interface. Thus, the apparent contact angle is the sum of all the contributions from the different phases, as shown by the equation:

$$\cos\theta_{CB} = f_1 \cos\theta_1 + f_2 \cos\theta_2 \quad (2.3)$$

Where θ_{CB} is the apparent contact angle in the Cassie-Bexter model, f_i is fractional area of the surface with a contact angle of θ_i ($f_1 + f_2 = 1$).

In this composite state, air parts of the surface can be considered perfectly non-wetting, and consequently the water contact angle is equal to 180°. By assuming that f_2 is fraction of air which the water is in contact with and consequently θ_2 = 180°, one can conclude that:

$$\cos\theta_{CB} = f_s(\cos\theta_s + 1) - 1 \quad (2.4)$$

Where f_s is the fractional area of the solid surface in contact with the drop.

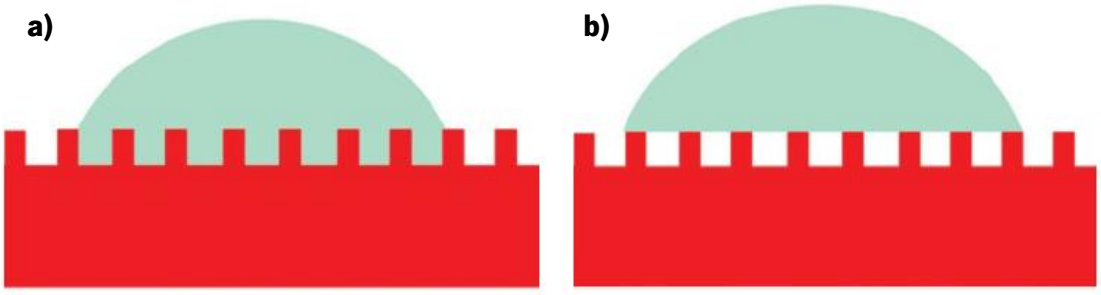

Figure 6 - Droplet behavior on solid surfaces. a) Wenzel Model. b) Cassie-Bexter Model. (Adapted from Forbes, 2008)

The Cassie-Bexter regime is characterized by a high apparent contact angle, promoting easy sliding of the liquid droplets on the surface. However, an high apparent contact angle is not sufficient to achieve the self-cleaning ability, a low contact angle hysteresis and high stability of the Cassie-Bexter wetting regime are also required (Bormashenko, 2015).

The composite interface, which allows the Cassie-Bexter state, is often fragile and can be irreversibly transformed into a homogeneous interface. There are several mechanisms that may contribute for its

destabilization such as condensation or accumulation of nanodroplets between the asperities, surface heterogeneity, among others (Michael & Bhushan, 2007). A multiscale or hierarchical roughness is often recommended in order to effectively resist these mechanisms and achieving a more stable Cassie-Bexter wetting state (Figure 7).

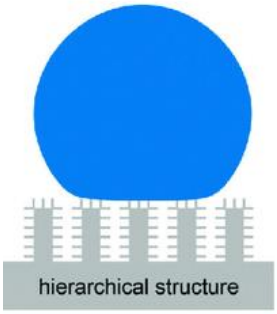

Figure 7 - Droplet in a surface with hierarchical structures. (Adapted from Michael & Bhushan, 2007)

However, when the initial Cassie-Bexter wetting state is not stable, the wetting transition namely the transition from the Cassie-Bexter to the Wenzel wetting may occur. The midterm wetting regime can also occur and is typical for superhydrophobic materials that present high contact angle hysteresis, i.e., the water droplet adheres to the substrate.

One of the first experimental studies that demonstrated the effect of increasing surface roughness on increasing the WCA of a polymer material was done by Garbassi and co-workers (Garbassi et al., 1994; Morra et al., 1989). In that study, a smooth PTFE surface was etched with oxygen plasma and the surface roughness increased as a function of etching time. The increase in surface roughness resulted in a significant increase in WCA (greater than 160°) compared to the WCA of the smooth surface (108°), clearly demonstrating the formation of a superhydrophobic surface.

2.3. Contact Angle Hysteresis

The ability of a droplet to move on a surface is determined by the contact angle hysteresis (CAH) (McHale et al., 2004). The hysteresis of a surface is related to its imperfections, which come from physical defects such as roughness or chemical variations (Verplanck et al., 2007).

If a surface on which a drop rests is slightly tilted, the drop remains at rest with differing contact angles at each side of the drop (Figure 8c). When the upper angle reaches the receding angle, θ_R, and the lower angle reaches the advancing angle, θ_A, the drop begins to move (McHale et al., 2004). It can be considered that the advancing angle is always higher and favors the flow of the droplet, while the receding angle resists the flow of the droplet (Yılgör et al., 2016).

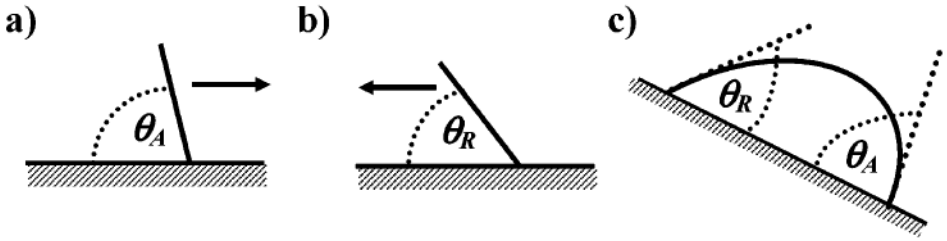

Figure 8 - Contact angle hysteresis. a) Advancing angle. b) Receding angle. c) Advancing and receding angle determined by tilting experiment. (Adapted from McHale et al., 2004)

The difference between these two angles ($\theta_A - \theta_R$) is called hysteresis and is responsible for the adherence of the liquid to the surface (Koch & Barthlott, 2009; Verplanck et al., 2007). Although hysteresis is a force that opposes the movement of the drop, the lower its value, the easier will be to move the liquid droplet (Verplanck et al., 2007).

Furmidge calculated the tilt angle, α, required in order for a drop to slide (Furmidge, 1962):

$$\frac{mg \sin \alpha}{w} \gamma_{LG} \left(cos\theta_R - \cos \theta_A\right) \tag{2.5}$$

Where m is the mass of the droplet, g is the acceleration of gravity, w is the width of the drop, θ_R,is the receding angle when the droplet leaves the surface and θ_A is the advancing angle when the droplet begins to move. The tilt angle required for a droplet to roll or slide on the substrate is referred to as the sliding angle.

In Young's model, it is assumed that there is no hysteresis because the surface is ideally flat and chemically homogeneous. Therefore, the three-phase line can move freely on the surface (Yılgör et al., 2016). According to Farshchian *et al.*, it is known that both the Wenzel and Cassie-Bexter regimes can form droplets with high contact angles, however, only in the Cassie-Bexter regime can low sliding angles be obtained. In the Wenzel regime, the droplet completely wets the surface, and therefore cannot easily move over it, and a contact angle hysteresis greater than 10° is obtained, due to the fixation of the droplet. In the Cassie-Bexter regime, since the droplet is in contact with a smaller solid area, it thus reduces the drag force (friction) on the droplet. As a result, the droplet can easily move over the surface with a low tilt angle. Therefore, only the Cassie-Bexter regime can fulfill the two requirements necessary for the self-cleaning ability (Farshchian et al., 2010).

Contact angle hysteresis can be controlled, and values lower than 1° can be achieved. In the case of hydrophobic or superhydrophobic surfaces it is intended that the tilt angle and consequently the contact angle hysteresis should be low, so that droplet could roll over the surface with a small tilt. A tilt angle of less than 10° is characteristic of superhydrophobic surfaces with self-cleaning properties (Koch & Barthlott, 2009).

2.4. Superhydrophobic and Self-Cleaning Surfaces in Nature

There are several surfaces in Nature that exhibit a high intrinsic ability for self-cleaning without any external help. This phenomenon, due to its unique mechanism and high adaptability, has attracted enormous scientific interest in recent decades. The concept of self-cleaning was initially based on the superhydrophobic nature of some plant leaves. Among them, the leaf of the lotus flower (*Nelumbo nucifera*) is considered one of the most relevant inspirations for the design of self-cleaning surfaces. Lotus flower leaves are able to stay clean in muddy water due to the way their surfaces are structured and water-repellent.

The underlying mechanism of the self-cleaning property of the lotus flower leaf was first investigated by Barthlott and Neinhuis (1997). It was found that micrometer-scale papillae and epicuticular wax play an important role in its superhydrophobicity, i.e., high water contact angle and low sliding angle, which was defined as the "Lotus effect" (Barthlott & Neinhuis, 1997). As observed in Figure 9b, micro-sized papillae with diameters between 5 and 9 µm are randomly distributed on the leaf surface. However, the fundamental mechanism of self-cleaning had not yet been fully clarified. In 2002, Feng *et al.* reported the existence of nanostructures in each papilla, with diameters of approximately 200 nm, which contributed to greatly increase the roughness of the leaf surface and effectively prevent the attachment of water droplets (Feng et al., 2002). Therefore, the effect observed on the leaf surface is due to the combination of the inherent hydrophobicity of the epiticular wax and the papillae with hierarchical roughness that are irregularly dispersed on the surface, granting superhydrophobicity to the leaf as water droplets form contact angles greater than 150° and a critical sliding angle of less than 2°. The water therefore creates droplets that roll off the surface, dragging the impurities that adhere to it (Figure 9c). As a result, the leaves are always clean – the principle of self-cleaning.

Thus, the so-called Lotus effect, which leads to the formation of self-cleaning surfaces, can be explained as the free rolling motion of water droplets due to the superhydrophobicity of the leaf surface and the ability of these same droplets to collect and drag debris from the surface (Figure 10) (Yılgör et al., 2016).

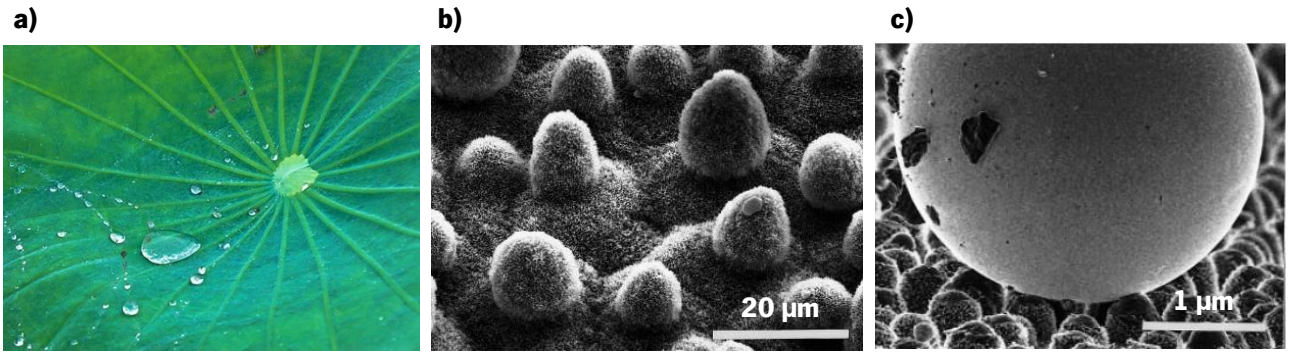

Figure 9 - Hydrophobic leaf surface of the lotus flower. a) Water droplets on the leaf surface. b) SEM images of cell papillae distributed on the leaf surface. c) Impurities adhere to the surface of the droplet and are removed when the droplet rolls over the leaf. (Adapted from Barthlott & Neinhuis, 1997)

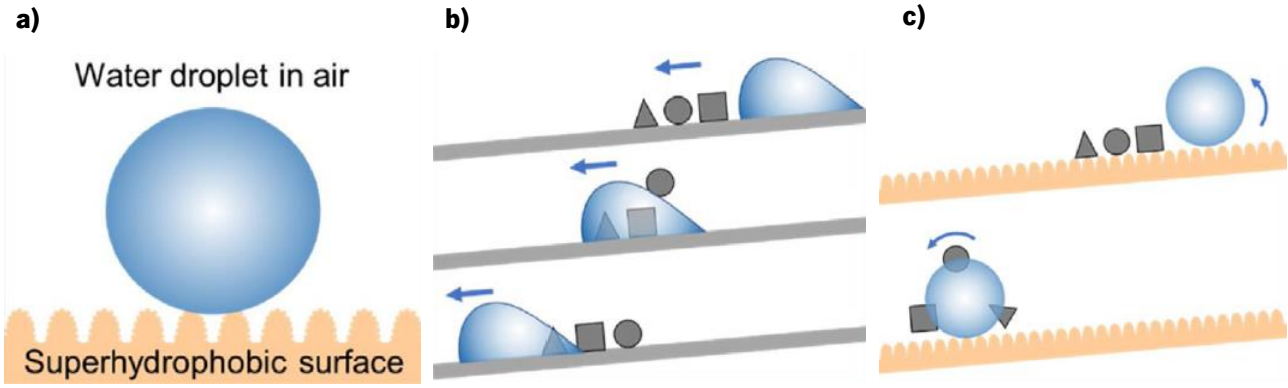

Figure 10 - Mechanism of the lotus effect. a) Schematic illustration of the lotus state. b), c) Schematic illustration of the cleaning by water droplets on smooth and structured surfaces, respectively. On the smooth surface, the particles are mostly redistributed by the water, while on the rough surface, they adhere to the surface of the droplets and are removed from the surface. (Adapted from Barthlott & Neinhuis, 1997)

Plants such as tulip, iris, eucalyptus, *ginko biloba*, and many others have leaves with this property. Another example of superhydrophobicity in nature is the eye of the mosquito (Figure 11a). The eye of this insect is covered by hexagonally closed-packed, micron-sized hemispheres called ommatidia (Yılgör et al., 2016). In addition, these microstructures are covered with hexagonally close-packed nanopillars. This micro/nano-hierarchical surface pattern gives the mosquito eye superhydrophobic and antifogging properties (C. Yu et al., 2020). Moreover, the hairs around the eye act as nucleating agents for water droplets, providing additional protection against fogging (S. Yu et al., 2015).

Cicada wings are also superhydrophobic and self-cleaning. Water droplets on the wing surface assume a spherical shape and roll easily with small inclinations (Yılgör et al., 2016). Cicada wings have been reported to consist of hexagonally closed-packed nanopillars (Figure 11b) (S. Yu et al., 2015). The nanometric surface pattern in combination with the wax layer on the surface allows the wing to exhibit a superhydrophobic character, although hierarchical roughness is not present. In addition to this, the wings of cicadas display high transparency and anti-reflective properties due to a single level of roughness consisting of regularly spaced nanopillars with sizes below the wavelength of propagating light (Darmanin, 2015).

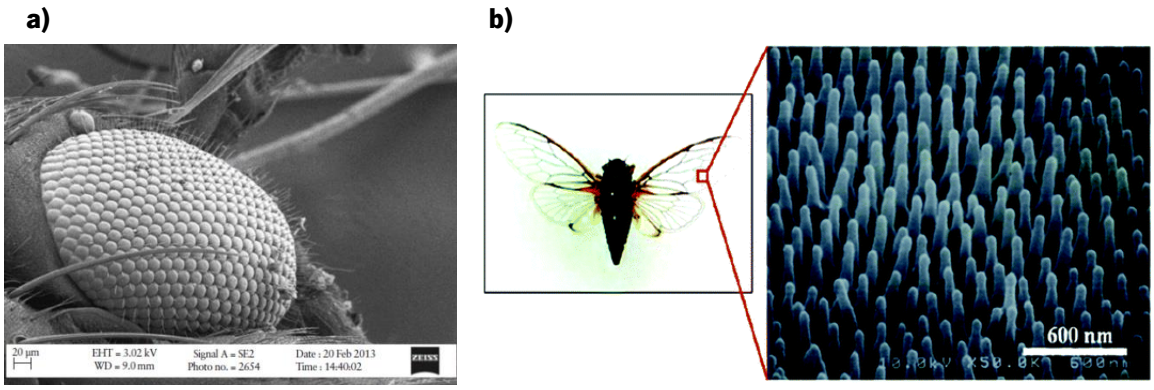

Figure 11 - Natural hydrophobic surfaces. a) SEM image of a mosquito's eye. b) Optical image of a cicada and SEM image of its wing. (Adapted from Yılgör et al., 2016; S. Yu et al., 2015)

Some insects, such as butterflies have their wings covered with shapes whose size and geometric shape lead to a superhydrophobic state and which is also at the origin of their colors (Verplanck et al., 2007). The wings of the *Morpho aega* butterfly possess flexible nanotips that are direction-dependent and are present on the top of ridging nanostripes and overlapped microscales. The quadrate scales overlap each other and there are several ridging stripes on the surface of each scale (Figure 12a-b). Therefore, there exists a hierarchical arrangement of micro and nanostructures made of nanotips, stacked nanostripes and microscales on the wings. This periodic arrangement delivers superhydrophobic and self-cleaning function to the butterfly wing surface (Figure 12a-b) (Malshe et al., 2013) . A peculiar feature of the wings of this butterfly is that the water droplets slide only in one direction, always outward from the animal's body (Figure 12e-g). Studies show that the droplet remains intact on the surface even when one tries to slide the liquid in the opposite direction, showing directional adhesive properties (Zheng et al., 2007).

The phenomenon of directional droplet movement on superhydrophobic surfaces can also be observed on feathers. Bird feathers exhibit strong water repellency that is mostly due to their porous structures and the grease coating on the feather surfaces. As demonstrated in Figure 12c and Figure 12d, feathers are composed of branches with different dimensions, including micro-scale dorsal spines, trunks and barbules, which facilitate the porous structure of feathers. The porous structures, as well as the grease coating with low surface tension, give the feathers a large liquid-gas interface, contributing to a water repellency differentiated from other (C. Yu et al., 2020).

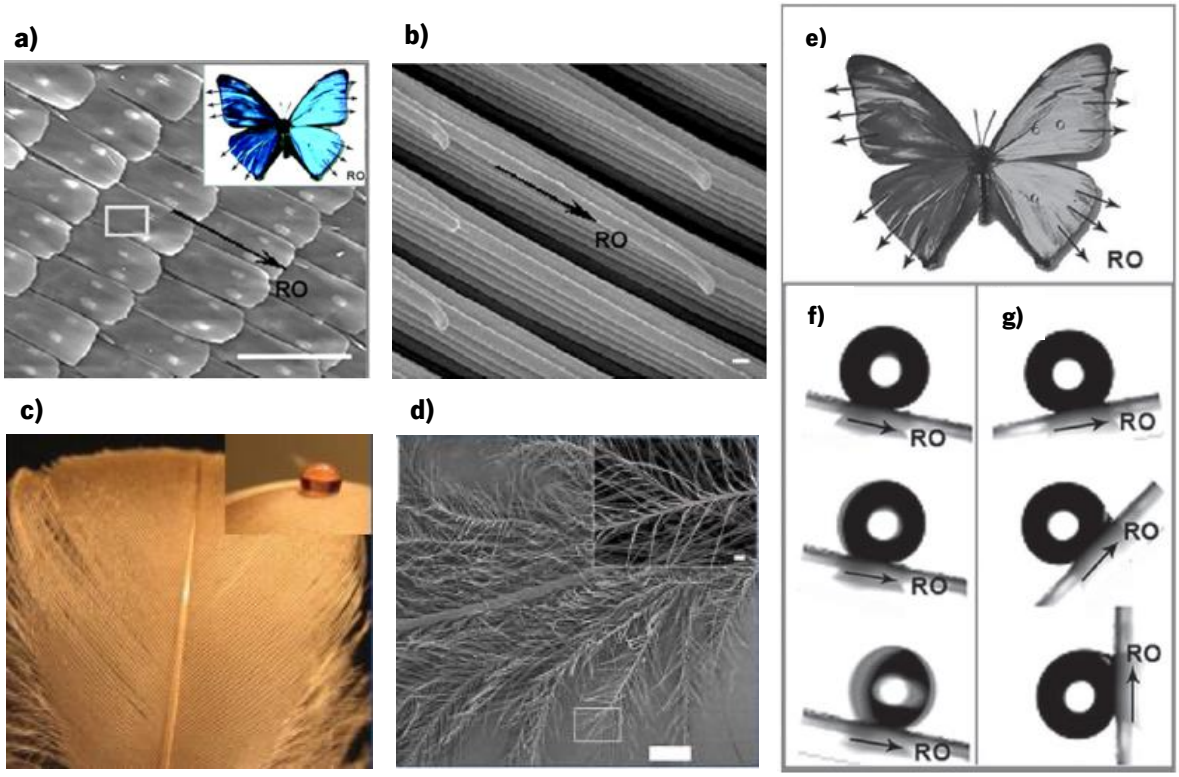

Figure 12 - Natural hydrophobic surfaces. a) SEM image of a butterfly's wings. b) Fine lamella-stacking nanostrips on the scales in butterfly wings. c) Optical image of a water droplet on a duck feather. d) Structures of duck feathers at various scales. e) Morpho aega butterfly with the direction of its directional adhesion indicated (RO - Radial Outward). f) The droplets glide easily in the RO direction and (g) in the opposite direction they show no movement. (Adapted from Malshe et al., 2013; Yu et al., 2020; Zheng et al., 2007)

2.5. Artificial Superhydrophobic and Self-Cleaning Surfaces

For a surface achieve the self-cleaning ability, the primary goal is to ensure that droplets can flow or roll off smoothly from the attached surface without any resistance. Based on the research about the natural superhydrophobic phenomenon, it is known that artificial superhydrophobic surfaces are more controllable under the combination of low surface energy materials or coatings and hierarchical roughness designed at micro and nano scales (Y. Lee et al., 2007; Yinyong Li et al., 2013; Sun, Li, et al., 2019). Several studies have confirmed that the combination of micrometric and nanometric scale roughness along with a material exhibiting low surface energy leads to apparent contact angles greater than 150°, low sliding angles and the self-cleaning effect (A. Nakajima et al., 2001). Based on the previously proposed models, it is possible for a surface to achieve the self-cleaning property by controlling surface structures to promote the free and spontaneous movement of a liquid droplet on the surface, allowing the removal of contaminants from the surface (Xu et al., 2016).

Conventionally, microstructures can be created to produce the required surface roughness for superhydrophobic surfaces. To achieve a desirable superhydrophobicity by creating microstructures, a high aspect ratio is required. Aspect ratio is defined as the ratio of height to width of a structure, the

increase of the aspect ratio, increases the water contact angle (K. Maghsoudi et al., 2017). Nevertheless, the production of high aspect ratio structures is limited due to processing constrains (Andersen & Taboryski, 2015). In addition, high aspect ratio structures are prone to faster wear and bending by mechanical forces (S. Lee et al., 2011). The introduction of nanostructures in order to create hierarchical micronanostructures can improve the performance of the produced surface in terms of wettability (Zhou et al., 2018). A dual-scale roughness not only establishes a more stable superhydrophobic condition, but it also allows a lower aspect ratio than a single-scale roughness, due to the formation of a more stable Cassie-Bexter regime (Khosrow Maghsoudi et al., 2020). Although, especially for production process and demolding issues, a lower aspect ratio is highly sought after, surfaces with hierarchical structures display lower mechanical durability in comparison with single-scale structures (J. Ma et al., 2018).

Since the first studies on the production of artificial superhydrophobic surfaces, a wide number of ways have been reported for producing rough surfaces that exhibit superhydrophobicity. In addition to water repellency, other properties such as transparency and color, reversibility of anisotropy, flexibility, anti-icing, anti-fogging and others have been incorporated into superhydrophobic surfaces (M. Ma & Hill, 2006; Xu et al., 2016).

In any case, both low surface energy and adequate surface roughness have been shown to be indispensable for processing superhydrophobic surfaces (Y. Lee et al., 2007). Techniques to make superhydrophobic surfaces can be simply divided into two categories, making a rough surface from a low surface energy material and modifying a rough surface with a material of low surface energy (M. Ma & Hill, 2006)

The most widely applied strategy involves roughening the substrate surface with micro- or nanofabrication processes, followed by a separate surface treatment or modification step, with the goal of lowering the surface energy. However, in practical applications, this type of approach requires two different steps, physical surface texturing and chemical surface coating, and has disadvantages such as peeling-off and degradation of the chemical coating (J. Li et al., 2018). To overcome this issue, it is desirable to roughen or texturize a surface that is inherently hydrophobic so that extra chemical treatment or coating is not necessary, as this increases the robustness and reliability of the superhydrophobicity of the surface.

Polymer materials have significantly lower surface free energy than metallic materials (Khosrow Maghsoudi et al., 2020). It is possible to achieve hydrophobic or superhydrophobic characteristics as long as the required roughness is fabricated on their surface (Zhou et al., 2018). Because of the excellent workability and processability for mass production, temperature resistance, high modulus of elasticity, low cost for high-volume fabrication and the wide range of material properties and surface chemistries available, the fabrication of polymeric superhydrophobic surfaces has been drawing the attention of many

researchers (Becker & Heim, 2000; Juang et al., 2002; Khosrow Maghsoudi et al., 2020; Zhou et al., 2018). Recently, thermoplastic polymers, such as low surface energy materials, have aroused large interest in recent years because of their strong hydrophobicity, electrical insulating, formable and flexible mechanical properties and chemical inertness to acids and alkali metals (J. Li et al., 2018).

Many researchers have explored the fabrication of superhydrophobic surfaces, based on these polymers. Zhou *et al.* presented a simple approach to fabricate high aspect ratio nanopillars and micro/nano combined structures via injection molding with the use of PC and PP grades (Figure 13) (Zhou et al., 2018). For both materials, the highest WCA measured was at highest mold temperature with hierarchical roughness (Figure 14). However, although the contact angle of the produced surfaces was above 150°, exhibiting excellent hydrophobic characteristics, the sliding angle of ~ 18,8° demonstrated that the surface did not possess self-cleaning abilities.

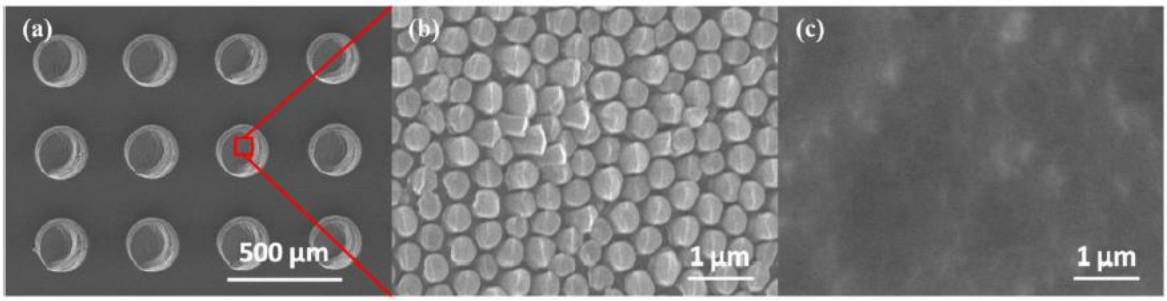

Figure 13 - SEM images of replicated structures on the surface of PC products by injection molding. (a) micropillar arrays (Tmold= 163◦C), (b) nanopillars (Tmold= 163◦C), (c) surface morphology replicated on the unprocessed AAO template. (Adapted from Zhou et al., 2018)

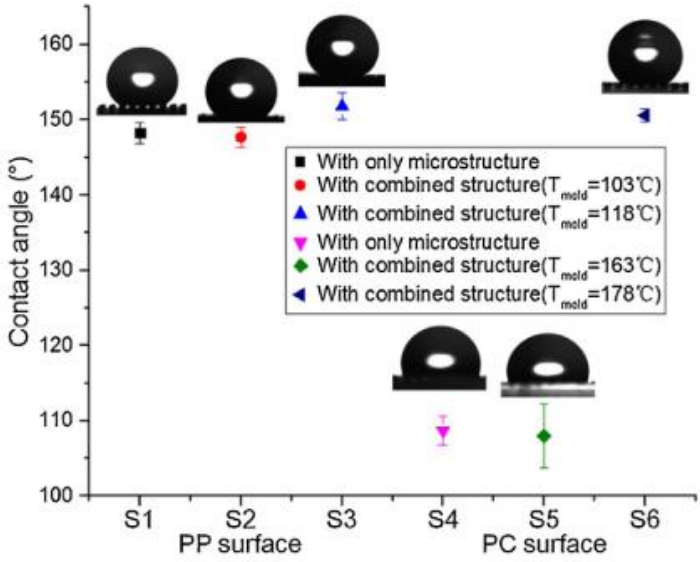

Figure 14 - Measured contact angles in PP and PC surfaces, with different surface structures. (Adapted from Zhou et al., 2018)

Bhushan *et al.* reported the fabrication of surfaces with micro-, nano- and hierarchical structures by replication of a micropatterned silicon surface using an epoxy resin and by self-assembly of alkanes to create hydrophobic nanostructures (Bhushan et al., 2009). Their study shows that the presence of single scale roughness (Figure 15a-b), both on nano and microscale, enhanced the WCA of the produced samples to the superhydrophobic regime, with the samples exhibit a WCA of 158 ° and 154 °, respectively. Concerning the CAH, the microstructured and nanostructured epoxy samples exhibited values of 23 ° and 36 °, respectively. However, the presence of a hierarchical structure (Figure 15c) was observed to boost even more the WCA of the surface (169 °) and decrease its CAH (2°), allowing the achievement of the self-cleaning property.

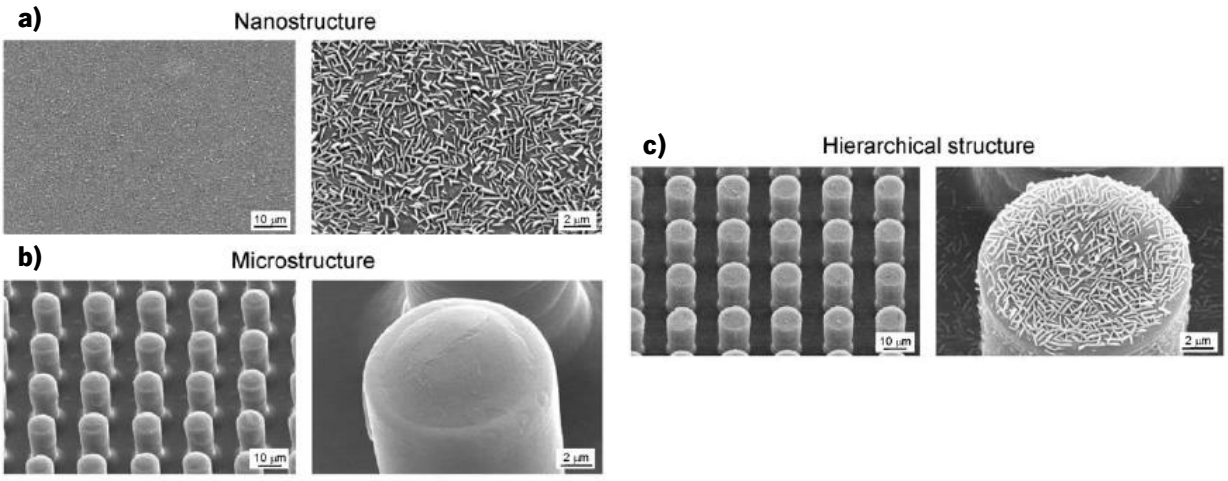

Figure 15 - SEM micrographs of the nanostructure,microstructure,and hierarchical structure. (Adapted from Bhushan et al., 2009)

In addition to self-cleaning surfaces, superhydrophobic polymeric surfaces can be used for a wide range of potential applications (Khosrow Maghsoudi et al., 2020). However, its developing can be really challenging, due to the difficulty to find the appropriate surface topography that boosts the WCA and lowers the hysteresis, in order to achieve the self-cleaning ability.

2.6. Optical Transmittance on Superhydrophobic Surfaces

Progression of materials and techniques used to fabricate superhydrophobic surfaces has led to the investigation of other properties desirable for many applications. There are many optical applications for superhydrophobic surfaces, which depend on a material being transparent (Roach et al., 2008). Almost all natural superhydrophobic surfaces and most synthetic ones are not transparent, limiting the applications in optics industry. To enable the applications of superhydrophobic surfaces to optical devices such as solar cell panels, smart windows, camera lenses, sensors, among others, it is critical to maintain high optical transparency in the desired wavelength.

Transparency is a physical property of materials, which allows light to pass through the material without significant scattering or absorption (Fei et al., 2020). Roughness, pores and grain boundaries will scatter light (Figure 16), significantly comprising transparency (Chen et al., 2012; Øgendal, 2019).

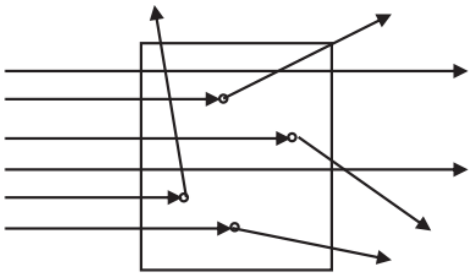

Figure 16 - Light scattering. (Adapted from Øgendal, 2019)

As mentioned, superhydrophobic surfaces or films require a large surface roughness and a low surface energy. From the point of view of surface roughness, hydrophobicity is competitive with transparency because it is the source of light scattering (Akira Nakajima et al., 2000).

Likewise, it is difficult to achieve both superhydrophobicity and high optical transmittance on the same surface, mainly because the surface features required for superhydrophobicity often leads to severe light scattering, resulting in nearly opaque or translucent surfaces (Fei et al., 2020; Karunakaran et al., 2011). An increase in surface roughness leads to a decrease in the optical transmittance due to Mie and Rayleigh scattering. Both theories assume that the surface roughness is created by spherical and non-absorbing particles that redirect the incident light. The relationship between particle size and incident light wavelength is used to categorize the scattering models. Mie scattering takes place when the diameter of the particle is close to the incident light wavelength, and Rayleigh scattering occurs when the particle size is much smaller than the wavelength of the incident light ($< 1/10\ \lambda$).

This phenomenon caused by surface roughness is mainly due to the Mie scattering effect. Mie scattering theory is described in the following equation:

$$C_{SCA} \approx \frac{\pi d^2}{2} \sum_{n=1}^{\infty} (2n+1)(a_n + b_n) \tag{2.6}$$

The scattering cross section (C_{SCA}) provides a quantification of light scattering as a function of particle diameter (d), where a_n and b_n are Mie coefficients of the order n, relating to the electromagnetic properties of the material. The C_{SCA} is directly proportional to the square of the particle diameter, indicating the existence of an upper limit beyond which the surface feature size, while providing a platform for superhydrophobicity, will result in significant light scattering, and thus reduce transparency (Fei et al., 2020). Therefore, precise control of roughness is required to satisfy both hydrophobicity and transparency. It is necessary to find the critical window, where the roughness is optimized for optical transmittance yet high enough for superhydrophobicity.

Based on research, surface roughness below the wavelength of incident light can help minimize Mie scattering (Fei et al., 2020; Yılgör et al., 2016). According to Liu *et al.* (2019), when the surface roughness is larger than ¼ of the wavelength of light, it causes light to scatter and thus loss of transmission depending upon the length and concentration of rough features (Y. Liu et al., 2019). It is believed that, to some extent, both transparency and superhydrophobicity of the surfaces can be obtained simultaneously. However, the required micro/nanostructures for superhydrophobicity are usually vulnerable to abrasion, exhibiting poor mechanical durability (Fei et al., 2020). The intrinsic contradiction of transparency and superhydrophobicity plus durability issues are a major challenge to overcome for preparation of self-cleaning surfaces with good optical transmittance.

Ngo *et al.* also investigated the effect of the micropillar step size upon the superhydrophobicity and transparency on a Polydimethylsiloxane (PDMS) sample (Ngo et al., 2015). They produced PDMS surfaces with cone-shaped micropillars arrays with an average height of 20 μm and base diameter of 23 μm, and tested five different step sizes: 40 μm, 60 μm, 80 μm, 100 μm and 120 μm. They reported that the transparency increased with the increase of the step size. With smaller distances between the structures, there was a higher concentration of the pillars, contributing to light scattering and consequently loss in transparency (Figure 17). They also found that the critical step size of 80 μm made it possible to achieve both superhydrophobicity, with WCA of 175 ° and a good transparency, with only 2% of transmittance loss over the 300-1000 nm spectral region.

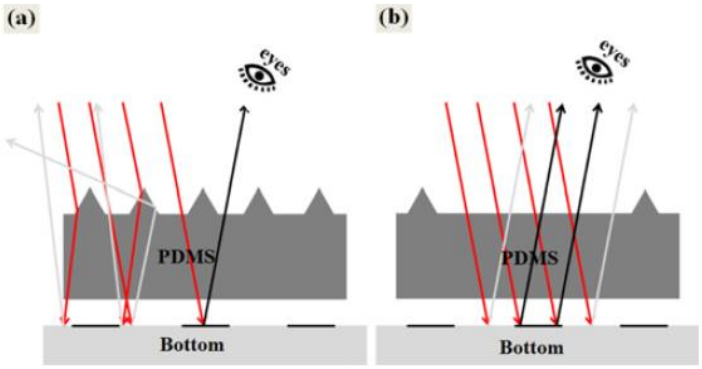

Figure 17 - Schematic diagrams illustrating the effects of step size upon the effects of step size upon transparency. a) small step size and b) large step size. (Adapted from Ngo et al., 2015)

The self-cleaning effect of superhydrophobic surfaces is especially critical for optical applications such as sensors, the main focus of this work, which should be dust-free for optimum efficiency. Studies have been carried out on designing and fabricating superhydrophobic and transparent materials through the control of the structure's dimensions, although is not straightforward how the surface topography dimensions can affect the transparency. According with the authors mentioned previously, for a surface to be transparent, surface structures should be smaller than the wavelength of the incident light, and the precise control of other roughness parameters are also important for the achievement of both properties.

2.7. Methods and Processes used for the Production of Superhydrophobic Polymer Surfaces

Before going into the description of the methods and processes used for the production of superhydrophobic polymer surfaces, it will be useful to list the critical structural features that must be incorporated onto polymer surfaces in order to observe superhydrophobic behavior. To prepare superhydrophobic polymeric surfaces with water contact angles superior to 150° and contact angle hysteresis below 10°, these following general requirements must be incorporated (Khosrow Maghsoudi et al., 2020; Yılgör et al., 2016):

i. Use preferably low surface energy substrates;
ii. Microstructures distributed throughout the surface with an average distance between them;
iii. Preferably the use of nanoscale roughness on the protrusions;
iv. High aspect ratio of the surfaces asperities to provide a large surface area for the structures;
v. Pillars lacking sharp edges to limit pinning of the water droplet;
vi. Tight packing of the structures to avoid destabilization of the solid/liquid/air composite;
vii. Small-sized asperities relative to droplet size.

Various physical and chemical methods have been developed to create superhydrophobic surfaces. In general, these approaches can be divided into three groups, bottom-up, top-down and combined approaches.

Bottom-up approaches, including chemical vapor deposition (CVD), electrochemical deposition (CBD), layer-by-layer (LbL), colloidal assembly and sol-gel methods, create surface roughness by depositing materials onto a surface. These methods produce micro/nanoscale superhydrophobic surfaces even from hydrophilic materials (Celia et al., 2013; X. M. Li et al., 2007; Khosrow Maghsoudi et al., 2020). However, they are limited in their use in industrial applications due to elaborated procedures and high costs of fabrication. In addition, micro/nanostructures produced via bottom-up approaches are not originated from the substrate, possibly leading to poor mechanical durability (Fei et al., 2020).

Top-down approaches, which include lithography, templation, micromachining, LIGA, plasma treatment, laser ablation and etching, are based on removing materials from the surface to create an appropriate surface roughness (Celia et al., 2013; X. M. Li et al., 2007; Khosrow Maghsoudi et al., 2020). The rough surface is an integrated part of the substrate and thus it has relatively high mechanical durability. The properties of the substrate are very crucial to the processability and quality of the surface. The low throughput and high cost of top-down approaches are the main limiting factors of their practical applications (Fei et al., 2020). The produced surface through this approach can also become a template in a polymer processing method to directly replicate the created roughness on a polymeric surface.

There are also methods based on the combination of both bottom-up and top-down approaches, for example, casting of polymer solution, phase separation and electrospinning. The combination of bottom-up and top-down approaches might have the apparent advantages of both methods and it is especially useful for the creation of architectures with a dual-scale roughness. The combination techniques often consist in two stages. Generally, the first step is the top-down approach for the creation of a rough surface and the second step is bottom-up process for the creation of the adequate roughness. However, some combination methods do not show a distinct two-stage process (X. M. Li et al., 2007). Moreover, these methods are not yet practical in an industrial context, most of these techniques suffer from process complexity, low level of automation, limitation of available materials and high specialization of the required equipment.

Given the interest in mass producing superhydrophobic surfaces, the application of polymer molding processes to the making of superhydrophobic surfaces arises as the main focus of this work.

2.7.1. Replication-based Methods

As mentioned previously, thermoplastic polymers have aroused wide interest for self-cleaning applications. Therefore, many researchers have explored the fabrication of superhydrophobic surfaces, based on these polymers, with various techniques, such as photolithography processes, etching techniques, among others.

Although the aforementioned techniques could generate superhydrophobic surfaces, the preparation of hierarchically structured superhydrophobic products still cannot meet the demands of large-scale industrialization. Therefore, there is still demand for the development of simple, efficient and economical fabrication methods that are capable of precisely controlling the dimensions and shapes of the surfaces structures (J. Li et al., 2018; Sun et al., 2019).

Alternatively, replication-based techniques have been regarded as a more cost-efficient and scalable processes. Replication-based techniques can be applied to already produced polymer surfaces, sheets and films, among others. Regular surface structures as well as relatively complex patterns can be created via replication-based techniques and the range of available polymer materials provides a wide selection and variety for fabricating patterned surfaces that meet specific properties (Guan et al., 2013; Khosrow Maghsoudi et al., 2020). Moreover, these methods are usually relatively simple and require less expensive equipment (Yeong & Gupta, 2017).

Replication-based methods generally involve three steps, template making, where a template with suitable structures is manufactured, a molding step, where a polymeric material is replicated on the template surface based on the specific processing technique being applied, and a demolding step, where

the structured polymer surface is very carefully detached from the template surface (Khosrow Maghsoudi et al., 2020).

There are some advantages attributed to the replication-based manufacturing of superhydrophobic polymer surfaces compared to other means of fabrication (Khosrow Maghsoudi et al., 2020):

i. Polymer processes are industrially practical methods that facilitate the mass production of superhydrophobic surfaces;
ii. Polymer processing techniques benefit from a high level of automation. They are usually simple processes, applicable to complex shapes and sizes, and that does not require excessive specialization of equipment;
iii. A wide range of polymers, including thermoplastics, thermosets, rubbers and thermoplastic elastomers can be processes using this type of techniques;
iv. Superhydrophobic polymer surfaces fabricated by replication-based methods can be highly resistant to mechanical damage, showing great durability. In replication-based method, the micro/nanostructures required for obtaining superhydrophobicity are a part of the bulk material. Therefore, these replicated surfaces benefit from high cohesive forces and thus a higher level of mechanical and chemical durability;
v. Due to the use of inserts or templates in an injection or compression mold cavity, the polymer surface can be produced directly. Moreover, the fabrication of micro/nanostructures on already produced polymer materials is also possible through the hot embossing technique.

However, despite the above mentioned advantages, several issues limit the wider application of replication-based methods, and further research is required to overcome many of this existing issues (Khosrow Maghsoudi et al., 2020):

i. The replication of some structure shapes, such as reentrant structures like T-shape, mushroom-like structures, among others, may provide the desired superhydrophobic property. However, these structures are often associated with serious demolding issues that prevent the successful fabrication of such structures;
ii. Currently, some approaches have been introduced to create nanostructures on a microstructured surface to create hierarchically structured surfaces, such as a combination of a two-level hot embossing via heating-cooling cycles and stretching of structures at higher molding temperatures when demolding. However, the fabrication of nanostructures using polymer processing techniques remains challenging due to complications during the filling and demolding steps;
iii. Polymer materials, have difficulty filling nanostructures due to their high viscosity and non-

Newtonian behavior. In case of thermoplastics, the manipulation of processing parameters, such as mold and melt temperature, can offer a solution for this issue;

iv. Micro/nanostructures are prone to damage from mechanical forces during demolding, being required a careful use of both produced samples and templates, and although and antistiction coating on the mold surface can be applied, this may create issues on the structures filling;

v. Template quality affects the replication quality of the produced surfaces. The micro/nanostructures of a template can be damaged by repetitive molding-demolding cycles due to mechanical forces or the filling by polymer materials. Although some studies have attempted to reduce damage during demolding, prolonging the template lifespan remains a major challenge.

2.7.1.1. Injection Molding

Among the diverse polymer processing techniques, injection molding is one of the most potential techniques to fabricate polymer products in large numbers (Figure 18) (Zhou et al., 2018). Injection molding profits from a low cost of fabrication of polymers parts in large quantities, the possibility of producing versatile shapes, short cycle times and simple automation (Khosrow Maghsoudi et al., 2020). The replication quality has been shown to be influenced by mold temperature, melt temperature, injection velocity, injection pressure, holding pressure and ejection temperature (Matschuk & Larsen, 2013). The greatest challenge in injection molding of micro/nanostructured surfaces is the proper filling of polymer into the structures. This difficulty emerges from the arduous filling of polymer melt into the micro/nanostructures and the fast cooling rate of the polymer material in the mold cavity, due to the heat transfer from polymer to the cold mold (Khosrow Maghsoudi et al., 2020; Matschuk & Larsen, 2013; Stormonth-Darling et al., 2014). High-quality replication requires both complete filling of the mold structures by the polymer melt and negligible deformation of the solidified replica during demolding (Matschuk & Larsen, 2013). For an improved control of the demolding quality, usually is applied an anti-sticking coating layer on the mold insert, especially for the high aspect ratio structures (Zhou et al., 2018).

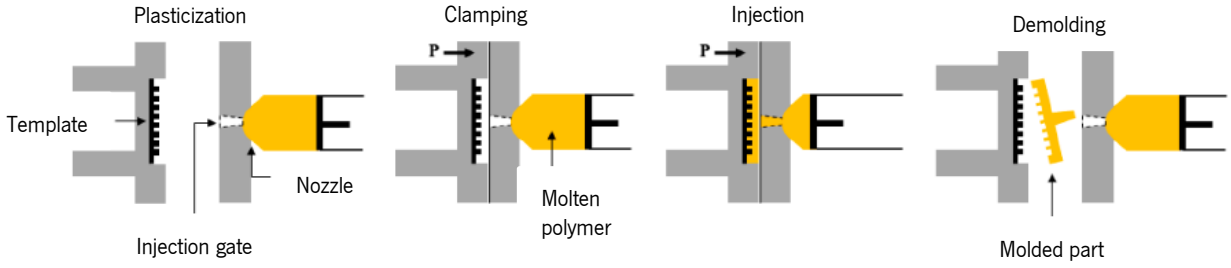

Figure 18 - Schematic of injection molding. (Adapted from Khosrow Maghsoudi et al., 2020)

2.7.1.2. Polymer Casting

Another promising technique is polymer casting, in which a polymer material having a suitable flowability is poured onto the template surface (Figure 19). The material can fill the micro/nanostructures without the need of any pressure, due to the low viscosity of the polymer. However, the filling is occasionally quite difficult, especially for nanostructures due to the presence of trapped air (Khosrow Maghsoudi et al., 2020). Nonetheless, filling can be achieved under vacuum. Given the specific properties that a polymer should possess for use in this technique, i.e., low viscosity and favorable flowability, PDMS is the main material used in this method (Hong et al., 2013).

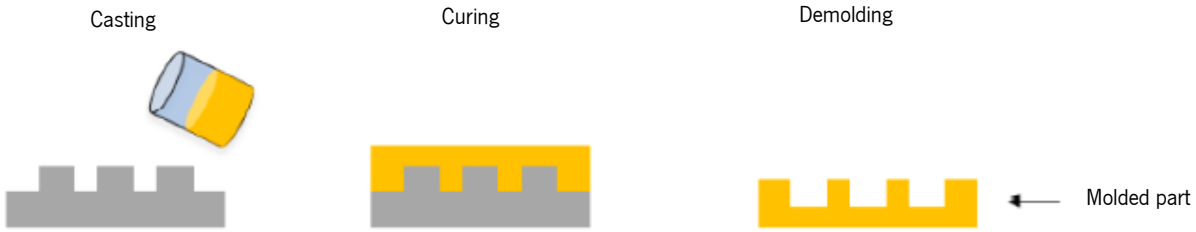

Figure 19 - Schematic of polymer casting. (Adapted from Khosrow Maghsoudi et al., 2020)

2.7.1.3. Hot Embossing

Hot embossing or the thermal nanoimprint technique is one of the most highly used processes for fabricating micro and nanostructured surfaces. Both amorphous and semicrystalline thermoplastic polymers and thermoplastic elastomer polymers can be replicated via hot embossing (Khosrow Maghsoudi et al., 2020). This process replicates a microstructured master, a so-called mold insert, in a polymer substrate. Hot embossing process relies on increasing the temperature of a polymer substrate up to its melting range in semicrystalline polymers or above its glass transition temperature in amorphous polymers and then on pressing a heated mold into the polymer for generating pressure to fill the surface structures (Omar, 2013; Worgull, 2009).

This method for fabricating micro and nanostructures on polymer substrate was firstly proposed by Chou S. Y. of Princeton University of the United States (Chou et al., 1995). Since then, this technology has attracted a significant interest among micro and nano replication processes due to the relatively simple set-ups and short lead times associated with its implementation.

In both academia and industry, this method is regarded as a more cost-efficient and scalable technique for the fabrication of high quality polymer structures, both on micrometer and nanometer scales, and also provides several advantages such as relatively low cost embossing tools, loss cost required for manufacturing, a single mold that can be used for mass production, simple operation and high replication

accuracy (Deshmukh & Goswami, 2020; Juang et al., 2002; Peng et al., 2014; Sun et al., 2019). Compared with other methods, this technique presents a much better processability ability for the fabrication of polymer micro/nanostructures, showing great precision forming at both micro and nano-scales (Sun, Zhuang, et al., 2019).

Up to date, the are mainly three kind of hot embossing technology, distinguished by the configuration of the molding tools, including Plate to Plate (P2P), Roll to Plate (R2P) and Roll to Roll (R2R) (Figure 20).

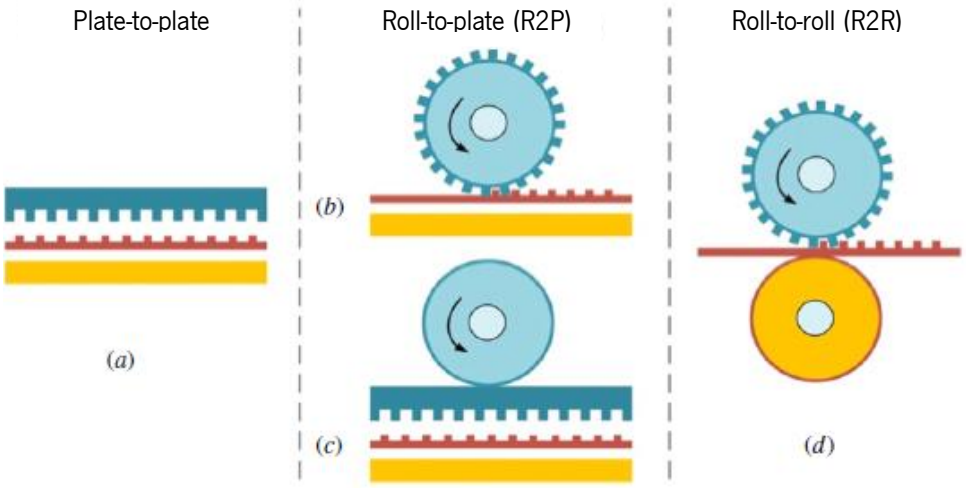

Figure 20 - Schematic diagrams of three modes of micro hot embossing. (a) P2P, (b) R2P—roller mold, (c) R2P—flat mold and smooth roller, and (d) R2R. (Adapted from Peng et al., 2014)

The R2R hot embossing is characterized by the use of two rotating cylinders, one is microstructured and the other one is the supporting roller. The polymer substrate in placed in between and is continuously passed through the roller (Deshmukh & Goswami, 2020). R2R embossing allows a high cylinder rotation speed and likewise is suited for the series production of large batches. The R2P is described by a rotating cylinder and a flat plate, where the cylinder can unwind. It is similar with the R2R principle, with the difference that the mold can be integrated in the plane area. The cylinder rolls along the microstructured mold and the embossing of the structures takes place on the contact line (Worgull, 2009). However, both of these principles can only be applied to the production of microstructures with low aspect ratios and a low heights due to demolding issues (Worgull, 2009).

Among these embossing technologies, the P2P hot embossing has advantages of high precision, good replication, flexibility in material choice and process controllability (Wu et al., 2016). The schematic of P2P hot embossing is illustrated in Figure 21, which contains a mold plate with microstructures and a substrate plate. As an advantage, the press force over the whole microstructured area allows the use of polymer melts, a prerequisite for molding high microstructures with high aspect ratios, making it the most suitable for the fabrication of superhydrophobic surfaces. Another advantage lies on the fact that structures can be demolded by a motion parallel to the structures. Hence, the risk of damaging the

structures is lower than the other principles. Due to these advantages and the fact that microstructures molds are typically produced on flat areas, this is the conventional method of hot embossing (Worgull, 2009). However, P2P hot embossing is a discontinuous batch-wise mode facing drawbacks of limited efficiency, high deformation force and small replication area (Peng et al., 2014).

The technological procedure of hot embossing comprises of four major steps (Figure 21): (1) heating the mold and substrate to molding temperature above its glass transition temperature, T_g, in case of amorphous polymers or melting temperature, T_m, for semicrystalline polymers, (2) embossing the microstructure patterns at embossing pressure, (3) after preset embossing time, cooling the mold and substrate to demolding temperature below T_g or T_m accordingly with the used polymer and (4) separating the mold from the substrate by opening the tools (deembossing).

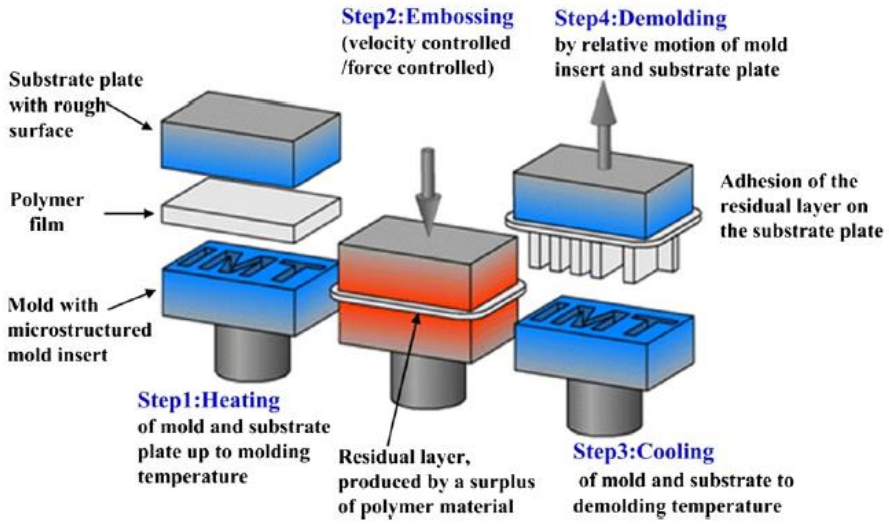

Figure 21 - Schematic representation of a typical micro hot embossing process including four major steps: heating, molding, cooling and demolding. (Adapted from Peng et al., 2014)

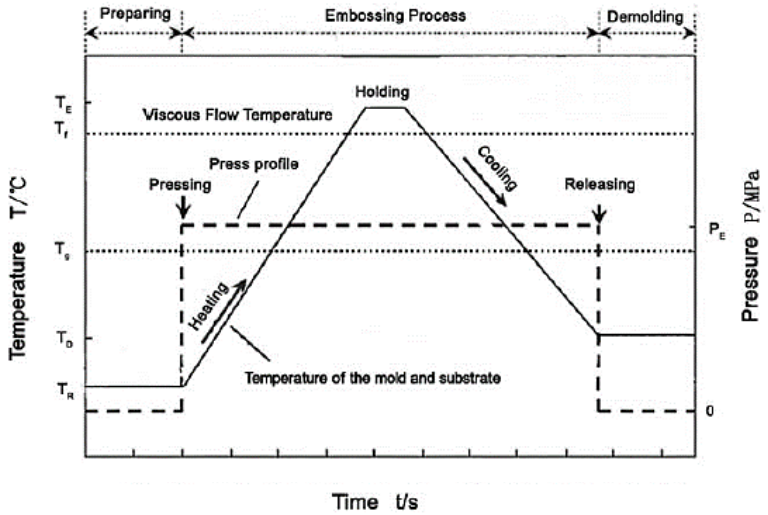

Figure 22 – Procedure's diagram of the traditional hot embossing process (P_p - preload pressure; T_R - room temperature; T_E – embossing temperature; T_D – demolding temperature; P_E – embossing pressure). (Adapted from Wu et al., 2016)

Figure 22 shows the procedures diagram of the hot embossing process, which in detail usually starts with the mold and the substrate being brough in contact with each other and heated under vacuum from the room temperature (T_R) to the embossing temperature (T_E). As a result of the contact, the heat transfer between the mold and the substrate is optimized, leading to a more homogeneous temperature distribution in the polymer. During the heating time the pressure is maintained at P_p (preload pressure). When the polymer temperature is close to the embossing temperature, the preload pressure is increased to the embossing pressure (P_E). This pressure is kept for a particular duration known as embossing time. During this time, the polymer deforms under constant load, which results in a decrease in the residual layer and the filling of the cavities. During the molding process, both temperature and pressure remain constant. The isothermal embossing under vacuum is important to fill the cavities of the mold completely, since air inclusions or cooling during the mold filling may result in an incomplete molding of the microstructures in particular with high aspect ratios. Upon the end of the embossing time, cooling of the mold and substrate starts while the pressure is maintained. Finally, when the demolding temperature of the polymer is achieved (T_D), the molded part is demolded from the mold by the relative movement between mold and substrate (Deshmukh & Goswami, 2020; Worgull, 2009).

In case of thermoplastic polymers, considered the most suitable materials, they experience two stages of deformation in the whole process: one is a stress concentration and strain hardening stage occurring in heating and embossing steps, and the other is a stress relaxation and deformation recovery steps which occurs in cooling and demolding steps (C. Liu et al., 2010; Sun, Zhuang, et al., 2019).

The stresses develop in a component after hot embossing is much less than in other methods. This could be attributed to the fact that in hot embossing, the polymer is stretched over a smaller distance from the bulk of the polymer substrate. The operating temperatures range in this technique is much less compared with other manufacturing methods, which helps in decreasing the shrinkage and frictional forces during the cooling and deembossing steps, respectively, leading to higher shape and dimensional precision (Deshmukh & Goswami, 2020; Sun, Zhuang, et al., 2019).

The pressure applied for replication in the hot embossing process is well distributed in the component, while in the injection molding process, for example, it is applied only at the injection gate and it dissipates throughout the mold cavity during the injection phase. On the other hand, the hot embossing cycle is relatively long if compared with injection molding, for example, due to the low cooling and heating rate of the bottom and top plates. This process could take up to 30 minutes depending on the mold design, machine and the replicated materials where the complex and high aspect ratio structures will prolong the process. Also the material viscoelastic behavior under embossing conditions which determines the replicability of the polymer will directly affect the processing time (Omar, 2013).

One of the major challenges faced during hot embossing is to arrive at optimum level of process parameters to ensure complete filling of the cavities on the embossing tool with the work material to achieve the maximum accuracy. Another challenge is to apply the optimum level of deembossing force in the cooling step to separate the mold from the polymer without damaging or distorting the replicated structure on the polymer (Deshmukh & Goswami, 2020). According to Worgull, demolding is the most critical process step of hot embossing, depending on the process parameters and the quality of the mold, demolding forces can vary by several factors (Worgull, 2009). The demolding-related defects, such as broken and distorted features, are important issues that limit the wide application of this method, especially in production of patterns with high aspect ratio. These phenomena may be attributed to the thermal contraction behavior of polymer being significantly different from that of the molds. As a result, large thermal stress during the cooling phase is generated because of this disparity, making it difficult to separate the features from the mold (Peng et al., 2014).

2.8. Factors Affecting the Replication and Part Quality in Hot Embossing

The molding parameters of hot embossing comprise process parameters, which are controlled by users, material parameters and influencing factors mainly from the embossing machine. Together, they influence the quality of the molded part. Therefore, their understanding and characterization is important to avoid defects or failures on the embossed parts.

The overall factors affecting the control of the process and the quality of the embossed parts can be separated into the five following groups:

i. Embossing machine;
ii. Embossing tool (alignment system, heating unit and cooling unit);
iii. Substrate Plates;
iv. Mold insert/Microstructures;
v. Process Parameters.

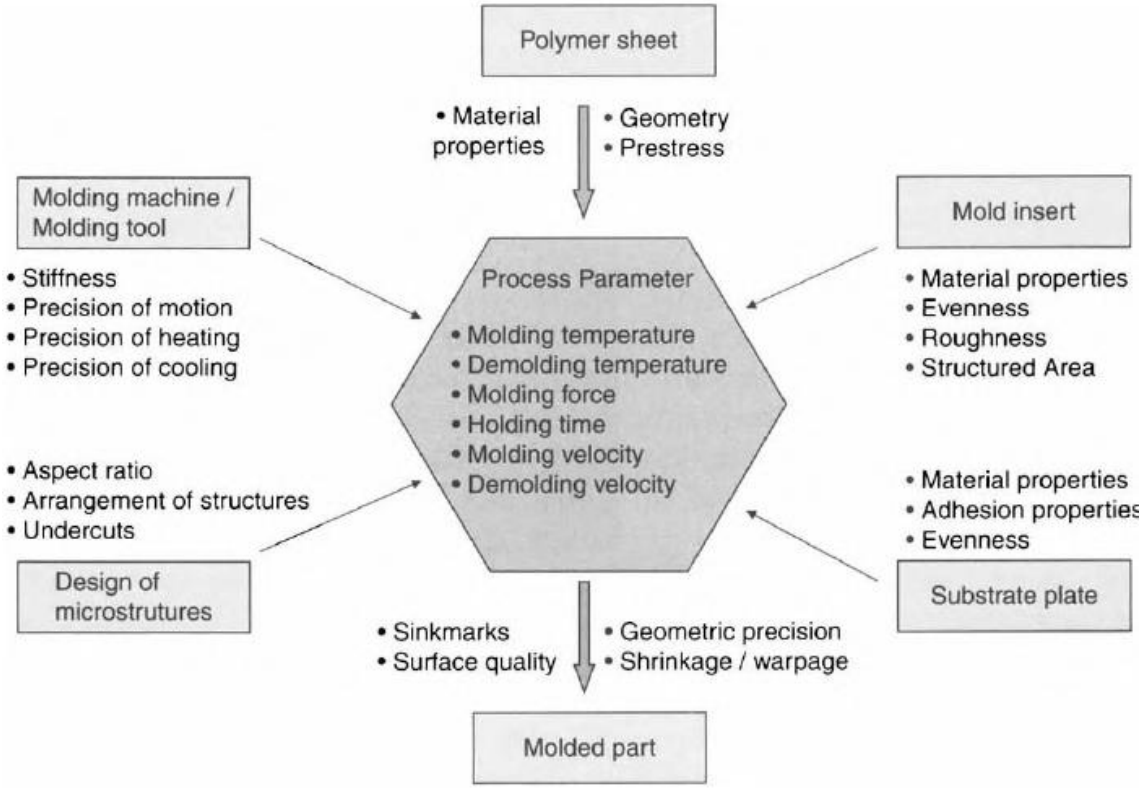

Figure 23 - Schematic view of the process parameters and factors influencing the quality of the replicated parts. (Adapted from Worgull, 2009)

The stiffness of the machine must be as high as possible in order to prevent bending of the plates under the embossing load, and consequently the possible damage of the structures during demolding. The precision of the plate displacement through the motion of the crossbars is responsible for the required parallel movement of the mold and the substrate material, which in turn influences the quality of the molded part. The lack of parallelism results in a gradient in the residual layer, a non-uniform-filling and the creation of high stress in one area, which may be the reason structures get damaged during demolding (Omar, 2013; Worgull, 2009). Furthermore, the evenness and the surface roughness of the plates is of particular importance to ensure a homogeneous thickness of the molded part over the complete embossing surface.

Another important factor is the homogeneous and stable temperature distribution during the heating and cooling phases. The accuracy of a homogeneous temperature distribution in the mold and substrate plate is essential for a successful molding. In particular, non-homogeneous temperature distribution during the heating stage could cause a non-uniform flow of the polymer melt and also, can contribute to variations in thickness of the residual layer. In the cooling stage, a non-homogeneous temperature distribution could be more problematic as it can result in an inhomogeneous solidification and anisotropic shrinkage, which can lead to warping of the produced replica (Omar, 2013).

The thermal properties of the polymer material are very important to control the embossing process, namely the molding and demolding temperature are crucial parameters for achieving high quality

replicated parts. The isotropic or anisotropic behavior of the polymer material will also affect the shrinkage and the warpage of a replicated part. Amorphous polymers are typically characterized with isotropic shrinkage, while semicrystalline polymers present anisotropic behavior. Therefore, the orientation of the crystallite structures determines the shrinkage and warpage of the molded parts. Furthermore, the molecular weight of a material will affect the cavities filling. The longer the polymer chains, the higher the embossing temperature has to be chosen above T_g in order to maintain a viscosity suitable for replication of the mold pattern into the polymer substrate, also resulting in an increase on the processing time due to long heating and cooling cycles (Schulz et al., 2005).

The mold material should also show chemical resistance to the polymer substrate, and a high heat conductivity of the mold material will also help reduce heating and cooling times, providing a more efficient cycle. In addition, the material properties of the mold are responsible for its deformation behavior when it is under load. Silicon molds can be broken easily under a small applied pressure and other molds made of relatively soft materials can be bent easily which can cause failures or defects on the final product (Omar, 2013). Evenness and parallelism of the mold are also essential for molding structures and achieving a uniform filling and a thin residual layer. Furthermore, the roughness of the mold surface is another factor responsible for high friction and demolding forces, that may cause the risk of damaging the structures during demolding. Another important factor is concerned with the mold machining defects like overlaps or the roughness of the vertical walls, as such surface features could damage or separate the polymer structures during the demolding step. To achieve a successful demolding, the surface roughness, especially of vertical sidewalls, should be reduced as much as possible (Omar, 2013; Worgull, 2009). In addition, the layout and the aspect ratio of the structures of the mold could cause filling problems during embossing and high forces during the demolding step (Omar, 2013). The use of mold coatings, lubricants and release agents can reduce friction, and thereby reducing the risk of damaging the structures during demolding. However, if its not an appropriate one, it can obstruct the structures and hinder the filling.

One of the most important factors which will affect the replication quality and accuracy is the controllable process parameters. The following process parameters, which can be controlled by the user during the setting up of a replication process on a hot embossing machine, define the hot embossing cycle:

i. Embossing temperature;
ii. Embossing pressure;
iii. Embossing velocity;
iv. Embossing time or holding time;

v. Demolding temperature;

vi. Demolding velocity.

A general hot embossing cycle cannot be defined due to the large variety of process variations, their individual adaptation to the requirements and the mold designs. Likewise, for each process the values of each parameter have to be set up individually, depending on the design of the structures, the molding material and the molding area.

With the rapid development of micro and nano manufacturing technologies and the in-depth studies on hot embossing processes, researchers generally agree that the main processing parameters for this method are the embossing temperature, pressure and time, as well as the vacuum environment when applied (Sun, Zhuang, et al., 2019; Telgarsky et al., 2004). Several researches investigated the effects of these factors and the generic conclusions were that an increase of these three process parameters leaded to improvements of the process performance (J. M. Li et al., 2008; Sun, Zhuang, et al., 2019). In particular, the embossing temperature was found to be of major importance for achieving better replication (Bhagat & Gupta, 2015; J. M. Li et al., 2008). Therefore, these results indicate that high values of process parameters can be used to ensure the complete filling of the cavities, however, it should be noted that such setting may also lead to negative effects such as an increase of the cycle time, degradation of the material, among others.

Li *et al.* investigated the effect of the process parameters on the polymer flow via online observation with stereo vision microscopy (J. M. Li et al., 2008). The results demonstrated that the embossing temperature had the most significant role in the replication accuracy of the width and shape of the structures, followed by the embossing pressure and time.

The main principle of determining the processing window of the hot embossing is to cover the temperature range where the polymer has enough flow or deformation ability filling in the cavities of the mold at available embossing pressure. According to Sun *et al.*, the embossing temperature needs to between 10 to 40 °C above the glass transition temperature for amorphous polymers, and in some cases, even higher than the melting temperature T_m or viscous flow temperature of the material T_f (Sun, Zhuang, et al., 2019). The temperature curve of the mold and substrate plate is also dependent of the quality of the heating system, heat conduction of the materials, and the amount and quality of heat transfer between the heating system and mold, which are also factors that affect the time needed for reaching the desired molding temperature.

Defects can occur during the principal process stages as follows:

i. During the filling stage, the main objective of the replication process is to obtain the complete filling of the structures since an incomplete filling leads to the geometric inaccuracy of the structures. Defects during this stage could happen due to the lack of required pressure to fill the cavities at a given temperature.

ii. In the cooling stage, sink marks can occur if the applied pressure is not enough to prevent shrinkage as it will induce poor contact pressure between the mold and the polymer. Moreover, the differences in shrinkage during cooling, due to the fact that thermal contraction behavior of polymers is significantly different from the molds, could cause a warpage of the structures or of the whole part. Furthermore, a short cooling time will increase the internal stress of the part as there will not be enough time for the relaxation of the shear stress during embossing and the orientation of the polymer molecules will be frozen too rapidly.

iii. The demolding stage is the most sensitive step which tends to cause the worst defects and limitations. Broken and pulled out structures as well as damaged edges could happen during this step as a result of high adhesion and friction forces between the mold structures and the polymer. Distorted features could happen due a non-vertical demolding and overstretching can happen due to the joint action of frictional force and high demolding temperatures.

The process parameters for hot embossing have to optimized depending on the feature size, geometry and shape of the pattern and finally the mold and substrate contact area in order to obtain the best replication accuracy. The parameters values must concern the highest value to assure the complete filling of the cavities, but in a range to avoid material degradation and other process defects. Also, to improve replication, technologies such as vacuum, to avoid incomplete filling of microstructures should be employed.

2.9. Hot Embossing of Micron-Sized Parts with High Aspect Ratio

As mentioned previously, to achieve a desirable superhydrophobicity by creating microstructures on a polymer part, a high aspect ratio is required. To emboss high aspect ratio structures, in line with what was abovementioned, there are process and material properties that have to be taken into account.

Becker *et al.* (Becker & Heim, 2000; Juang et al., 2002) have suggested the following processing conditions for hot embossing of polymer parts with micron-sized features:

i. The thermal cycle, defined as the temperature range between embossing and deembossing temperatures, should be 25°C to 40°C in order to minimize the thermally induced stresses;

ii. The embossing pressure should be around 0,5 to 2 kN/cm^2;

iii. Automated deembossing is required if the structures have vertical walls and a high aspect ratio;

iv. For embossing structures with high aspect ratio, the side wall surfaces of the mold must be kept as smooth as possible in order to minimize the friction force between the mold and the polymer substrate. The microstructure is destroyed if the frictional forces become larger than the local tensile strength of the polymer. For making structures with aspect ratio higher than 0,5, the empirical limit is 80 nm RMS.

v. The above-described friction between the mold and substrate is particularly critical in microstructures with vertical side walls. A small draft angle eases this constraint, as mechanical contact between the mold and polymer is immediately lost in the demolding. If the application and mold fabrication allows angles different from 90 °, this advantageous in the fabrication process.

vi. The thermal expansion coefficients of the mold and the polymer substrate also must be taken into consideration, because of the additional force caused by the difference in shrinkage between the mold and the polymer;

vii. To minimize adhesion between the mold and the polymer material, which creates an additional force in the deembossing step, both surfaces should offer as little chemical surface bonding sites as possible. Although mold release agents and plasticizers can be added to the polymer, in the fabrication of a biochemistry or biomedical devices, these components are not desirable, owing to sample contamination or an increased fluorescence background.

2.10. Hot Embossing in the Production of Superhydrophobic Surfaces

Several studies have been investigating the production of superhydrophobic surfaces through the hot embossing technique.

Bhagat *et al.* presented an approach for large-scale microstructure replication on PC surfaces (Figure 24a) with the use of silicon (Si) wafer masters (Bhagat & Gupta, 2015). In summary, they demonstrated that microtexturing alone through hot embossing can lead to superhydrophobic behavior of polycarbonate, without the need of surface chemical modification. Moreover, it was shown that the hydrophobic properties of the PC surfaces could be tailored over a wide range through a proper control of temperature of the master during the replication. By increasing the temperature from 155 to 175 °C, the average height of the micropillars on the PC surfaces increases from 1,34 to 6,68 μm. As a consequence, this

change in the micropillar height enhanced the WCA from 82 ° to 155 °, demonstrating the existence of strong correlation was between the average height of micro-pillars on the PC surface and the resulting WCA (Figure 24b). The PC surfaces obtained at 175 °C exhibited a contact angle as high as 155°, a sliding angle of 9° and a contact angle hysteresis of 7°. The results reported on this study prove that a single scale roughness on a microscale level, can boost the WCA of an intrinsically hydrophobic PC surface to the superhydrophobic regime and the self-cleaning property.

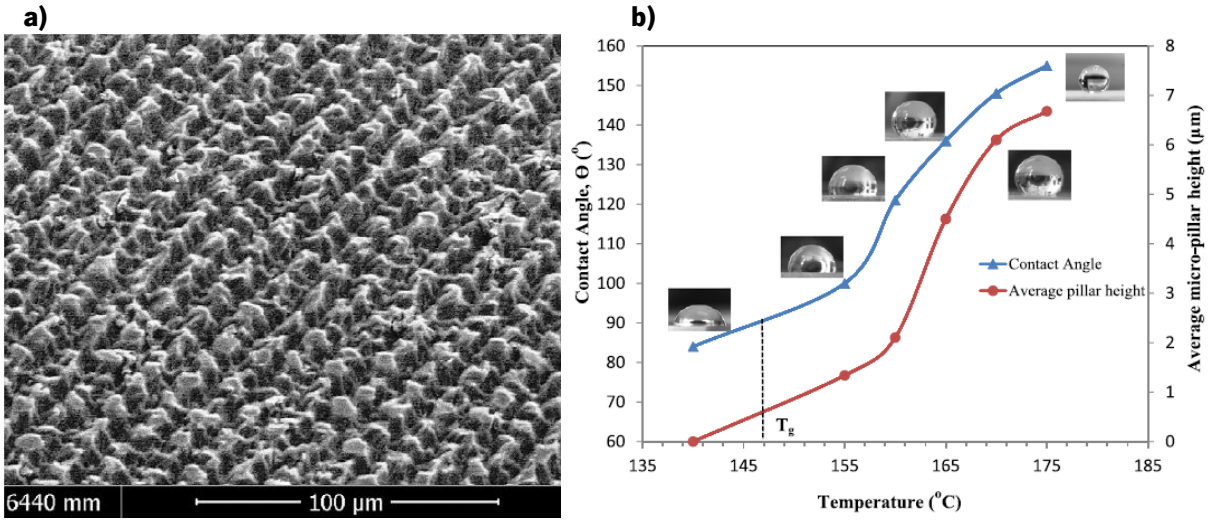

Figure 24 - PC surfaces obtained through hot embossing. (a) SEM images of replicated polycarbonate using microtextured Si master. (b) Contact angle variation as a function of average microtexture height for polycarbonate surfaces replicated at various temperatures. Contact angle values were reproducible within ±1°. (Adapted from Bhagat & Gupta, 2015)

K. Li *et al.* successfully fabricated hierarchical micro/nanostructures comprising nanopillars superimposed on micropillars on a thermoplastic cyclic olefin polymer (COP) substrates through hot embossing (K. Li et al., 2020). First, an array of nanopillars in the shape of circles or ellipse were fabricated on a Si wafer (Figure 26), using photolithography and deep reactive ion etching (DRIE) process for pillar diameters between 300 m and 500 nm. Secondly, an array of circular shaped micropillars with either square or hexagonal arrangements and nominal pillars sizes of 15 µm or 20 µm diameter were etched to a depth of 20 µm or 30 µm using photolithography and DRIE processes. Subsequently, the master mold was transferred to a flexible FEP working mold, followed by the replication of the hierarchical micro/nanopillars into the COP substrate by hot embossing. They fabricated thermoplastic hierarchical micronanopillar surfaces were superhydrophobic with WCA above 150 °. However, they reported that the hydrophobicity was enhanced with the decrease of the size of the nanopillars superimposed on the micropillars and with the use of circular pillars instead of elliptic. Likewise, by further decreasing the size of the nanopillars down to 150 nm, as well as a post-fabrication fluorocarbon coating, they were also able to achieve WCA large as 167 ° and sliding angles of 2.5 °. This study demonstrated that its possible to produce a hierarchical structure on a polymer surface through hot embossing (Figure 25), and those self-cleaning properties can be achieved.

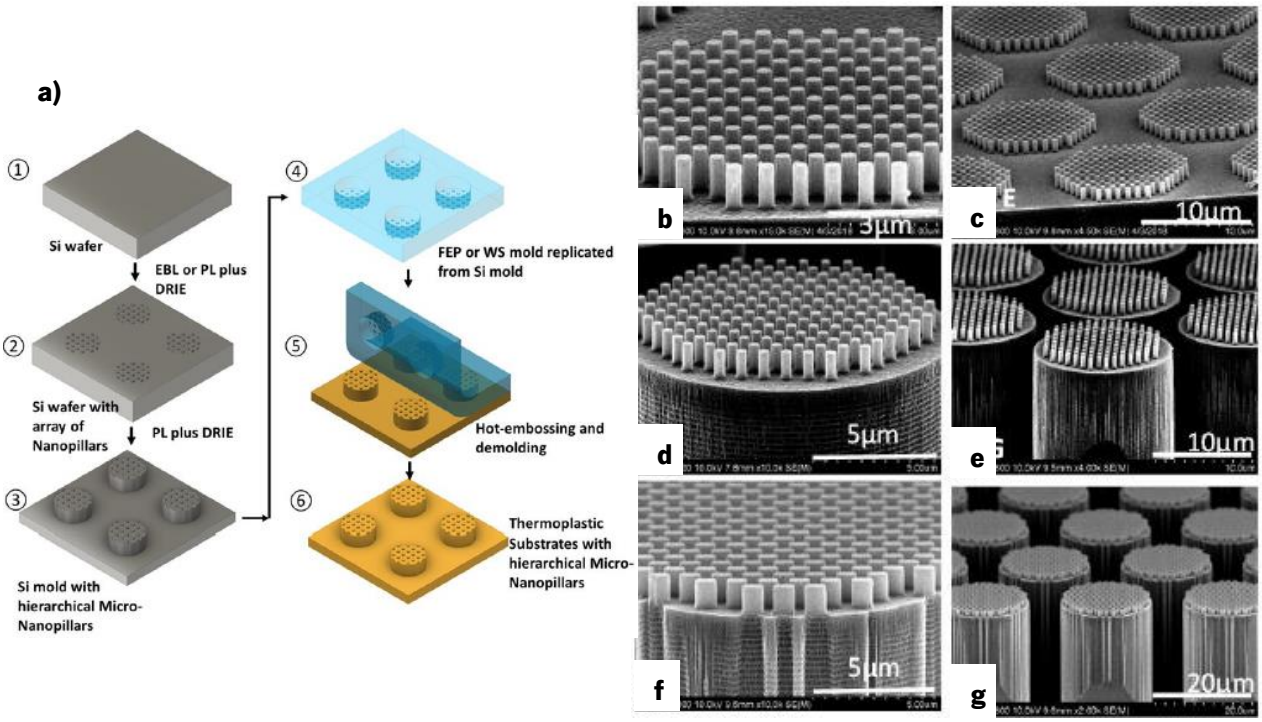

Figure 26 - Fabricatica of hierarchica roughness on the mold. a) Process flow chart of the fabrication of hierarchical micronanopillars on thermoplastic substrate. b-c) SEM images of an array of nanopillars on Si substrate. d-g) SEM images of hierarchical micro-nanopillars on Si substrate. (Adapted from K. Li et al., 2020)

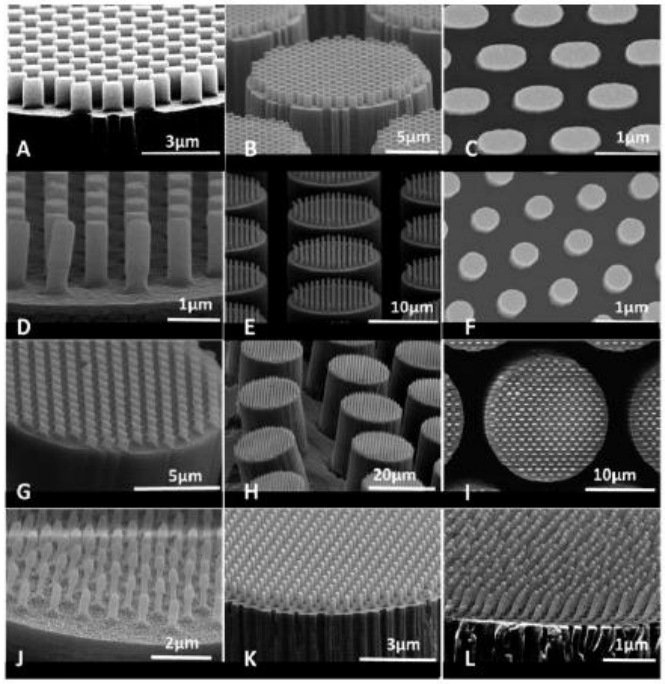

Figure 25 - SEM images of hierarchical micro- nanopillars replicated through hot embossing. a-c) SEM images of a sample with elliptic nanopillars (450 nm by 880 nm) superimposed onto a micropillar (19 µm diameter).d-f) SEM images of a sample with round nanopillars (450 nm diameter) superimposed onto a micropillar (15 µm diameter). g-i) SEM images of a sample with elliptic nanopillars (250 nm by 680 nm) superimposed onto a micropillar (19 µm diameter). j) SEM image of a sample with round nanopillars (250 nm diameter) superimposed onto a micropillar (19 µm diameter). (Adapted from K. Li et al., 2020)

Röhrig *et al.* developed a combination of the classical hot embossing process, hierarchical hot embossing and hot pulling to fabricate a gecko-inspired three-fold hierarchy of micro-nanostructures on a PC surface (Röhrig et al., 2013). The presented process involves a hot embossing step to create micropillars, a second step to create quadrangular pillars and a hot pulling step to create nanohairs having an aspect ratio as high as 10. This study does not show if superhydrophobicity can be achieved with this combination, however due to the characteristics of the produced surface it is a promising method for this application.

The develop technique is a combination of a two-level hot embossing: the first creates microstructures, and the second creates an additional level of submicro or nanostructures. This method is only applicable for thermoplastic polymers as two heating-cooling cycles are needed. Besides being completely automatic process, the introduction of an electromechanical sensor principle allows the precise fabrication of hierarchies, as it allows the detection the first hierarchical level structures when the second level is about to be imprinted. Lastly, the application of the hot pulling step promotes the elongation of the polymer structures. In contrast to hot embossing, where the material is solidified before demolding by cooling the tool, in the hot pulling step, the temperature of the mold insert is maintained above the material softening temperature. Therefore, softened polymer chains are elongated due to adhesion and normal forces during demolding. Benefiting from this phenomenon, the stretching effect, high aspect ratio nanostructures are produced on the polymer surface and superhydrophobicity may be achieved in a very cost-effective way.

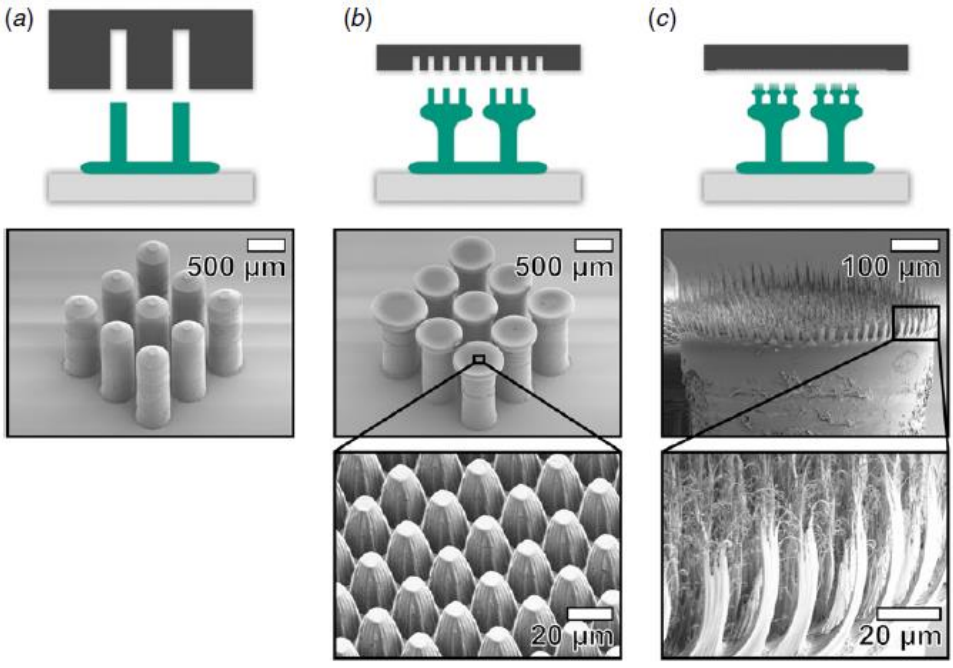

Figure 27 - Combining classical hot embossing, hierarchical hot embossing, and hot pulling a threefold hierarchy of micro- and nano-structures was fabricated successfully on a PC surface. (a) In a classical hot embossing process the lowermost pillars were replicated first. (b) With a second mold, quadrangular pillars were molded on top in a hierarchical hot embossing step. (c) Applying hot pulling, filigree high aspect-ratio hair were pulled out with a nanostructured mold insert. (Adapted from Röhrig et al., 2013)

CHAPTER 3 – MATERIALS, PROCEDURES AND METHODOLOGIES

This chapter comprises the materials, procedures and methodologies used in the experimental work defined for this dissertation. First, it is presented a brief description of the experimental procedure, followed by an overview of the production techniques, materials, and productive tools.

3.1. Experimental Planning

The experimental procedure defined for the present dissertation consist in the study of two different materials in order to determinate the optimal conditions for its use in hot embossing for the production of a prototype of a POW with self-cleaning characteristics. For its application on a LiDAR sensor to be efficient, it is necessary that the produced samples exhibit superhydrophobic properties and an optical transmittance in the required range (905 nm and 1550 nm) above 85%.

The experimental work is divided in three studies:

1. Determination of the optimal conditions for the embossing of PC through an improvised hot embossing technique and the influence of the microstructure's configuration and geometry on its hydrophobicity and optical transmittance. And also, the establishment of the number of cycles that the mold can handle without the need for cleaning, and, consequently, downtime for the process;
2. Application of a hydrophobic coating, by spin coating, on PC samples produced with the optimal conditions determined in study 1, and the study of its influence on the hydrophobic behavior and optical transmittance;
3. Study of the operative conditions for PMMA in the hot embossing process, taking into account the results obtained with the conditions of the study 1, and the influence of the replicated pattern on the optical and hydrophobic properties of the produced samples.

3.2. Hot Embossing

The replication of surface features at the micro and nano scale is highly dependent on the technology used to transfer the geometries from one substrate to another. As mentioned previously, hot embossing is regarded as a cost-efficient and scalable technique for the fabrication of high precision and high-quality polymer structures. As this technique presents a better processability ability for the fabrication of polymer micro/nanostructures in comparison with other above-mentioned methods (section 2.7.1), it was the

selected process to produce the prototype of the protective optical window for the LiDAR sensor.

Since a hot embossing machine was not available, the process had to be simulated with an improvised station by using an existing hydraulic press in the laboratories of DEP at the University of Minho (Figure 28). A jig was also produced in order to easily place the insert between the center of the hydraulic press plates in order to ease the procedure and to obtain a more uniform process in terms of pressure and temperature distribution over the sample area (Figure 30a-b).

The hydraulic press is composed by an upper and lower plate. The lower plate was the one where the jig with the microstructured insert and sample was placed, so it could be heated up above the glass transition temperature of the used polymers materials in order to transfer the replication pattern. The upper plate was the one responsible for applying the defined pressure, and it was heated below the glass transition temperature of the polymers, so it would not affect the side of the sample where there should be no replication. At the same time, the use of a hot upper plate is important to achieve a uniform replication, as it not only helps to keep the substrate under a positive pressure but also kept it warmer, otherwise, a significative difference between the temperature of the plates would result in unwanted deformation of the material. Also, in order to maintain the face of the sample without replication completely flat, with no change in its surface topography to obtain better optical properties, it was also produced a polished metal plate that is screwed to the upper plate, preventing the direct contact between the sample and the plate of the press and the consequent transfer of roughness (Figure 30c-d).

The process has a similar approach as the one used in hot embossing, except it was not possible to apply a vacuum phase and the demolding of the part had to be manual since the press was not equipped with an extraction system, which may cause the defects already listed in Chapter 2, such as incomplete molding or distorted and broken features.

Figure 28 - Improvised hot embossing station.

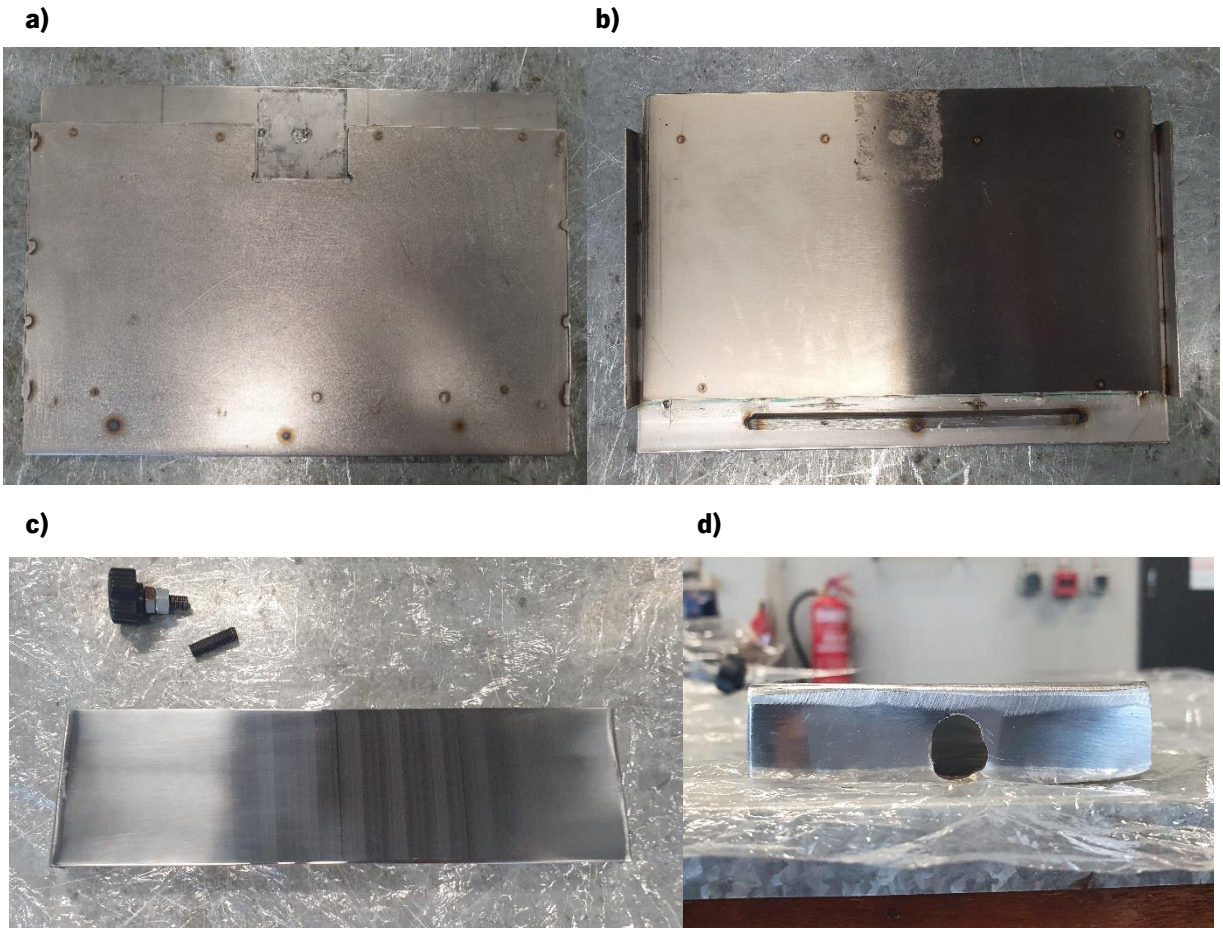

Figure 30 - Acessories produced to optimizate the process. a) Frontview of the jig. b) Backview of the jig. c) Polished metal plate and respective screws. d) Side holes of the metal plate that allow the fixation to the upper plate.

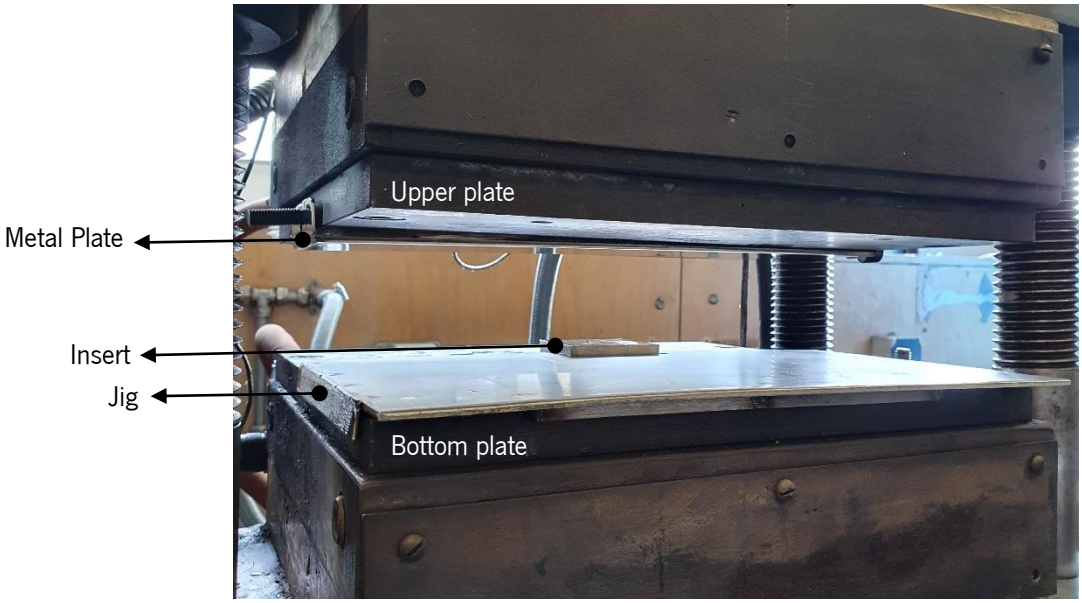

Figure 29 - Configuration of the acessories and the insert on the press.

3.3. Processing Materials and Production of the Substrate

The materials used to produce the protective optical window for the sensor were chosen especially concerning their capacity of transmitting light within the LiDAR wavelength range, the infrared. However, there are other specifications that the materials must fulfill, such as adequate mechanical and thermal properties given its application, and a good processability to facilitate the microstructures filling.

Polycarbonate and Poly(methyl methacrylate) are one of the most convenient and frequently used polymers in optic devices, such as contact lenses, due to their excellent transparency, showing optical properties similar to glass (Her et al., 2013). In addition, they are also emerging as the materials of choice for the hot embossing process due to their low cost and good processability (Kiew et al., 2009). However, despite these advantages, both PC and PMMA surfaces exhibit water contact angles well below the superhydrophobic regime (Table 1), which severely limits its widescale exploitation in applications where water repellency is of paramount importance. Meanwhile, several attempts through hot embossing have been successful in transforming hydrophilic materials into hydrophobic ones (Bhagat & Gupta, 2015).

Likewise, according with the requirements of the part, the polymer characteristics, cost and availability, it was chosen one grade from PC and one grade from PMMA to perform the experimental work.

i. PC Makrolon 2407 (black) by Covestro;
ii. PMMA Plexiglas 8N (black) by Evonik Industries.

Usually, the polymer substrates used in hot embossing processes are obtained through extrusion, with some advanced lines aligning the extrusion and embossing equipment in series. However, other molding methods can be used to obtain the polymer substrates. In this study, the polymer substrates with approximate dimensions of 50 x 50 x 2 mm for the hot embossing process were obtained through injection molding of the PC and PMMA grades.

Immediately before any of the substrate's plates were used in the hot embossing process, they were firstly cleaned with compressed air to remove any particles that may be in the surface, and, secondly, if stains and other impurities were still visible, they were also cleaned with isopropyl alcohol. The cleaning of the samples is not only important to assure the proper filling of the structures during the process but also to ensure that the optical properties of the part are not affected through damage caused by these particles.

3.4. Microstructured Insert

Replication of microstructures requires the preparation of tools to achieve the desired surface structure. The key element in replication-based manufacturing methods is the use of a high quality template for the production of multiple samples (Khosrow Maghsoudi et al., 2020).

The templates used in this study were projected for development of a protective optical window through injection molding in a previous dissertation inserted in the same project where a steel insert was used as a nickel deposition substrate to replicate the required micropattern (Martins, 2020).

Martins opted for using nickel as the material for the template because previously it was shown that silicon (Si) inserts, due to their fragile nature, broke during the injection phase due to the high pressures used in injection molding, and it also broke in the manual demolding step of the hot embossing process ((Martins, 2020; Pereira, 2018). Therefore, in the selection of a less brittle material that could support high pressures and with an easy fabrication, nickel was chosen in order to determinate the optimal conditions to obtain parts with a high replication degree.

The surface microstructure is composed by circular holes with the dimensions present in Table 2 (Figure 31). The dimensions and shape of the microstructures were developed taking into account the existing reports in literature about the hydrophobic behavior and its production requirements. The structures present a circular shape in order to facilitate the part demolding from the mold, since surface details without corners are the best approach to ease the process and cause less damages in the features.

Table 2 - Dimensions and shape of the structures in the insert.

Shape	Diameter (µm)	Depth (µm)	Pitch (µm)
Circular	5	10	15

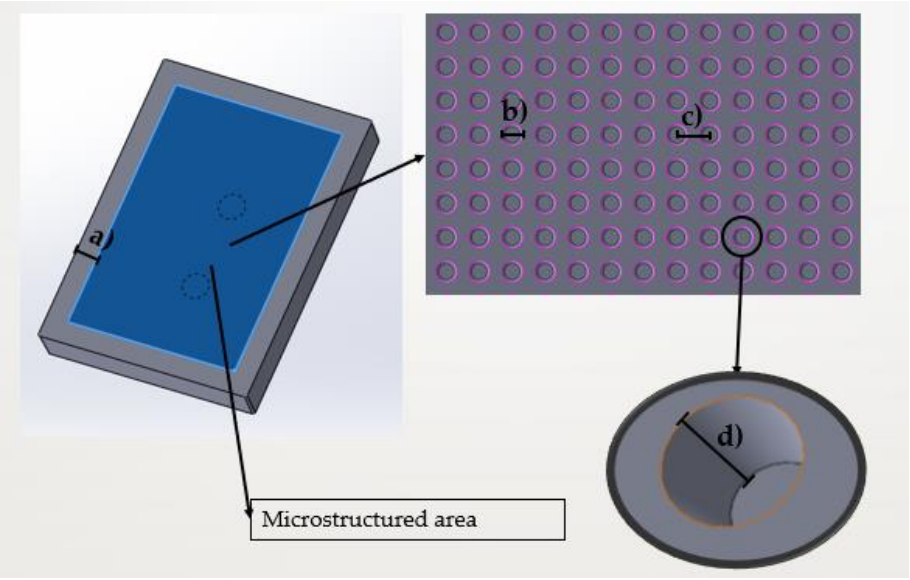

Figure 31 - Scheme of the microstructured insert plate with cylindrical holes. a) Area of the part without holes. b) Cylinders hole diameter. c) Distance between holes. d) Cylinders depth.

The method used in the production of the pattern was UV lithography, a technique based on transferring a pattern from a mask to a surface using a radiation source, such as UV light (C. H. Lee et al., 2010; Pinto et al., 2018). For this process, a photoresist, a photosensitive material, is exposed through a photomask to UV light, whereas the exposed areas suffer a change in their chemical properties to create a pattern (Figure 32). After the substrate is coated with a semiconductor layer, the photosensitive material is deposited over the substrate by spin-coating, forming a thin and uniform layer. The photomask, which is a transparent plate with patterned areas printed on it, is placed between the source of radiation and the photoresister. After the shape and size of the features are defined, it is performed an etching process in order to define the height or depth of the feature by removing the surface layers not covered by the photomask. Then, a developer solution is used to dissolve the photosensitive material in the exposed areas, in case of a positive photoresist material, leaving the substrate with the pattern of the photomask. In case of a negative photoresist, the unexposed areas are removed with the developer solution, leaving the substrate with the opposite pattern of the photomask.

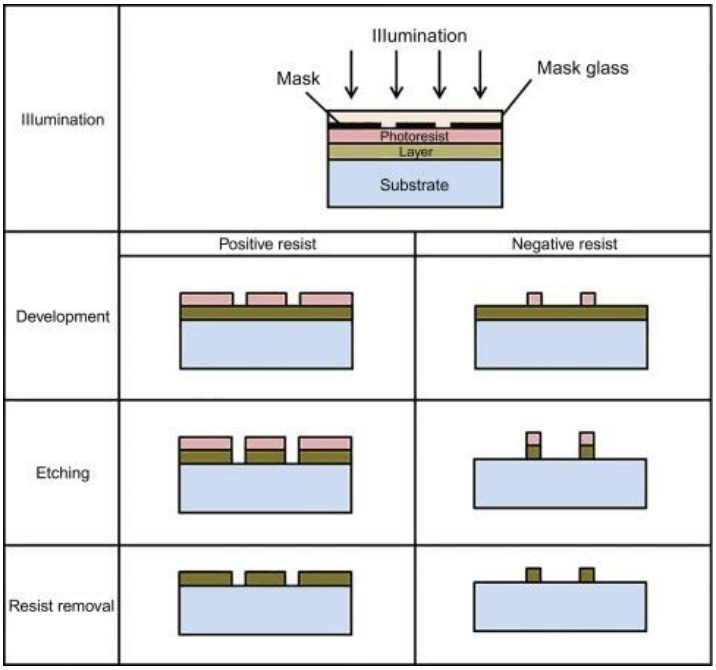

Figure 32 - Scheme of a UV lithography process (Pinto et al., 2018).

To obtain the defined microstructure of the used mold, the tone of the photomask had to be reverted to use a negative photoresist in order to achieve almost vertical walls (Figure 33b), which was not possible with the positive approach (Martins, 2020). After optimizing the UV lithography process to achieve pillars with enough height, the nickel deposition was made to reproduce the requested height (Figure 33c). Subsequently to the deposition and lithography, ultrasonic frequency vibrations were applied in order to clean organic residual on the formed holes, obtaining the microfabricated insert (Figure 33d).

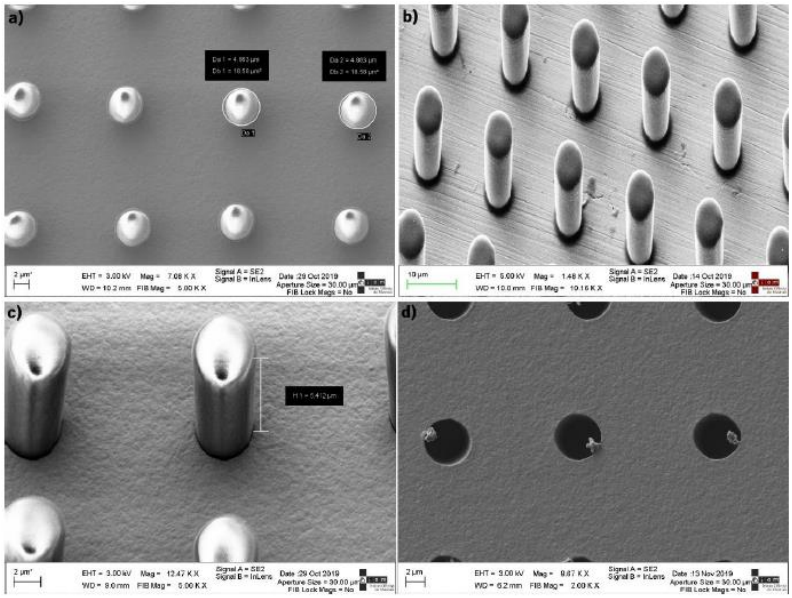

Figure 33 - Nickel deposition. a) Upper view of the pattern. b) Photomask with negative resist, after finished. c) Nickel deposition process. d) After nickel deposition, before cleaning the organic residuals. (Adapted from Martins, 2020)

For this study, there were two equal nickel inserts available to be used. One of them, the mold 1, was already damaged from its use in previous studies (Figure 34a), and the mold 2 was in perfect conditions. Likewise, it was initially decided to use the mold 2 in the embossing of PC and PMMA to obtain high quality samples. However, during the first preliminary experiments with the PC samples, it was noticed that the mold was suffering degradation on its surface, and that this degradation was increasing with the number of cycles (Figure 34b). With the intention of minimizing the damage to the mold and preserving the future possibility of using it in the confirmation experiments of the study, in order to have more realistic results, it was decided to use the mold 1 for the definition of the optimal conditions. Therefore, it was defined that for the PC study, as it was a more intensive study with a large number of experiments, the mold 1 was going to be used for the definition of the optimal conditions, and then it would be produced a small number of samples through the confirmation experiment with the optimal condition for the PC with the mold 2 to obtain more reliable results. As for the study of the PMMA, as it is known that it would be performed much fewer experiments, all the samples of the study would be performed with mold 2 while maintained a close monitorization of its condition.

During the experiments, the molds should be evaluated using optical microscopy with the purpose of observing if the cavities are filled with material, as it would prejudice the replication quality. Always, if necessary, the insert would be cleaned using a toluene bath with ultrasounds.

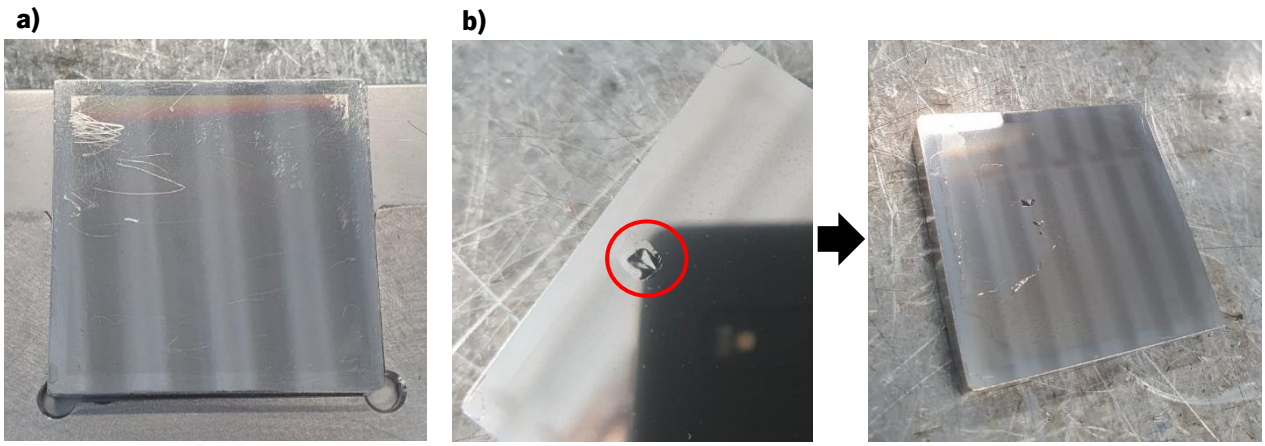

Figure 34 - Nickel inserts available to be used in this study. a) Mold 1 (50 x 50 mm) - Damaged mold from previous studies. b) Mold 2 (50 x 50 mm) – Mold that suffered degradation on its surface, starting with the formation of a bubble and then starting to peel off in some regions with the increase of the number of experiments performed.

3.5. Processing Conditions for Hot Embossing

At an early phase of the study, it was only defined the processing conditions for the primary study, the embossing of PC (T_g = 143 °C). The embossing temperature, pressure and time are considered the most important parameters for hot micro/nano-embossing technology (Sun, Zhuang, et al., 2019). Likewise, its important to concentrate the study on reaching the optimal values for these parameters. For the embossing of microstructures using polycarbonate, the processing conditions were defined taking into account the existing reports in literature (Becker & Heim, 2000; Bhagat & Gupta, 2015; Juang et al., 2002), the embossing station used, the technical datasheet of the material and previous testing experiments performed to validate the process that enable the definition of the stationary parameters.

Table 3 - Processing parameters applied in the embossing of PC samples.

Pre-heating time (min.)	Top Plate Temperature (˚C)	Replication Temperature (˚C) (bottom plate)	Replication Time (min.)	Replication Pressure (Ton.)	Demolding temperature (˚C)
5	100	165	10	2	120
		175	15	4	
				6	

For the study of the embossing of PMMA, the processing conditions would only be defined after the analysis of the results obtained in the PC study. The values of the replication time and the replication pressure, especially because the substrate samples of both materials have the same area, could be similar in both studies, only the temperature used has to be adapted to the processing material.

3.6. Design of Experiments

The design of experiments (DOE) is an essential statistical tool for a successful product development and improvement, and provides an efficient and scientific approach to obtaining meaningful information (Anderson & Whitcomb, 2000). DOE is defined as a branch of applied statistics that deals with the planning, analysis, and interpretation of controlled tests in order to evaluate the factors that control the value of a parameter or group of parameters. It allows various input factors to be manipulated, determining the cause/effect relationship on a desired output (response). DOE is a relevant tool, not only in an investigational environment but also in industrial applications.

3.6.1. Design of Experiments using the Taguchi Approach

The DOE by means of the Taguchi method was selected to help identify the effects of the parameters and the optimal set of parameters among the effective factors by cutting down a number of experiments in the study 1.

The Taguchi method is a statistical technique that allows to minimize product variability through robust, multi-parameter optimization that employs a smaller number of experiments in order to identify and optimize the parameters to achieve the desired response. Thus, it represents a simple and systematic solution to determine the effect of variables on the responses and the optimal condition of the variables. This method aims to produce high quality products at a low price for the manufacturer.

The Taguchi method uses a complete fractional design called orthogonal matrices and ANOVA as an analysis tool. Orthogonal matrices are the minimum set of experiments that represent the various combinations of factors and allow to organize the parameters that affect the process and the levels at which they should vary.

In this way the Taguchi method, allows obtaining the necessary data to determine with the necessary confidence, the factors that most affect the quality of the product with a considerable reduction in the experimental tests performed, thus saving time and resources, thus marking the difference between the conventional statistical technique, in which it is necessary to test all possible combinations.

The major steps to complete an effective designed experiment are (Pareek & Bhamniya, 2013):

i. Factors selection;
ii. Selection of orthogonal array and factor levels;
iii. Conduct experiments described by trials in orthogonal arrays;
iv. Analyze and interpret results of the experimental trials.

In this experiment, as mentioned previously, the factors taken into considerations are only the replication temperature, pressure and time, i.e., 3 factors. As observed in Table 4, this experiment presents 1 factor with 3 levels and 2 factors with 2 levels. By using the software Minitab, it was possible to create a mixed-level Taguchi experiment, producing an L_{12} orthogonal array. Therefore, for the study of the embossing of PC, it is needed to perform twelve different experiments (runs). For each run, it was produced four samples to be analyzed.

Table 4 - The experimental factors of the PC study and their levels.

Experimental Factors	Experimental Level		
	1	2	3
A: Replication Temperature (˚C)	165	176	-
B: Replication Time (min.)	10	15	-
C: Replication Pressure (Ton.)	2	4	6

Table 5 illustrates the experience plan to be performed during the first study. The level 1 corresponds to the lower level and level 2, in case of the temperature and time, and level 3 for the pressure, corresponds to the highest level.

Table 5 - Experiences plan of the PC study.

Exp.	A: Replication Temperature (˚C)	B: Replication Time (min.)	C: Replication Pressure (Ton.)
1	Level 1	Level 1	Level 1
2	Level 1	Level 1	Level 2
3	Level 1	Level 1	Level 3
4	Level 1	Level 2	Level 1
5	Level 1	Level 2	Level 2
6	Level 1	Level 2	Level 3
7	Level 2	Level 1	Level 1
8	Level 2	Level 1	Level 2
9	Level 2	Level 1	Level 3
10	Level 2	Level 2	Level 1
11	Level 2	Level 2	Level 2
12	Level 2	Level 2	Level 3

3.6.2. ANOVA Analysis

Analysis of variance, or ANOVA, is a statistical decision-making tool used to detect differences in mean performance and test the significance of the factors and their interactions (Asghar et al., 2014). ANOVA uses F tests (Snedecor distribution) to test for equality between means and accept or reject the null hypothesis. If the null hypothesis is rejected, the alternative hypothesis is necessarily true.

The generic null and alternative hypotheses are:

$H0$: The result of mean values using different levels of variation is equal;

$H1$: The result of mean values using different levels of variation is different.

If the null hypothesis is rejected when performing the F test, it means that there are significant differences between the sample means, that is, the factors are affecting the responses (Montgomery & Runger, 1994). If the null hypothesis could not be rejected, then, the factors being studied had no influence on the response.

The analysis of variance was performed after the production of the samples resulting from the experience plan and its characterization in order to test the factors significance and influence in the process.

3.7. Coating Application

As stated in Chapter 2, the most widely applied strategy used to achieve superhydrophobic surfaces involves the roughening of the surface, followed by a separate surface treatment, such as deposition of a coating, with the aim of lowering the surface energy. In order to test this approach, it was elected the Cytonix® coating, a hydrophobic resin of direct application, to deposit over some selected microstructured samples through spin coating.

Spin coating is a procedure used to apply uniform thin films to substrates (Tyona, 2013). A typical process involves the deposition of a small puddle of a fluid resin onto the center of a substrate and then spinning the substrate at high speed. Centrifugal force will cause the resin to spread eventually off the edge of the substrate originating a thin film of resin on the surface. The final film thickness and other properties will depend on the nature of the resin and the parameters chosen for the spin coating, such as the rotation speed and acceleration.

Figure 35 - Laurell WS-650MZ-23NPP spin coater.

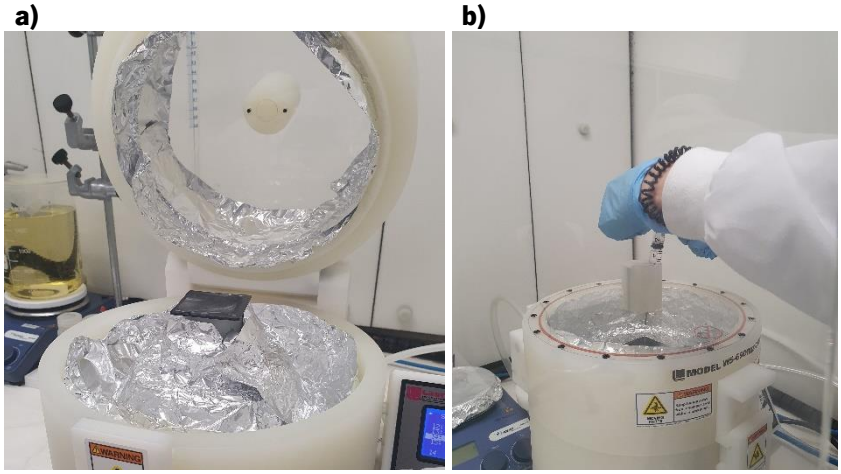

Figure 36 - Spin coating. a) Substrate fixed by vacuum. b) Deposition of 2,5 ml of the solution on the center of the substrate to then be spun at high speed.

The deposition tests were performed using the Laurell WS-650MZ-23NPP spin coater, available at PIEP (Figure 35). In this method, the substrate is fixed by means of a vacuum (Figure 36a). By spinning the substrate, the coating is spread evenly over its entire surface, due to the centrifugal force applied (Figure 36b). Therefore, 2,5 ml of the solution (Cytonix®) was dispersed on the substrate according with the parameters listed on Table 6 and Table 7. Subsequently, the samples were cured for 24 hours at room temperature.

Table 6 - Parameters used on the spin coater.

Velocity (rpm)	Acceleration (rpm/s)	Time (s)
180	30	30

Table 7 - Velocity steps applied during the spin coating process.

Steps (s)	Velocity (rpm)
2,5	90
5	90
25	180
26	144
27	108
28	72
29	36
30	18

Its was defined that the coating is only going to be applied on samples of PC produced with the optimal conditions determined in study 1. Due to time and project constraints, it was not possible to apply the coating on PMMA samples.

CHAPTER 4 – CHARACTERIZATION

This chapter contains the descriptions of all the tests performed for the characterization of the protective optical window prototype samples obtained during the course of the thesis, namely the evaluation the surface roughness, wettability and optical performance.

4.1. Surface Topography Analysis

In order to characterize the surface topography, the device used was the InfiniteFocus SL by Bruker Alicona, located at PIEP (Figure 37). This equipment is an optical 3D measurement system that allows the measurement of the surface topography.

Figure 37 - InfiniteFocus SL by Alicona.

The equipment possesses a measurement field of 50 x 50 mm. The surface to be measured is scanned and a dataset that can be displayed in true color or in pseudo color as a height map is obtained. The output values are determined by tracing a profile line that allows the software to calculate the amplitude parameters through the profile roughness over the specified line length.

The most important parameters are described below:

i. Ra, the average roughness of profile, is the integral of the absolute value of the roughness value (shaded area divided by the evaluation length, l) (Figure 38).

$$Ra = \frac{1}{l}\int_0^l |z(x)|\ dx \qquad (4.7)$$

ii. Rq is the Root-Mean-Square roughness of profile, corresponds to the standard deviation of height distribution.

$$Rq = \sqrt{\frac{1}{l}\int_0^l z^2 \, dx} \tag{4.8}$$

iii. Rt is the maximum peak to valley height of the roughness profile.

iv. Rmax is the maximum peak to valley height of the roughness profile within the sampling length.

v. Rz is the average peak to valley height of the roughness profile, corresponds to the difference between the average of the selected the five highest peaks and the five lowest valleys along the profile length, in agreement with the ISO system (Figure 39).

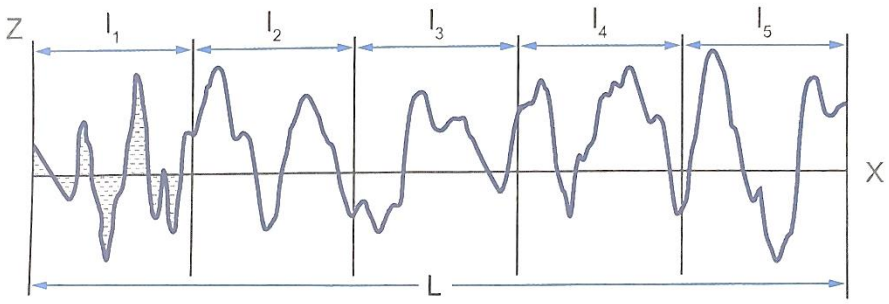

Figure 38 - Representation of the definition of Ra.

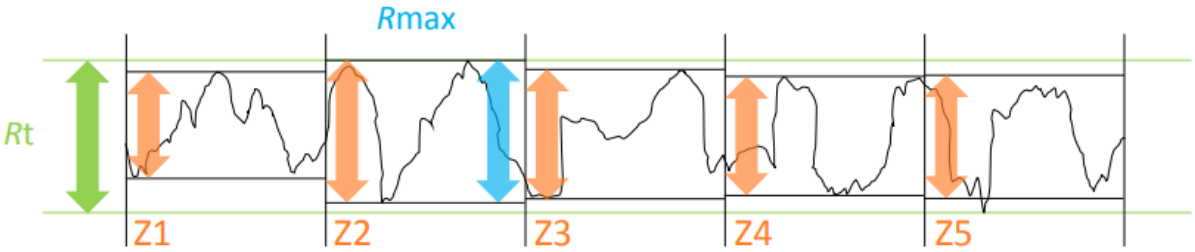

Rz = Mean value of Z1, Z2, Z3, Z4, Z5

Figure 39 -Representation of the definition of Rz.

For this study, only the Rt and Rz were used to characterize the roughness. In addition to the roughness parameters, the software also allows a profile form measurement, which permits the measurement of the height or depth of peaks or valleys (Figure 40). This functionality was used to characterize all the samples obtained through the studies on the PC and PMMA surfaces in three different spots, as it was possible to export the data for profiles comparison and data treatment of the heights of the structures.

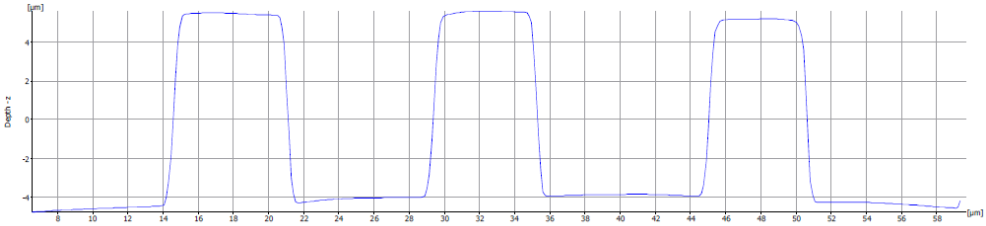

Figure 40 - Example of an output profile from the Alicona profile form measurement functionality.

4.2. Scanning Electron Microscopy (SEM)

Scanning Electron Microscope (SEM) produces three-dimensional images of a sample surface by scanning it with a high-energy beam of electrons in a raster pattern. The incident electron beam scans the surface of the sample, and the backscattered or the secondary electrons emitted are detected by a collector, showing the 3D image in display (Khare et al., 2019).

SEM also requires that the sample is electrically conductive to prevent charge buildup in the sample, that affects the incoming primary and emitted secondary electrons, resulting in poor and distorted images (Lampamn et al., 2003). Therefore, as most polymers are not electrically conductive, they must be coated with thin conductive layer. In this study, it was applied a thin a gold layer in the analyzed samples in order to increase the image resolution.

Figure 41 - FEI Nova 200 available at SEMAT.

The equipment used to perform the SEM analysis of the samples was a FEI Nova 200 available at SEMAT in the University of Minho (Figure 41). Since it is an expensive and destructive test, this characterization was only performed in some selected samples. The choice fell on the characterization of two samples, one microstructured PC sample and one microstructured PC sample covered with the Cytonix® coating layer.

4.3. Water Contact Angle Measurement

As mentioned previously in Chapter 2, the water contact angle is a quantitative measure of the surface wettability. Therefore, is a direct way of perceiving if the modification of the surface roughness had any influence in the surface hydrophobicity, one of the main characteristics for a surface being considered self-cleaning.

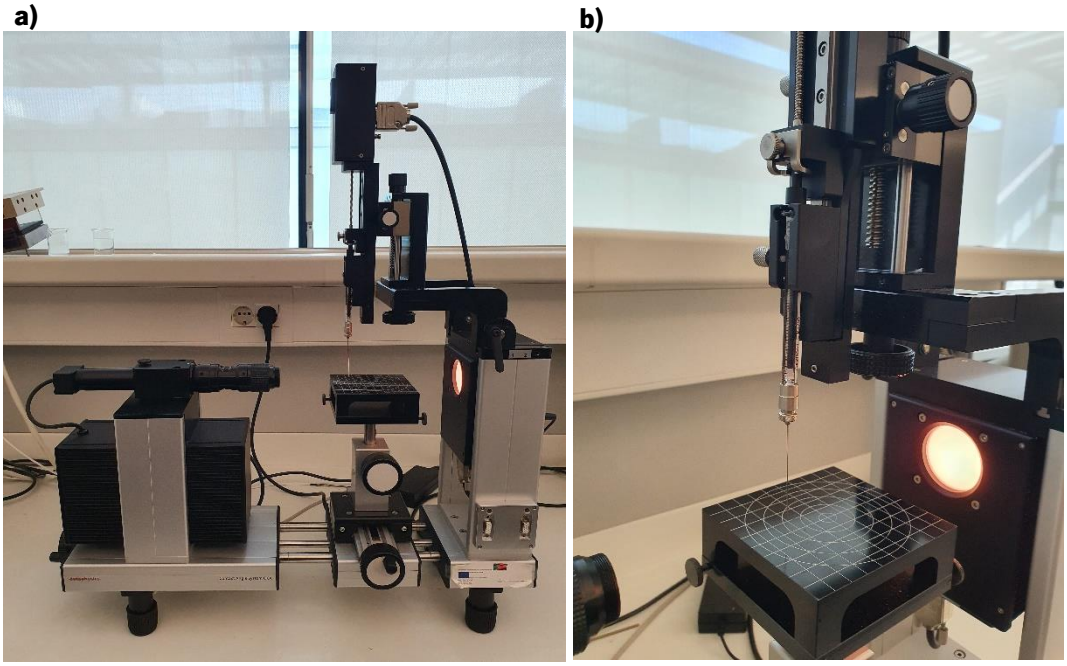

Figure 42 - OCA model 20 by Data Physics. a) Full equipment display. b) Water droplet dispensing needle above the mobile platform.

The water contact angle measurement was executed in an OCA model 20 by Data Physics, available at DEP laboratories (Figure 42). The device consists of a movable platform where the sample is placed, a syringe and a camera with associated software.

The water contact angle was measured in all the microstructured samples in 10 different points, including the ones where the coating layer was applied, and also in samples without microstructures in order to constitute the control sample.

The method of measuring was through the sessile drop technique. The syringe releases the water droplet, according to the defined parameters in the software (Table 8), on the sample that was previously placed on the platform. The system allows the regulation of the platform to move along the xyz axis enabling a precise placement of the droplet. The camera captures the moment the droplet gets in contact with the sample, and through the definition of the baseline, the software assumes an approximation of the droplet contour and calculates the value of the water contact angle (Figure 43).

Table 8 - Parameters used in the WCA measurement.

Drop Volume (µL)	5
Volume Rate (µL/s)	2

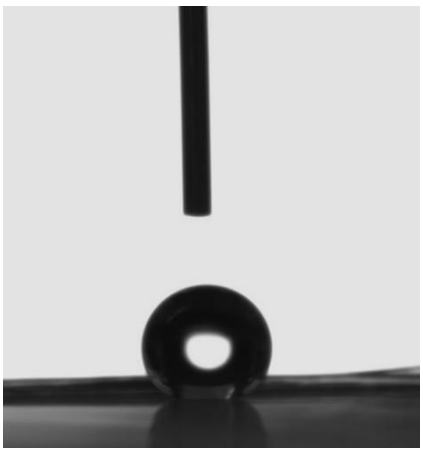

Figure 43 - Water droplet on a sample.

4.4. Optical Transmittance

The efficiency of light transmittance in the infrared range is the most relevant characteristic on a protective optical window of a LiDAR sensor in order to achieve a correct functioning. It is defined that for the sensor to work properly, it is needed that the protective optical window presents an optical transmittance of at least 85% in the wavelengths where the sensor in study operates, i.e., 905 nm and 1550 nm.

Optical transmittance is defined as the fraction of incident light of a specific wavelength that passes through a sample, that is the fraction of light that is neither absorbed nor reflected by the material. It takes form as a numerical value with a range between 0%, no light is transmitted, and 100%, total transmittance of the light.

Figure 44 - Shimadzu UV-2401PC spectrophotometer.

The device used for the measurement of the transmittance of the samples was a Shimadzu UV-2401PC spectrophotometer available at DEP laboratories (Figure 44). This equipment can measure the optical transmittance for wavelengths between 190 nm and 1100 nm. The results are presented on the associated software, giving the percentage of transmittance for each value according with the chosen range.

The measurement of the optical transmittance was applied to all the PC and PMMA samples produced throughout the study, and it was measured in 2 different points of the surface. For its measurement it was defined that the wavelength range for the analysis was between 650 nm to 1100 nm, since the transmittance at 905 nm was the most relevant for the case study and the optical transmittance of both materials below 700 nm is almost null. In addition, one microstructured sample of PC produced with the determined optimum condition from study 1 and one sample of PC with the coating application from study 2 were chosen to have their optical transmittance tested in the wavelength of 1550 nm, in the equipment available at Bosch since the equipment available at the DEP did not allow measuring at this wavelength.

CHAPTER 5 – RESULTS AND DISCUSSION

The results concerning the experimental work are presented in this chapter, which is divided in three different sections related to the three performed studies.

The first study (section 5.1) showed the optimal conditions for the embossing of a PC substrate and the replicated microstructured pattern influence on the surface hydrophobicity and light transmittance. The second study (section 5.2) showed the influence of a coating application on the wettability of a microstructured samples and its optical transmittance. Lastly (section 5.3), due to its excellent optical properties, the PMMA processability through hot embossing was studied in order to understand its viability for a protective optical window application.

5.1. Study 1 – Production of PC Samples through Hot Embossing

In this first study, the goal consists in testing different conditions through the simulation of the hot embossing process in order to reproduce a microstructured pattern on a PC substrate and verify the replication degree and its influence on the surface hydrophobicity and optical transmittance.

As mentioned previously in Chapter 3, there were two equal nickel inserts available, the mold 1, which was already damaged from previous experiments, presenting scratches on its surface, and the mold 2, which during the preliminary experiments started to degrade. As explained before, in order to spare the mold 2 for its use in the production of PC parts with the optimal condition determined in this study and in the PMMA study, it was decided to use the mold 1 for testing the different conditions on the PC substrate. However, its known that the scratches on its surface influence its roughness, and thus it will influence the replication and the part quality, hence the need for a confirmation experiment of the optimal condition with the mold 2 in order to have more accurate results.

Figure 45 - Representative non-microstructured PC sample used in the replication process for obtaining microstructured parts (50 x 50 x 2 mm).

The conditions or runs performed in order to evaluate the effect of the process parameters in the replication quality are available in Table 9.

Table 9 - Conditions performed on the PC samples.

Condition	Replication Temperature (˚C)	Replication Time (min.)	Replication Pressure (Ton.)
1	165	10	2
2	165	10	4
3	165	10	6
4	165	15	2
5	165	15	4
6	165	15	6
7	175	10	2
8	175	10	4
9	175	10	6
10	175	15	2
11	175	15	4
12	175	15	6

It is important to mention that all the characterization tests were performed in parts of the samples where there were no scratches or other damages visible, in order for a more reliable evaluation of the effect of the process parameters in the replication degree and quality.

5.1.1. Surface Topography

After the performance of all the defined conditions or runs, the first characterization test was the profile roughness measurement to determine the replication degree of each sample produced. During the surface topography analysis, it was taken into account the value of Rz (Mean peak to valley height of roughness profile), Rt (Maximum peak to valley height of roughness profile), the profile of the structures and the height map obtained.

Firstly, the profile roughness values (Figure 46) and height maps showed that all the conditions were able to cause changes on the surface of the samples, an indication that the polymer flowed into the microcavities of the mold, even with the combination of the lowest temperature, time and pressure.

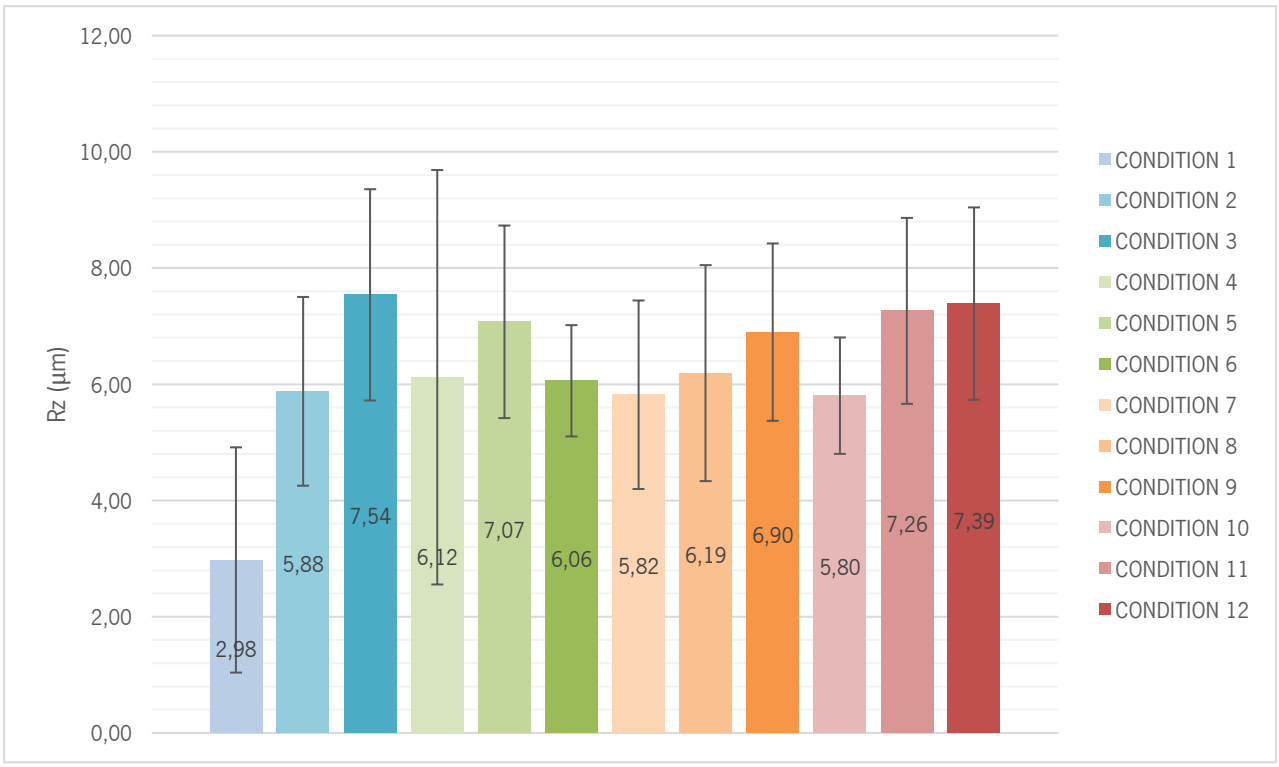

Figure 46 - Values of Rz obtained through the profile roughness measurement. Rz is the average of all the heights measured in the profile.

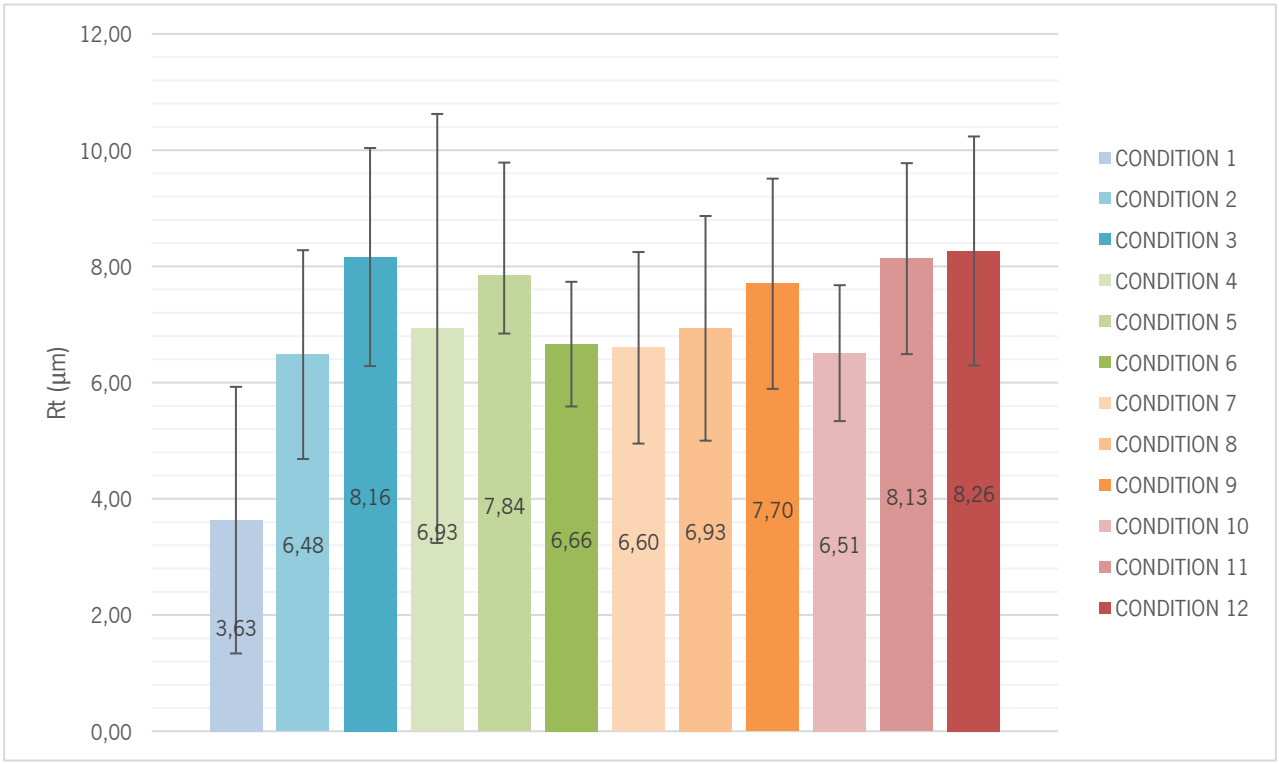

Figure 47 - Values of Rt obtained through the profile roughness measurement. Rt is the highest value measured between the peaks and the valleys.

As stated in Figure 46, it was possible to achieve up to 75 % of the desired replicated height (10 μm), even with no ideal conditions. The microstructures with the highest average heights were achieved with the conditions 3 (165 °C × 10 min. × 6 Ton.), condition 11 (175 ° × 15 min. × 4 Ton.) and condition 12 (175 ° × 15 min. × 6 Ton.). These conditions presented average heights superior to 7 μm (Figure 46) and the highest micropillars found in its surface had average heights superior to 8 μm (Figure 47).

However, a good reproducibility of the replication pattern throughout the surface was not achieved, with most samples showing significative standard deviations due to superficial defects and incomplete filling of the cavities. The samples demonstrated defects in some areas such as distorted features (Figure 48e-f), pull out structures (Figure 48a-b) and areas with an alter pattern due to scratches present on the mold that automatically replicated to the substrate (Figure 48c-d). These defects could be due to diverse reasons, especially related with the conditions that were available for the study, such as:

i. The press not being able to maintain a complete stable temperature value and pressure distribution during the process. Any change of these parameters will affect the polymer substrate fluid resistance, resulting in pattern defects such as incomplete filling of the cavities and deformation of the structures;
ii. The mold being damaged, as the defects present on its surface can alter the surface roughness and do not make it possible for a perfect replication of the mold pattern, directly influencing the replicated structure;
iii. The demolding of the parts being manual and the adhesion between the mold and the polymer. Some defects associated with demolding, such as distorted features, overstretched features and broken and pulled out microstructures influence the replicated pattern, having a direct influence above the replicated height of the structures. The adhesion between the polymer and the mold insert, which may deform and even destroy the structures, along with the manual demolding, affected the quality of the polymer replica;

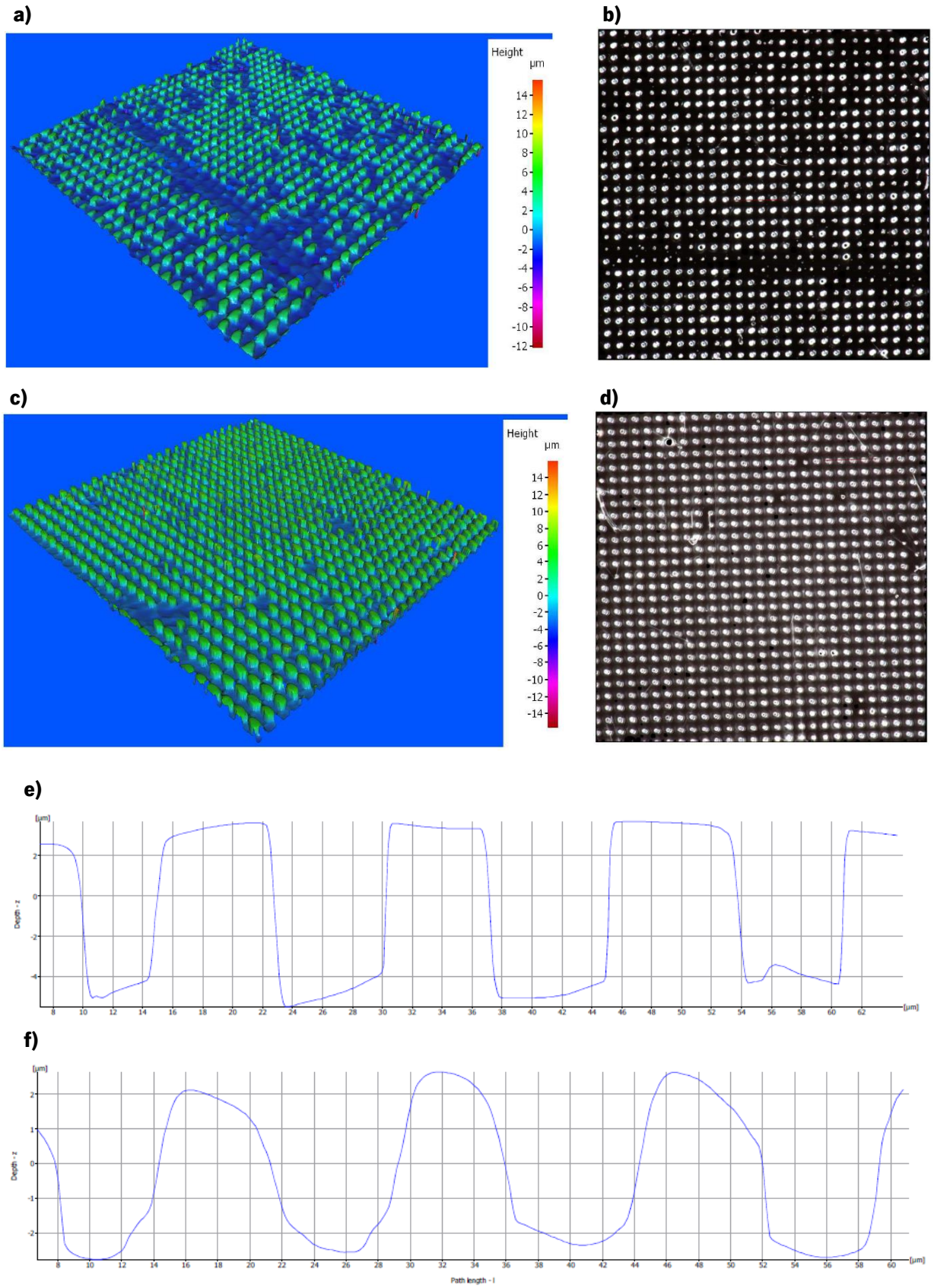

Figure 48 - Defects present on the samples. a) Pulled out structures visible through the height map of the samples. b) Pulled out structures visible through the microscopical image obtained through InfiniteFocus SL. c) Defects of the mold replicated on the surface on the samples, visible through the height map produced, clearly affecting the surface replication. d) Defects of the mold replicated on the surface of the samples, visible through the microscopical image obtained through InfiniteFocus SL. e) Profile of distorted microstructures obtained through the profile roughness measurement, evidencing a clear dislocation of the structures during the demouling phase. f) Profile of distorted microstructures obtained through the profile roughness measurement, evidencing a clear deformation of the structures.

Based on the experimental results, an analysis of variance (ANOVA) was performed in order to assess the contribution of each processing parameter to the resulting mean replicated height (Rz). Table 10, Table 11 and Figure 49 show the significance of each factor, the response of each parameter and the main effects plots, respectively.

Table 10 helps to understand the significance of each parameter and interaction for the relationship between the factors and the response. If the p-value is inferior or equal to 0,05, then, the factor is significant for the variation of the response in study. If an interaction effect is significant, the main effects have to be interpreted considering the interaction effects. In this case, the determinant factors are the replication temperature, the replication time, the replication pressure and the interaction between the replication time and pressure since they all present p-values below 0,05.

Table 10 - Analysis of variance for Rz.

Source	DF	Sum of Squares	Mean Square	F-value	P-value
Replication Temperature	1	2,8131	2,8131	6,77	0,023
Replication Time	1	3,8410	3,8410	9,24	0,010
Replication Pressure	2	13,8041	6,9021	16,61	0,000
Replication Temperature*Replication Time	1	0,4859	0,4859	1,17	0,301
Replication Temperature*Replication Pressure	2	1,0159	0,5079	1,22	0,329
Replication Time*Replication Pressure	2	5,0780	2,5390	6,11	0,015
Error	12	4,9877	0,4156		
Total	23	38,6086			

It is observed from Figure 49 that, generally, an increase of temperature, time or pressure increases the height of the structures, as already reported in literature by Lin et al (Lin et al., 2013) and Singh et al (Singh & Dupaix, 2012). This observation for the effect of the replication temperature was expected given that the viscosity of a polymer is directly dependent on its processing temperature. In particular, an increase of temperature eases the polymer flow during processing as it increases its deformation ability, facilitating the filling of the cavities. The effect of the replication time can be explained by the melt behavior of polymers, as melt is a time-depended phenomenon and extending the time where the embossing pressure is applied will benefit the flow of the material into the cavities. As it is obvious, an increase of pressure will lead to a bigger capacity of the polymer to fill the cavities, and, consequently, a better replication.

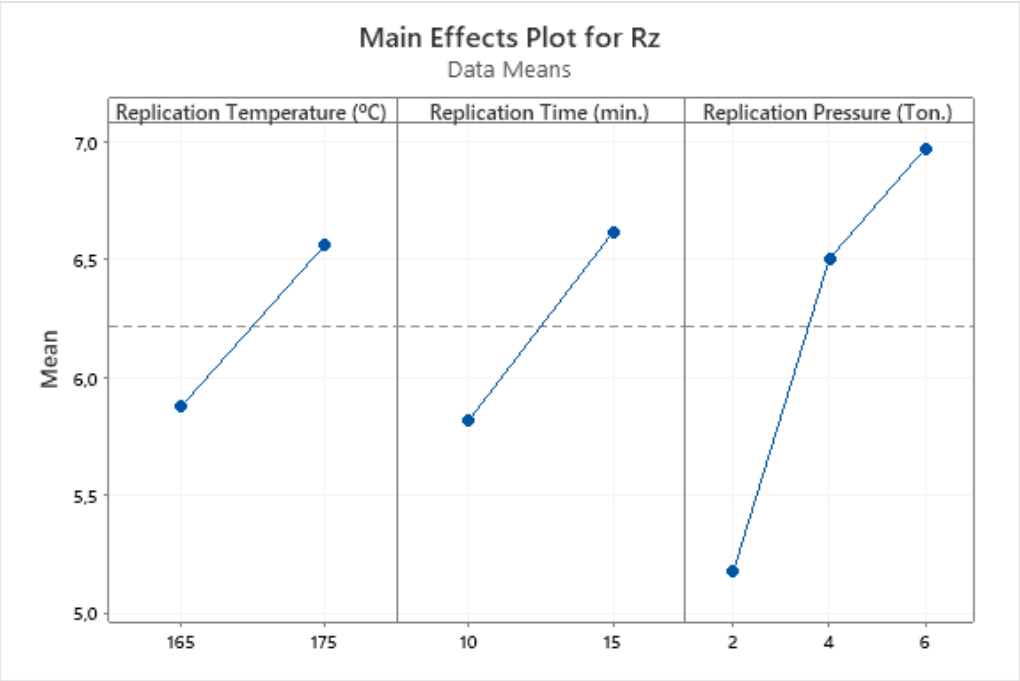

Figure 49 - Main effects plot for Rz.

The interaction effect (Figure 50) indicates that the relationship between the replication pressure and Rz depends on the value of the replication time. For example, if a pressure of 2 tonnes or 4 tonnes is applied, a replication time of 15 minutes is associated with the highest mean height. However, if a pressure of 6 tonnes is applied, a time of 10 minutes is associated with the highest mean height. This shows that although the main plot effects show that the increase of time was beneficial to the replicated height, that is not always the case, in this study this is also essentially dependent on the level of pressure applied.

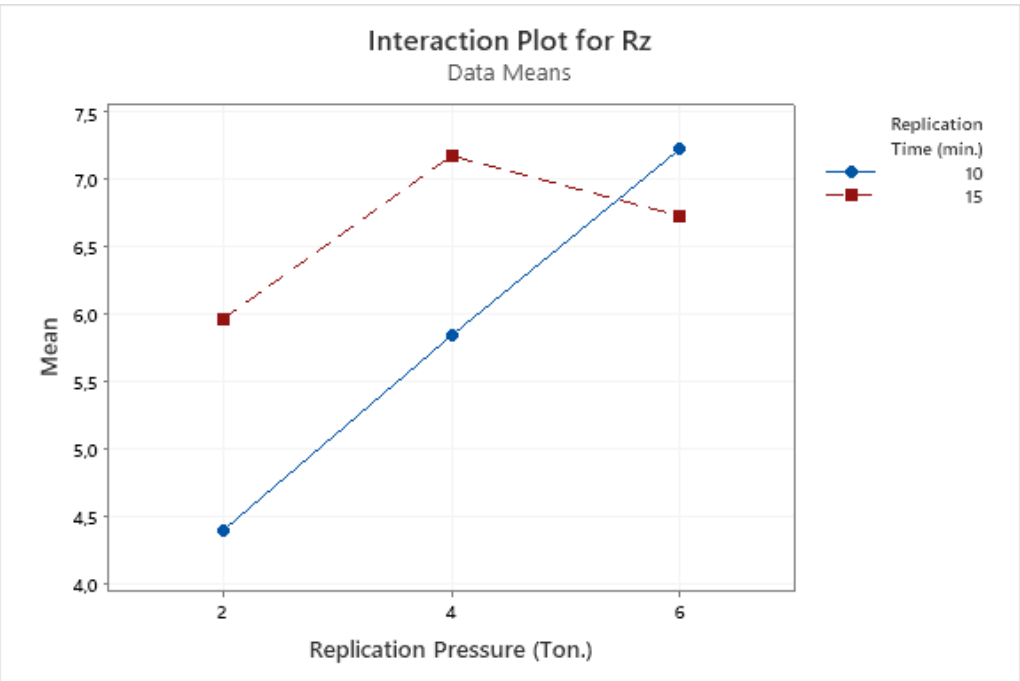

Figure 50 - Interaction plot between the replication pressure and replication time for Rz.

From the response table (Table 11), it is apparent that the most influential parameter in this study for the replication height was the replication pressure and the least important parameter was the replication temperature. However, the influence of the replication pressure was bigger in the transition between level 1 and level 2 (1,324) in comparison with level 2 and level 3 (0,467).

Table 11 - Response Table for Means of Rz.

Level	Replication Temperature	Replication Time	Replication Pressure
1	5,876	5,818	5,180
2	6,561	6,618	6,504
3	-	-	6,971
Delta	0,685	0,800	1,791
Rank	3	2	1

As mentioned previously, through the observations of the Figure 46, it is possible to determine that the conditions that were able to produce higher structures, closer to 10 µm, are condition 3, condition 11 and condition 12 (Figure 51). When analyzing Figure 49, the main effect plot suggests that the maximization of the values of all the parameters would offer higher structures. However, the interaction plot (Figure 50) suggested that a combination of a pressure of 6 tonnes and a time of 10 minutes followed closely by a combination of 4 tonnes and 15 minutes was more beneficial for obtaining higher replication heights than the combination of the maximization of both parameters in question.

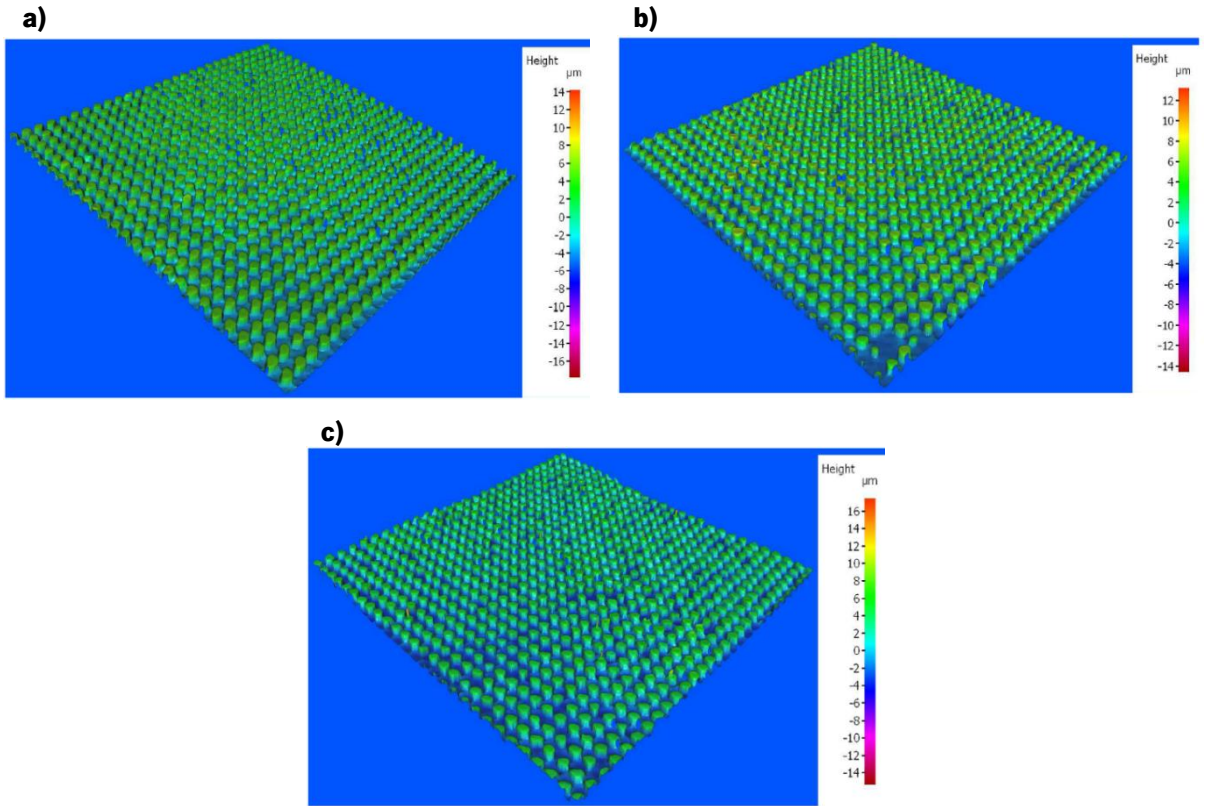

Figure 51 - Height maps of the better conditions for obtaining higher micropillars. a) Height map obtained from a sample produced with condition 3. b) Height map obtained from a sample produced with condition 11. c) Height map obtained from a sample produced with condition 12.

Nevertheless, when visually observing the produced samples, it was possible to observe that the samples produced with the conditions 8 (175 °C × 10 min. × 4 Ton.), 9 (175 °C × 10 min. × 6 Ton.), 11 (175 °C × 15 min. × 4 Ton.) and 12 (175 °C × 15 min. × 6 Ton.), showed that the surface was with a melting appearance and unwanted deformation with the latter also showing material degradation due to the combination of pressure, time and temperature (Figure 52). Likewise, this proved that the combination of 175 °C and 4 and 6 tonnes did not produce viable samples, invalidating the use of this temperature value and consequently the condition 11 and condition 12.

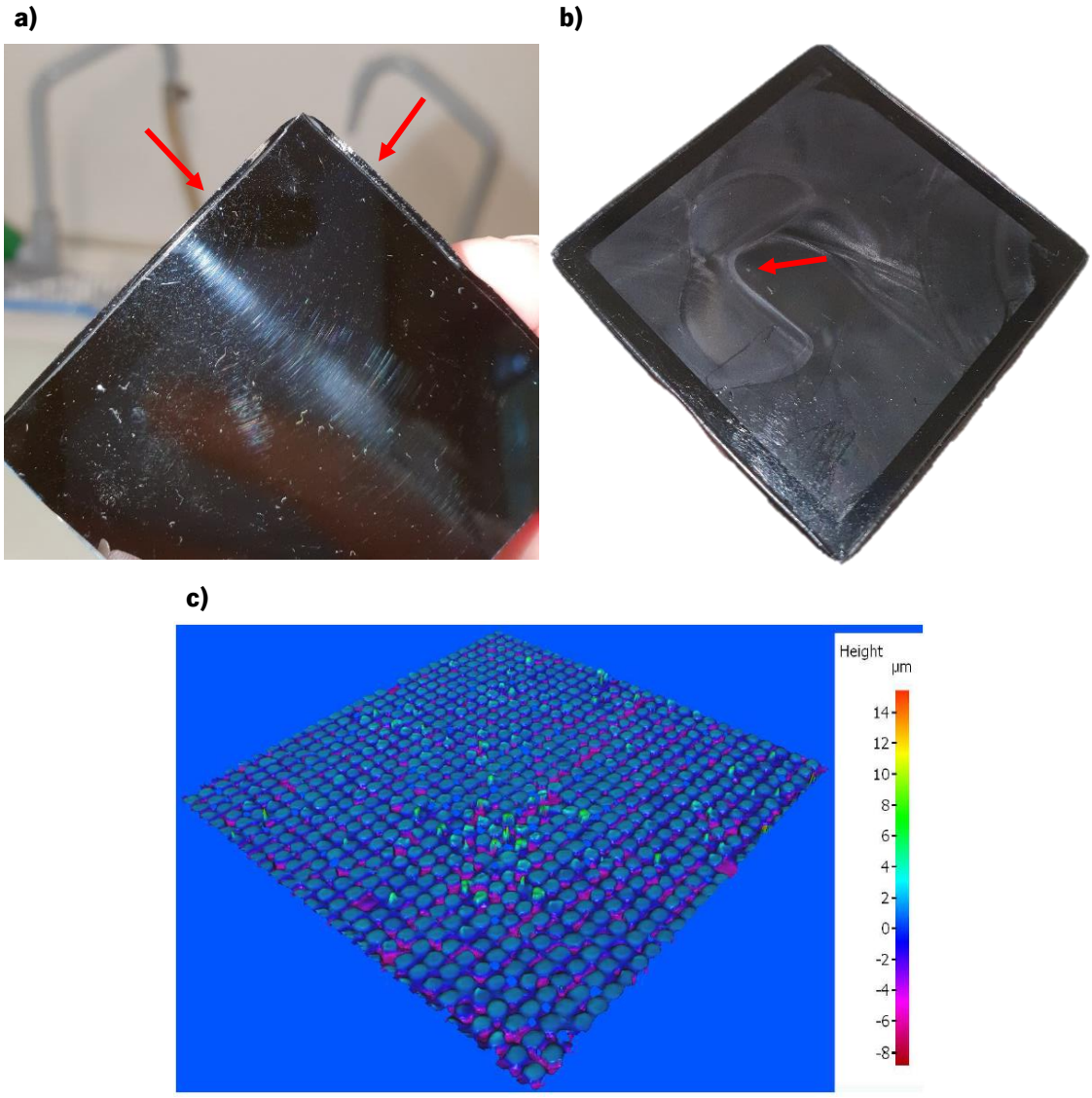

Figure 52 - Defects who invalidate the conditions 11 and 12. a) Melting and unwanted deformation on the surface of the samples produced with conditions 8, 9, 11 and 12. b) Material degradation on the surface of a sample produced with condition 12. c) Height map showing the replication on a degraded spot.

During the study, it was also demonstrated that with the lowest embossing temperature applied (165°C), the mold could handle 12 cycles without needing to be cleaned using the toluene bath with ultrasound, while when a higher temperature (175°C) was applied the mold could only produce a maximum of 8 samples until the cavities started to get filled with material. A higher temperature seemed to create a greater tendency for the material to be stuck in the cavities of the mold after demolding, increasing the need for its cleaning in order to produce quality parts. Likewise, in terms of production, a lower replication temperature is advantageous for the process and lifetime of the mold.

Therefore, taken into account all the aspects mentioned previously, the best condition for obtaining the better replication was condition 3 (165°C × 10 min. × 6 T), which enable around 75 % of the intended replication height with an acceptable surface quality and permits the minimization of the downtime of the production.

5.1.2. Water Contact Angle

In order to understand if the increase of roughness had influence on the hydrophobicity, it was necessary to measure the water contact angle, as the WCA is a consequence of the replicated pattern.

Firstly, a non-microstructured sample was measured in order to conclude the real influence of the microstructured pattern had on the surface wetting property. The measurement of a control sample of the PC Makrolon showed water contact angles in the hydrophilic regime, with an average of 75,95 ° ±4,69 (Figure 53). Although PC has status of an hydrophobic material due to his chemical nature that contains non-polar groups (Bhagat & Gupta, 2015), a great quantity of grades such as the one applied to this study are formulated to be optically smooth, which is sufficient for the material to fall into the hydrophilic regime.

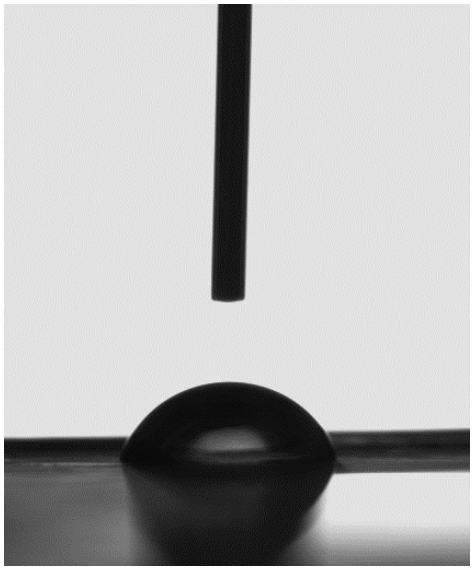

Figure 53 - Water droplet placed on a non-microstructured PC sample (WCA = 75,9 °).

Subsequently, the measurement of the microstructured samples manufactured with the various conditions produced the values of WCA present on Figure 54.

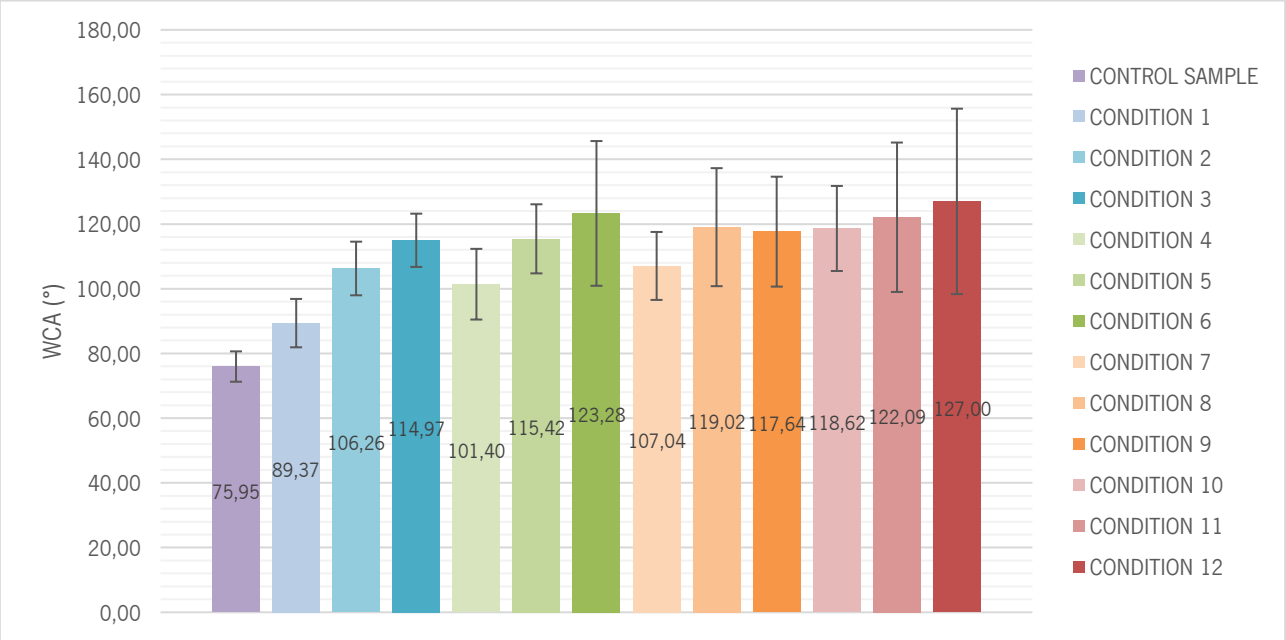

Figure 54 - Water contact angles measured in the samples with the various conditions.

The results of the microstructured samples measurement suggested a clear enhancement of the hydrophobic property, with practically all samples in the hydrophobic regime. A water droplet on the microstructured PC surface could exhibit contact angles on average as high as 127 °. This implies that the maximum contact angle that can be achieved for PC using its inherent chemistry is 75,95 ° and that the surface roughness plays a crucial role to improve its hydrophobic properties.

The condition 3, which provided the best parameters combination for obtaining higher micropillar height, which previously showed up to only 75 % of the desired replicated height, demonstrated an average increase of the WCA of more than 50 %. When a more intensive study of the WCA was performed, with more areas of the samples measured, the maximum WCA found in the samples produced with the condition 3 was 168,2 °, an angle clearly in the superhydrophobic state (Figure 55f). Angles above 150° were not constant through the surface, and this could be due to the lack of uniformity of the surface structures (Figure 55). However, the presence of these values is an optimistic sign that in an optimum environment, superhydrophobicity could be achieved with this microstructured pattern, although it obviously needs to be tested for confirmation.

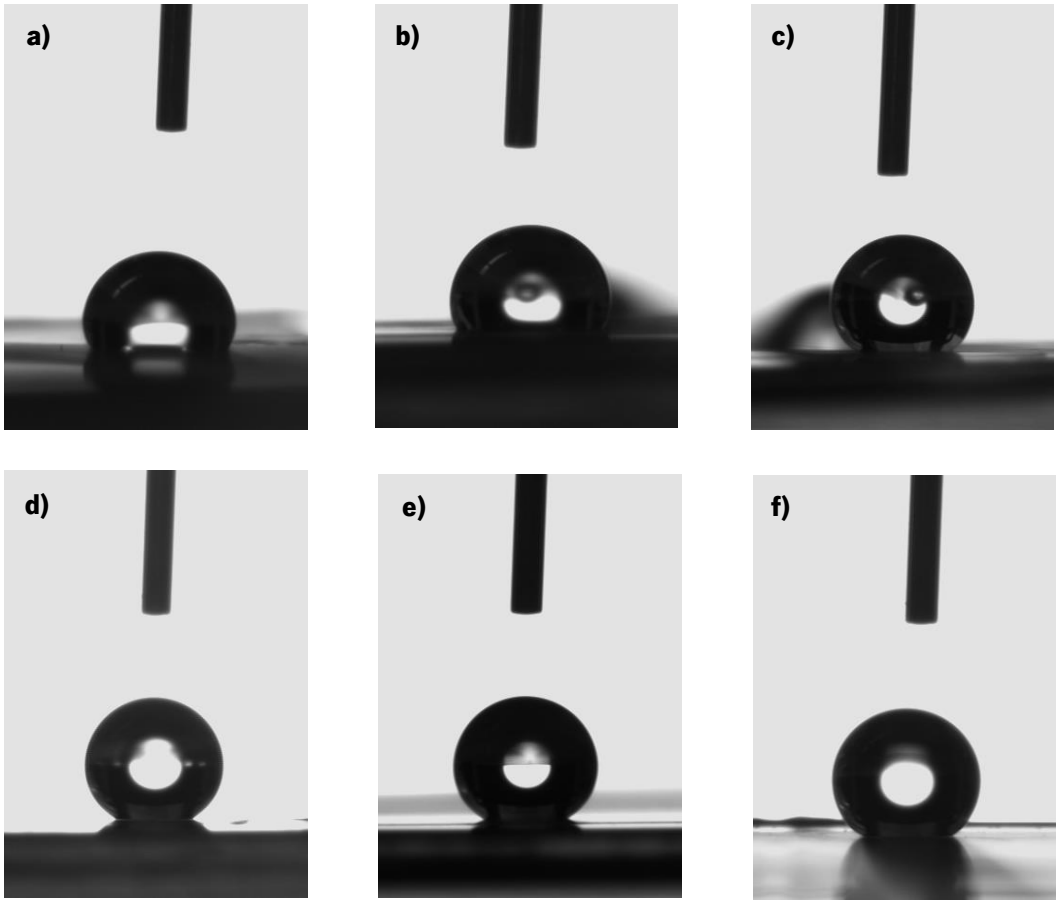

Figure 55 – Examples of the variety of angles found on the PC samples produced with the condition 3. a) WCA = 114,5°. b) WCA = 122,7°. c) WCA = 130,3°. d) WCA = 151°. e) WCA = 155,2°. f) WCA = 168,2°.

Condition 6, 8, 9, 10, 11 and 12 all showed on average higher water contact angles than the condition 3 (Figure 54), although all of them on average also presented inferior values for the micropillars heights (Figure 46). Despite having higher average WCA values than condition 3, these conditions also possess considerable standard deviations between the water contact angles measured on its surface, reveling the lack of uniformity for the angles related to the presence of lower and uneven microstructures. In particular, the condition 12, with the maximization of all the parameters, was the run which showed on average higher WCA, however, it also had the biggest standard deviation among all conditions, with the appearance of low angles in the hydrophilic range and very high angles in the superhydrophobic range (Figure 56). This could be due to the material degradation on its surface as observed previously (Figure 52b-c), since the WCA on degraded spots created smaller contact angles due to degradation of the structures.

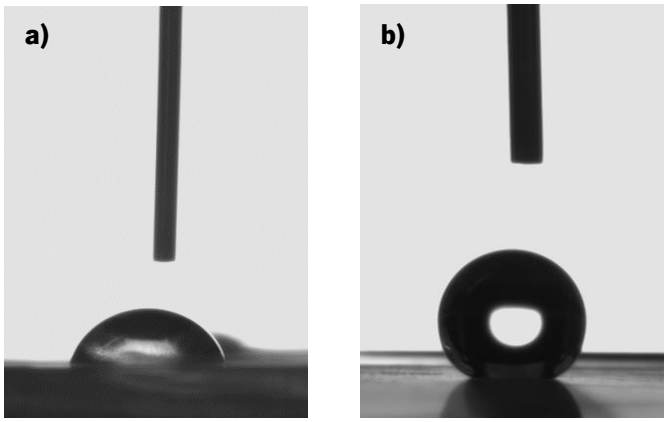

Figure 56 - Different angles obtained in the measurement of the samples produced with the condition 12. a) WCA = 86,3°. b) WCA = 169,6°.

It is also relevant to state that some of the droplets placed on the surface had the tendency to spread after a few seconds or minutes, not maintaining the original angle, especially when they were above 150°. When the angles were in the superhydrophobic regime, in 1 to 3 minutes the water droplet suffered a decrease on average of 25 % of its original value (Figure 57). However, some droplets showed a much slower rate of decrease as observed in Figure 58. These phenomenon's could be related with diverse causes such as the water penetration between roughness gaps, especially in superhydrophobic angles, which could represent a transition of state between Cassie and Wenzel related to the instability of the surface caused by the lack of hierarchical roughness, for example (Bormashenko, 2015; Teisala et al., 2011). Although more unlikely, water absorption into the polymer material could also have caused a decrease on the WCA, or even submicron impurities in the water when the rate is more accelerated, as stated by Park *et al.*, which reports that on a hydrophobic surface, the CA of an evaporating droplet decreases with time and becomes smaller, however when there is some impurity in the water the decrease of the CA is remarkably accelerated with time (L. Feng et al., 2014; C. I. Park et al., 2009; J. K. Park et al., 2012). However, further tests in order to evaluate the evolution of the wetting regime would have to be performed in order to detect the real cause.

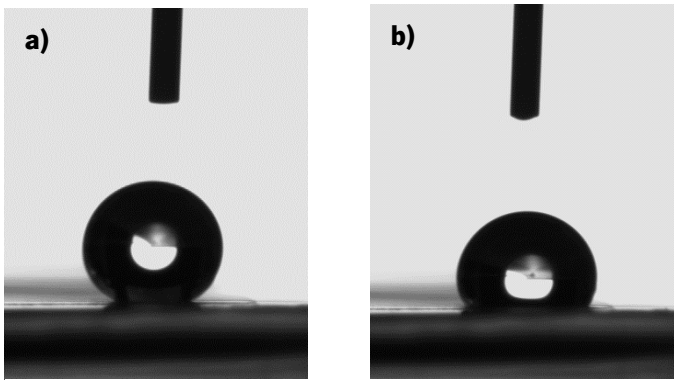

Figure 57 - Decrease of the WCA with time. a) t=0s, WCA = 164,4°. b) t=60s, WCA = 126,7° (decrease of 22,9% in comparison with the original value).

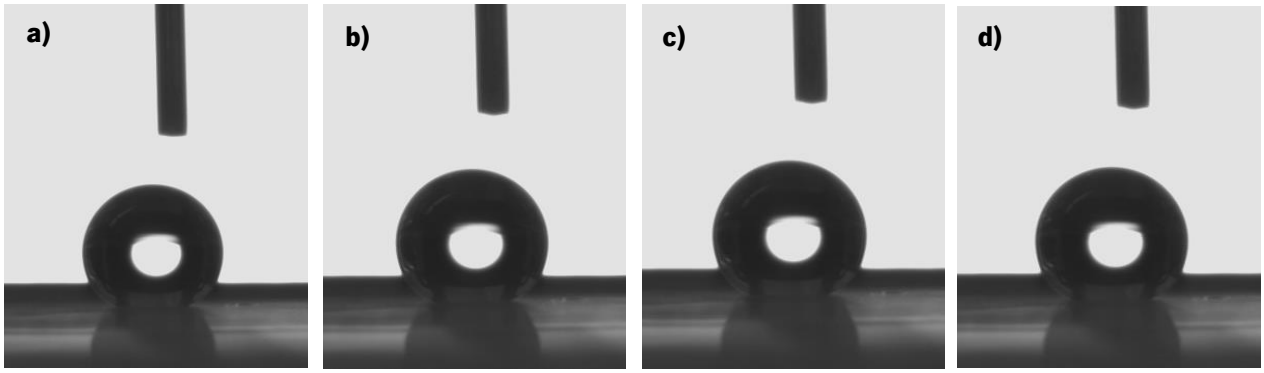

Figure 58 - Decrease of the WCA with time. a) t=0s, WCA = 162,5°. b) t=60s, WCA = 162,5°. c) t=120s, WCA =158,7° (decrease of 2,3% in comparision with the original value). d) t=180s, WCA = 143° (decrease of 12% in comparision with the original value).

5.1.3. Optical Transmittance

After the validation of the satisfactory replicated height of the micropillars and its influence on the surface hydrophobicity, the next characterization consisted in the measurement of the optical transmittance of the samples in order to understand the effect of the replicated structures on the optical transmittance performance in the main wavelength required by the manufacturer, the 905 nm.

A non-microstructured sample of PC Makrolon offers a transmittance of 82,25 % ± 2,37 at 905 nm. As seen in Figure 59, the transmitted light values suffer a significant decreasing across all samples, with the presence of average values well below the control sample value. This decrease was influenced greatly by the increase of the surface roughness because of the light scattering promoted by the microstructures.

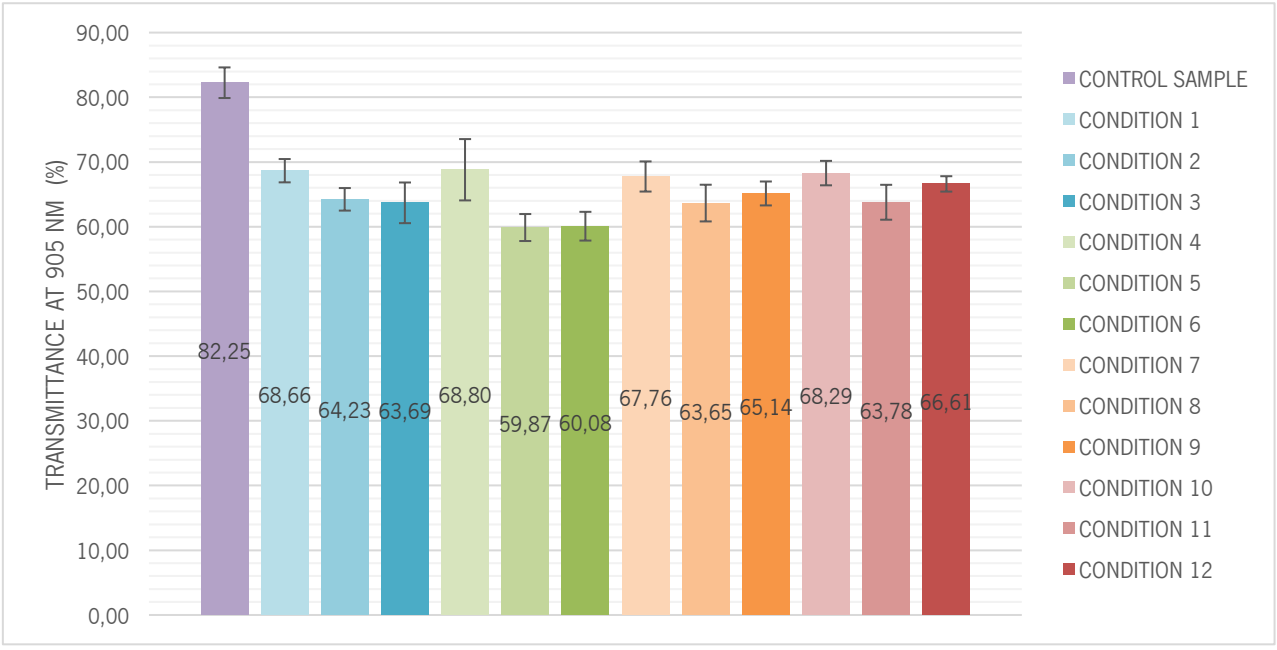

Figure 59 - Optical transmittance measured at 905 nm with the samples from the various conditions performed.

However, it is believed that these values could be improved if the handling during the injection and embossing process was optimized in order to not create any further optical damage on the part. Also, the scratches already present on the mold who were transferred to the samples, and the ones created during the handling on the non-microstructured face of the samples could contribute for measurement errors due to the spot of the sample where the transmittance was measured, that could have a greater or smaller number of scratches that were invisible to the naked eye and, likewise, impossible to control.

In any case, with these results it is possible to conclude that this microstructured pattern has a negative influence on the optical transmittance of the part, which invalidates its use on a protective optical window for a LiDAR sensor that must have at least 85% of light transmittance in the required range.

5.1.4. Optimal Condition for the Hot Embossing of Polycarbonate

After the establishment of the optimal parameters for the embossing of the microstructured pattern on a PC substrate through the preliminary study, five samples were produced with the mold 2 in order to obtain more accurate and reliable results about the replication and its influence on the surface hydrophobicity and optical transmittance.

Table 12 - Optimum condition for the embossing of PC.

Pre-heating time (min.)	Top Plate Temperature (˚C)	Replication Temperature (˚C) (bottom plate)	Replication Time (min.)	Replication Pressure (Ton.)	Demolding temperature (˚C)
5	100	165	10	6	120

The profile roughness measurement demonstrated that microstructures with an average of 10,37 μm ± 1,16 were achieved, showing that a complete filling of the cavities can be achieved with this condition. The highest micropillars present on the surface had an average of 11,18 μm ± 1,26, which confirms the existence of overstretched structures on its surface that could result from high adhesion and friction between the structure and the mold during demolding and/or from a high demolding temperature.

The samples 2, 3 and 5 did not achieve an average of 10 μm of height (Figure 60), and this could be due to the distortion of features during the demolding. Samples 1 and 4 showed that the microstructures suffered a significant overstretch during the demolding leading to structures higher than the desired height (Figure 60). Through the analysis of the Rt values, it could be said that a stretching of the structures was generalized through all the samples, with the highest peak always above 10 μm (Figure 61). These defects could be improved with the application of an adequate release agent, an automatic demolding system, and a vacuum system in order to optimize the process to have more reproducibility.

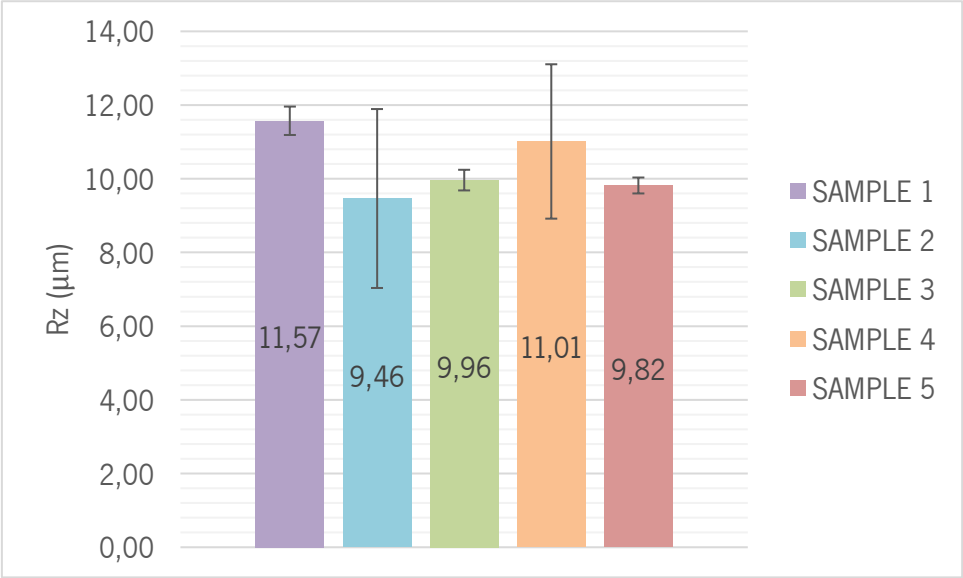

Figure 60 - Values of Rz obtained through the profile roughness measurement.

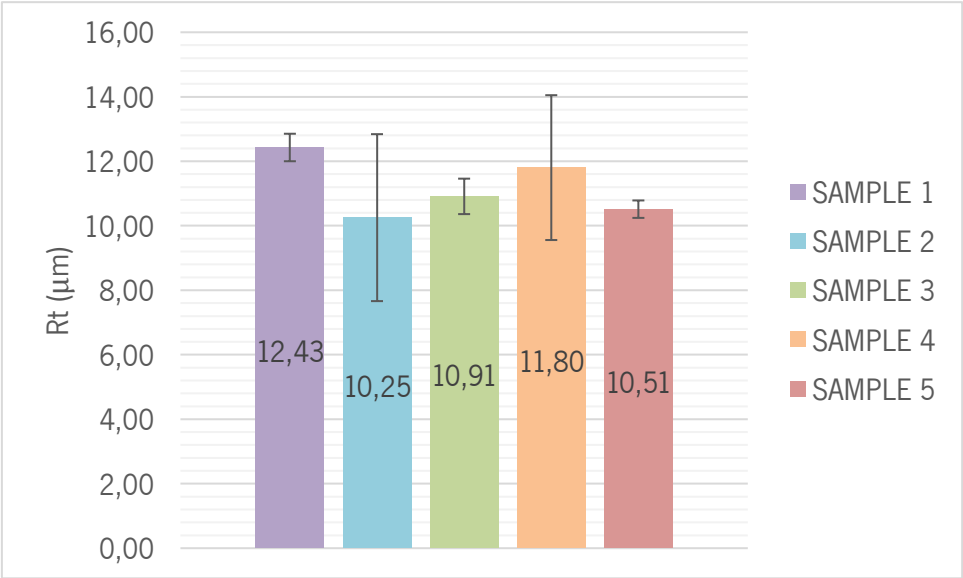

Figure 61 - Values of Rt obtained through the profile roughness measurement.

Analyzing the height maps and the profile roughness obtained with the InfiniteFocus SL, it is possible to observe well-defined structures, with less apparent distortion in comparison with the structures produced with the mold 1 (Figure 62a-c). Apart from some distortion on some features, it is also possible to observe that some structures were pulled out probably during the demolding stage (Figure 62b). However, its already possible to assume that with the use of mold 2, the surface quality of the samples improved, with less appearance of defects, except for the already existing demolding issues.

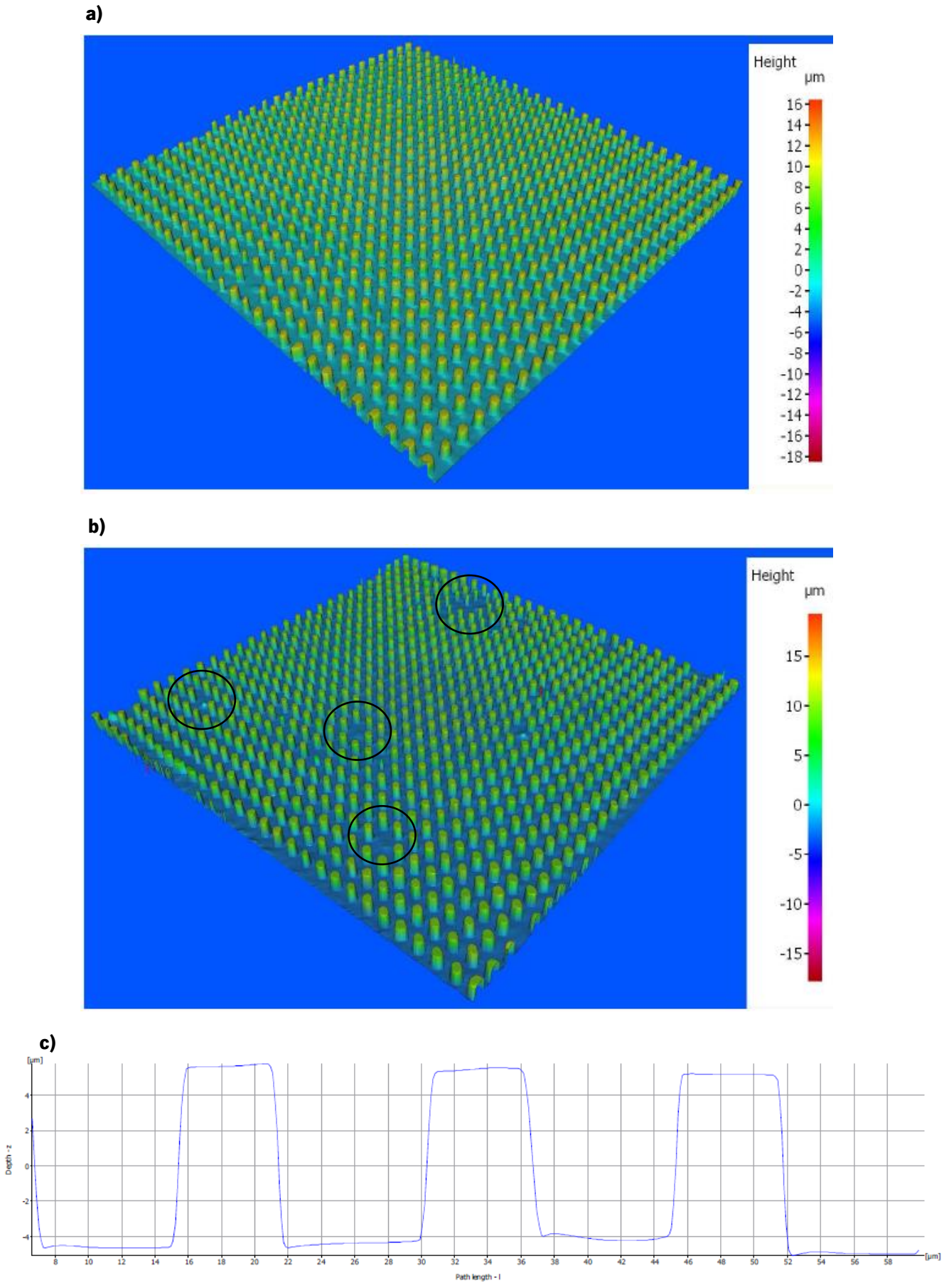

Figure 62 - Example of the height maps and profile roughness obtained in the measurement of the samples. a) Height map showing a more defined and uniform replication. b) Pulled out structures are visible on the surface due to demolding issues. c) Profile of the structures demonstrating more structural fidelity with well-defined vertical edge.

Scanning the surface of one of the samples through SEM, a clearest image of the microstructures was provided (Figure 63). Through the SEM images it was possible to observe the replication of the structures, which was well-defined as well as defects in some structures (Figure 63)(Figure 64). The defects present on the surface are essentially related to demolding. Distorted features are visible, with the structures slight tilted and/or deformed, which may be one of the reasons some structures are under 10 μm (Figure 64b-c). Along the surface it is also possible to observe broken and pulled out micropillars (Figure 64a). In addition, on top of a few structures it is possible to see a defect that could be material residue from previous moldings, or an excess of the gold used to coat the samples for the SEM analysis giving that aspect to the structure (Figure 64d).

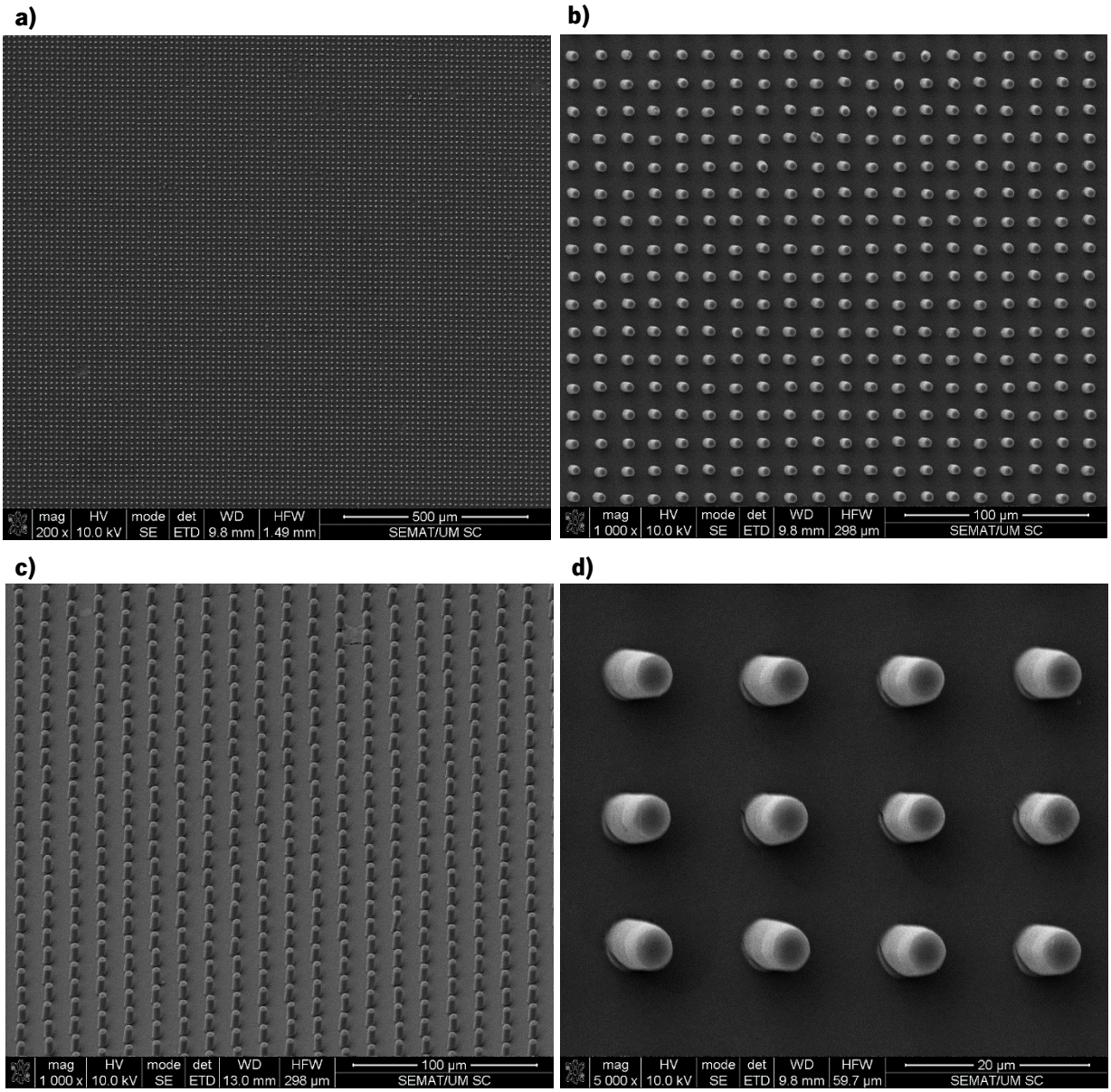

Figure 63 - SEM images of the structures. a) 200x magnification of the surface pattern. b) 1000x magnification of the surface pattern, showing the top of the features. c) 1000x magnification of the surface pattern. d) 5000x magnification of the surface pattern, showing the top view of the features.

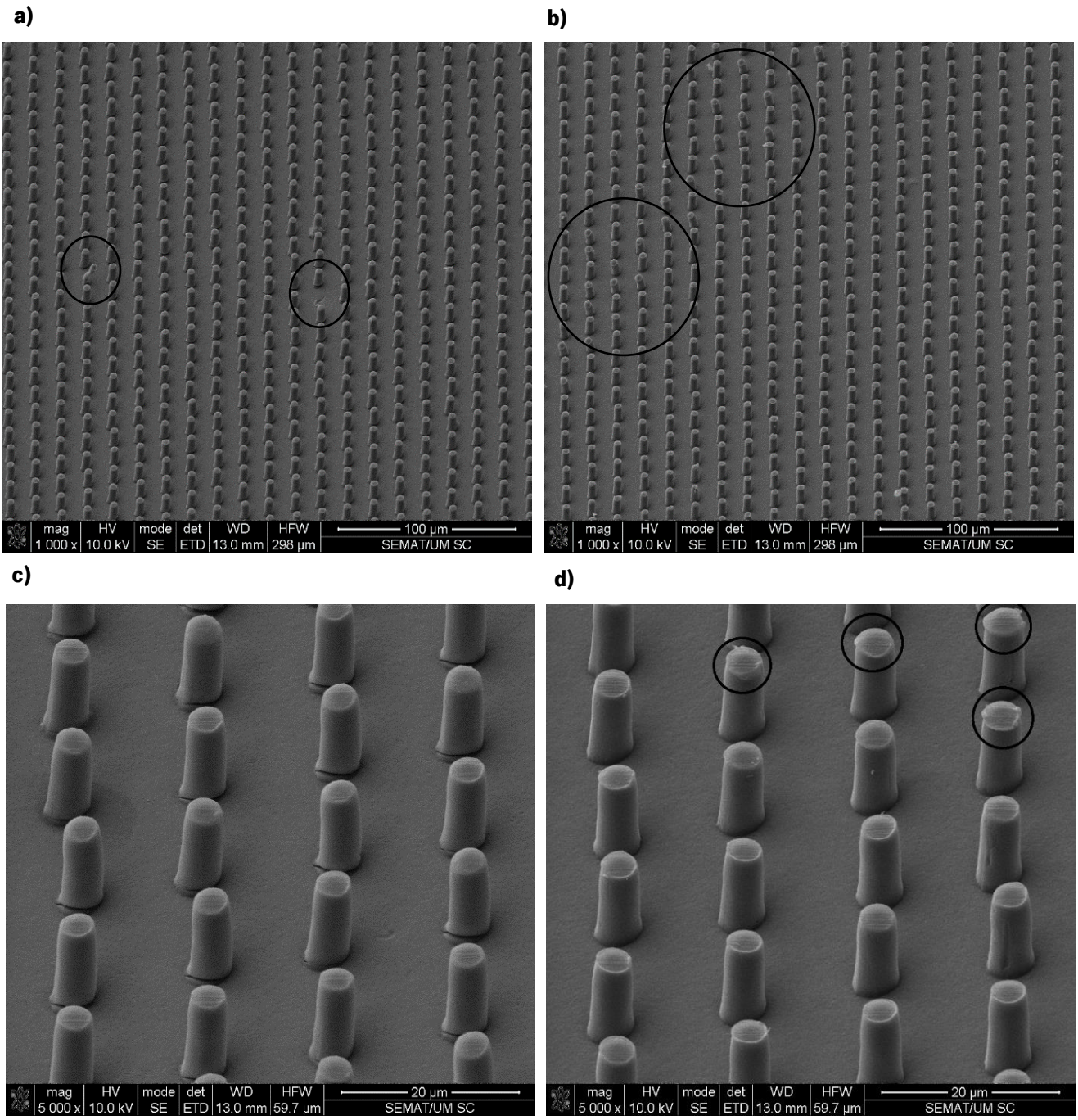

Figure 64 - SEM images of the surface defects associated with demolding. a)1000x magnification of the surface showing pulled out and broken structures. b) 1000x magnification of the surface showing distorted features. c)5000x magnification of the surface showing slight tilted and distorted features. d) 5000x magnification of the surface showing what could be material residue from previous moldings or an excess of the material used to coat the samples for the SEM.

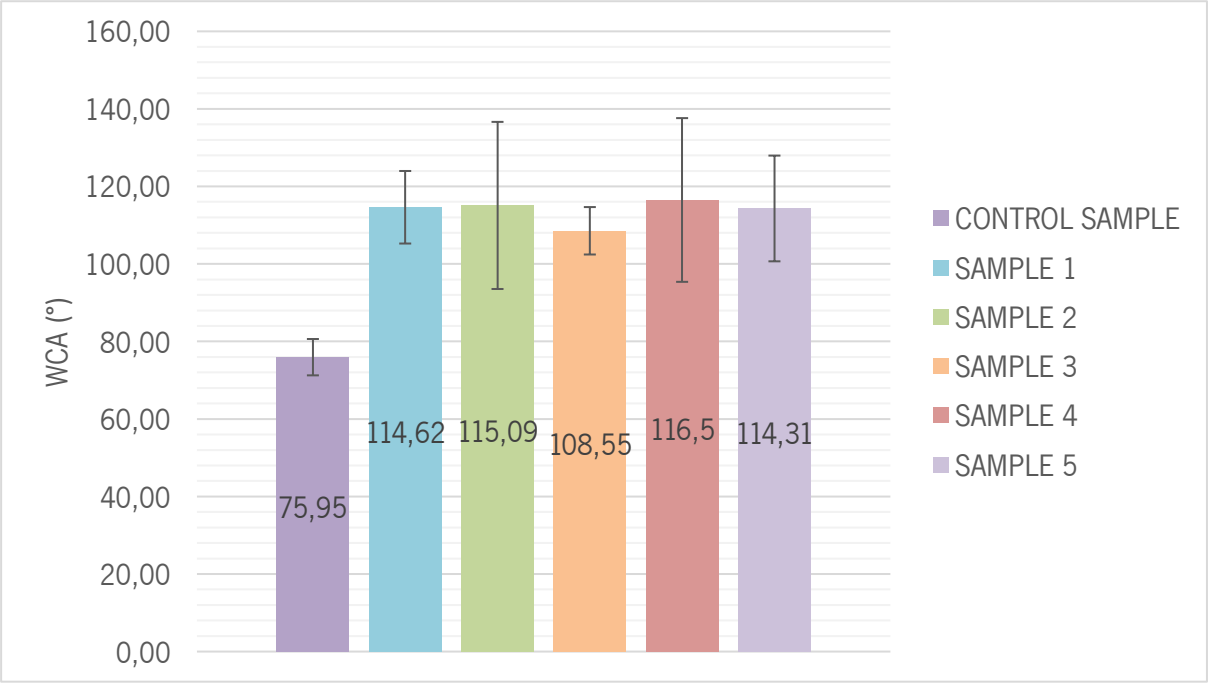

Figure 65 - Water contact angles measured in the PC samples.

The measurement of the water contact angle showed that the samples produced with this set of parameters had on average a WCA of 113,81 ° ± 15,87. Which in comparison with a non-microstructured sample suggests an increase of the WCA of practically 50 % due to the existing micropillars on its surface. In a more profound measurement of the WCA on the samples, where a further 15 spots of the sample were measured, it was possible to obtain even higher values of WCA, on average the samples provided a water contact angle of 134,88 ° ± 15,64. The highest angle measured was about 167,2 °, demonstrating once again that parts of the surface were superhydrophobic and given positive signs that superhydrophobicity could be achieved in a more controlled environment of processing (Figure 66).

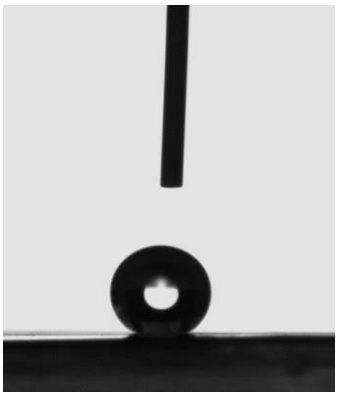

Figure 66 - Highest WCA measured across all PC samples (WCA = 167,2°).

Similar to what happened in the preliminary study, the majority of water droplets with WCA above 150°, spread on the surface after some time. In this case, the majority of the droplets showed a decrease on its WCA 60 seconds after being attached to the surface. However, it was observed very different rates of WCA decrease in the droplets, some presented a much slower rate than others (Figure 67).

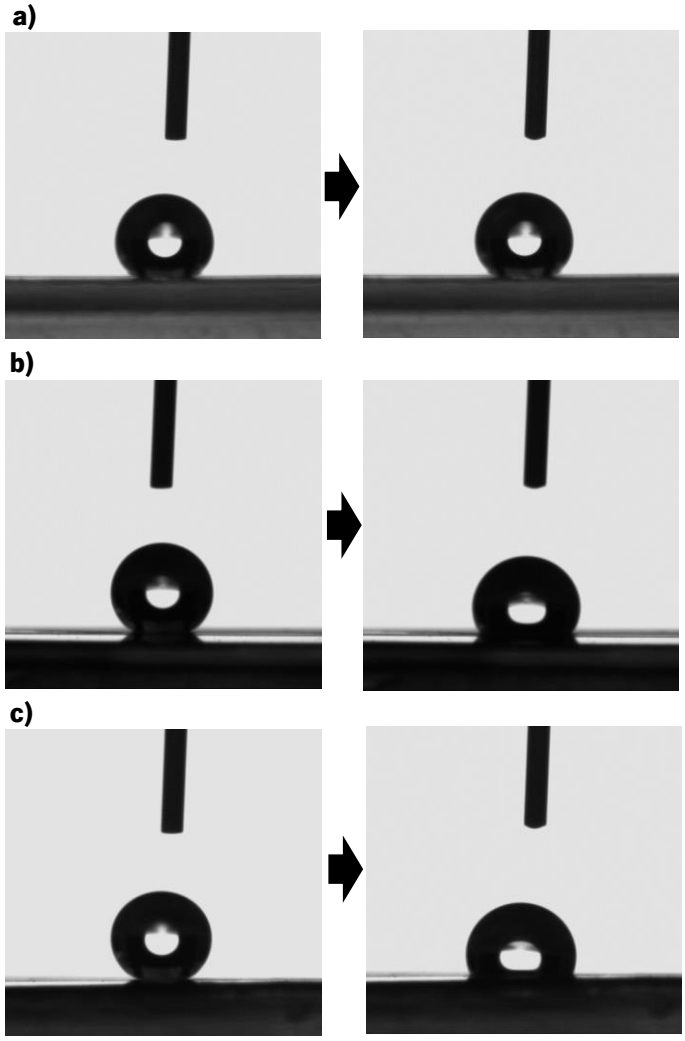

Figure 67 - Water droplets spreading in the surface at different rates. a) WCA = 151,3° (t=0s), WCA = 144,5° (t=60s) (decrease of 4,5% in comparison with the original value). b) WCA = 162,9° (t=0s), WCA = 132,9° (t=60s) (decrease of 18,4% in comparison with the original value). c) WCA = 167,2° (t=0s), WCA = 121,1° (t=60s) (decrease of 27,5% in comparison with the original value).

With these results, it is possible to state that this microstructured pattern affects the wettability of a surface leading to hydrophobic properties, with the surfaces exhibiting majorly a Wenzel State type of wetting with the majority of the angles being below 150 °. Moreover, the results show that the hydrophobic behavior does not vary among most of the samples, indicating that the hot embossing process is reproducible. As there exists the presence of angles above 150 ° in parts of the surface, the replication of the PC with this mold pattern in a more controlled environment and with a proper machine should be studied in order to understand if the achievement of superhydrophobicity with this pattern is possible.

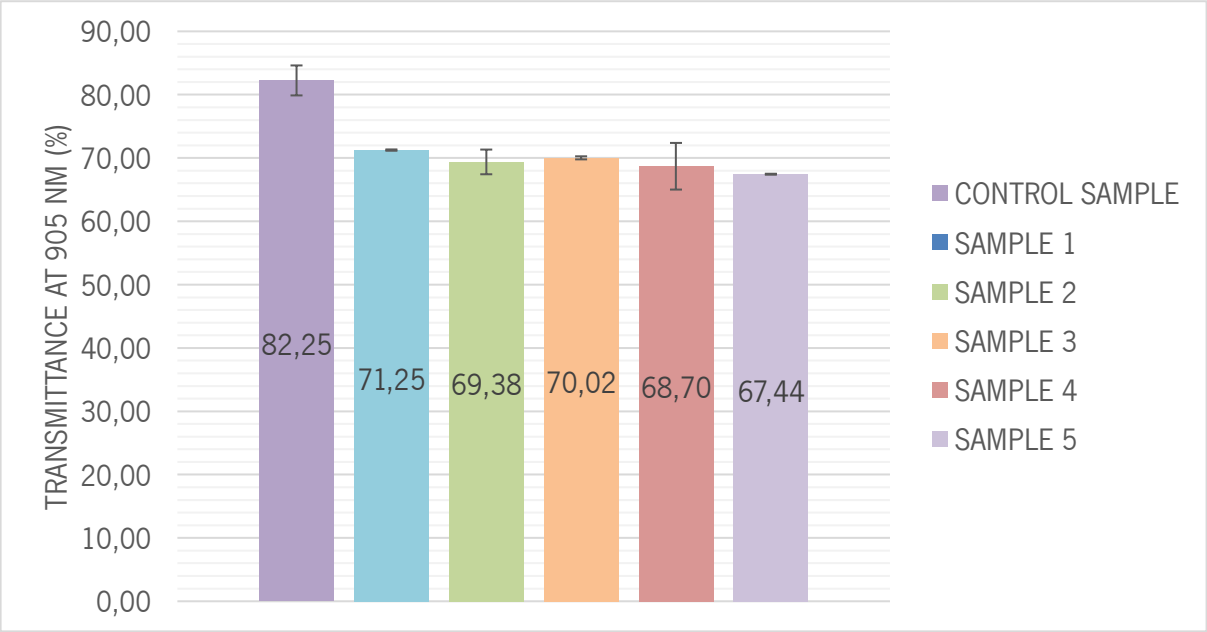

Figure 68 - Transmittance values at 905 nm of the PC microstructured samples produced with the optimal condition.

The optical transmittance of the samples at 905 nm was on average of 69,36 % ± 2,26. In comparison with the optically smooth surface, there exists an average decrease of 12,89 % in the optical transmittance of the samples due to the increase of the surface roughness. The results also show that optical transmittance does not vary among the samples, with the samples presenting close average values and minor standard deviations, also indicating good reproducibility of the process (Figure 68).

In one of the samples, it was also possible, resorting to Bosch, to measure its optical transmittance at 1550 nm, which was another value of interest in the project. At 1550 nm, the sample produced with this set of parameters with an undamaged mold offers an optical transmittance of 62,75 %.

In conclusion, these measurements demonstrated that the microstructured pattern influenced the optical transmittance, which is not ideal for the application in question. Considering that the optical transmittance should be at least 85% in both required wavelengths, these results invalidate the application of this microstructured pattern in a protective optical window for a LiDAR sensor, as it causes significant light scattering, resulting in a substantial decrease of the optical transmittance value.

5.2. Study 2 – Coating Application on PC Samples

The second study consisted in the deposition of a coating by spin coating on four PC microstructured samples produced with the optimal condition (Figure 69) (Figure 70). This study had the purpose of studying one of mostly applied strategies to achieve superhydrophobic surfaces, where after roughening the surface, a coating is applied with the aim of lowering the surface energy.

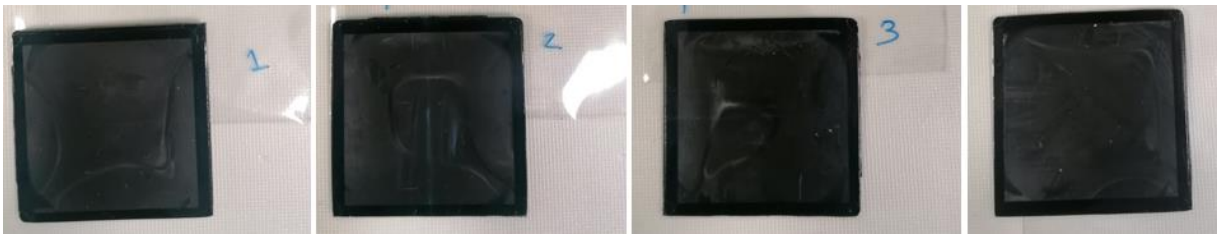

Figure 69 - All the samples after the coating application by spin coating.

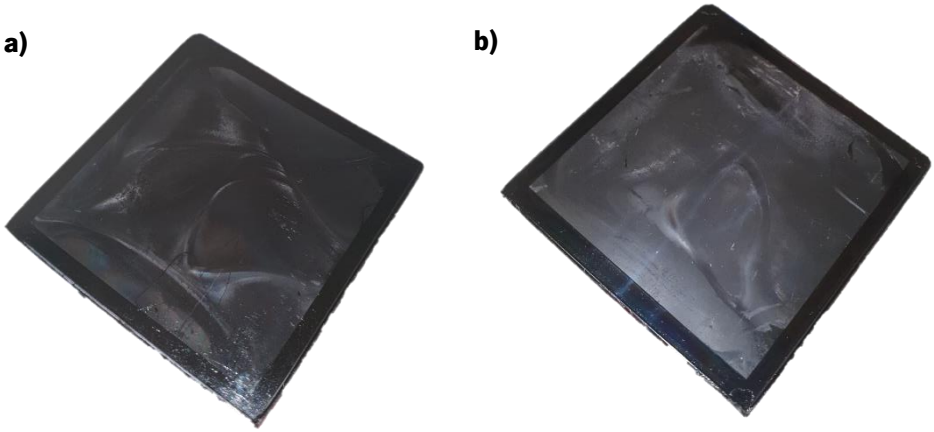

Figure 70 - Samples before and after the coating application. a) Sample before the coating application. b) Sample after the coating application, with a duller appearance.

Subsequently to the deposition, the surface topography was analyzed, however, as the coating was transparent and the InfiniteFocus SL was an optical device, some of the images were affected by the difficulty of the device to analyze the surface with the coating, making it difficult to measure some spots of the samples.

Table 13 - Rz values before and after the coating application on the samples.

Rz	Average	Standard Deviation
Before the coating application	10,24	2,26
After the coating application	7,90	1,19

Table 14 - Rt values before and after the coating application on the samples.

Rt	Average	Standard Deviation
Before the coating application	11,03	2,42
After the coating application	8,79	1,35

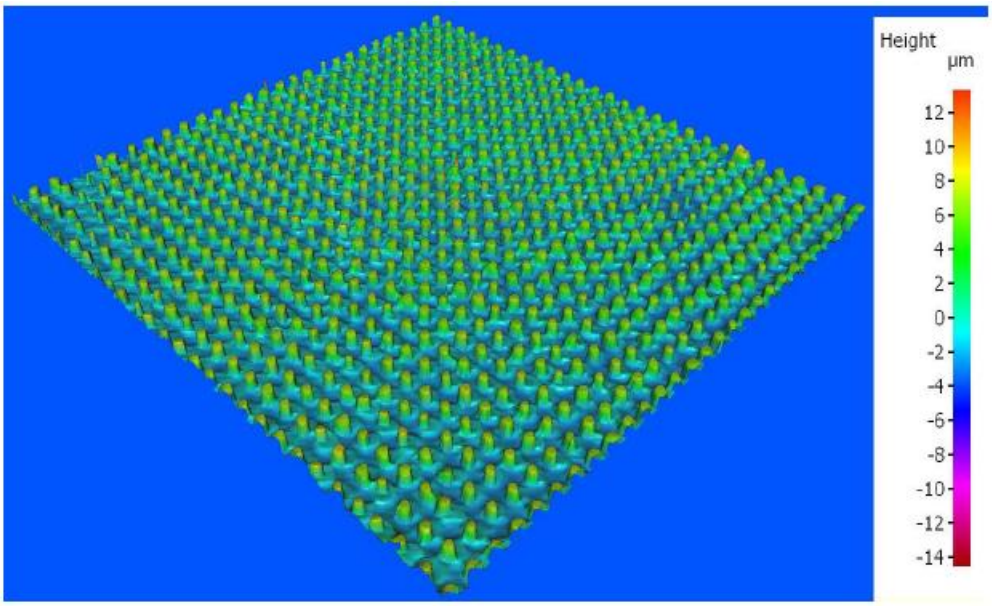

Figure 71 - Height map of a microstructured sample with coating obtained through the InfiniteFocus SL.

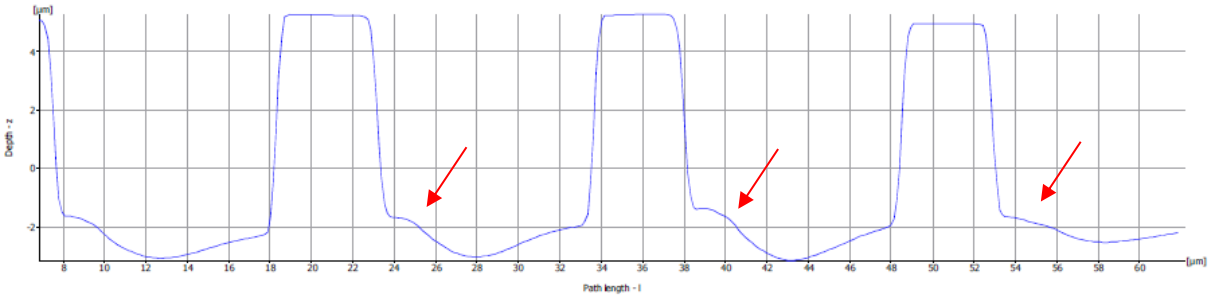

Figure 72 - Example of a profile of the structures covered by the coating, showing well-defined pillars and what could be the presence of the coating layer above the surface.

Through the height maps it was already possible to observe the presence of the coating above the surface (Figure 71). The measurement of the profile roughness showed an average decrease of 22,8 % on the mean height of the structures. This decrease is expected due to an increased layer of coating on top of the surface, leaving the structures with an apparent smaller height. With the coating, the micropillars showed on average a height of 7,90 µm ± 1,19, with the highest structures present on the surface with an average of 8,79 µm ± 1,35. This could mean that the layer of the coating deposited above the surface, near the bottom of the structures, has an average of 2,3 µm of thickness.

Observing the SEM images, that provide a more accurate representation of the surface, its possible to see that a large part of the pillars are slightly tilted, which immediately affects the height of the structures obtained, and through the surface is also possible to observe broken and pulled out structures, mostly likely also related to the demolding during the replication process, as these were very common defects (Figure 73). The SEM images also reveal that the coating seems to be evenly spread in the surface, indicating a good uniformity over the sample area (Figure 73b-c).

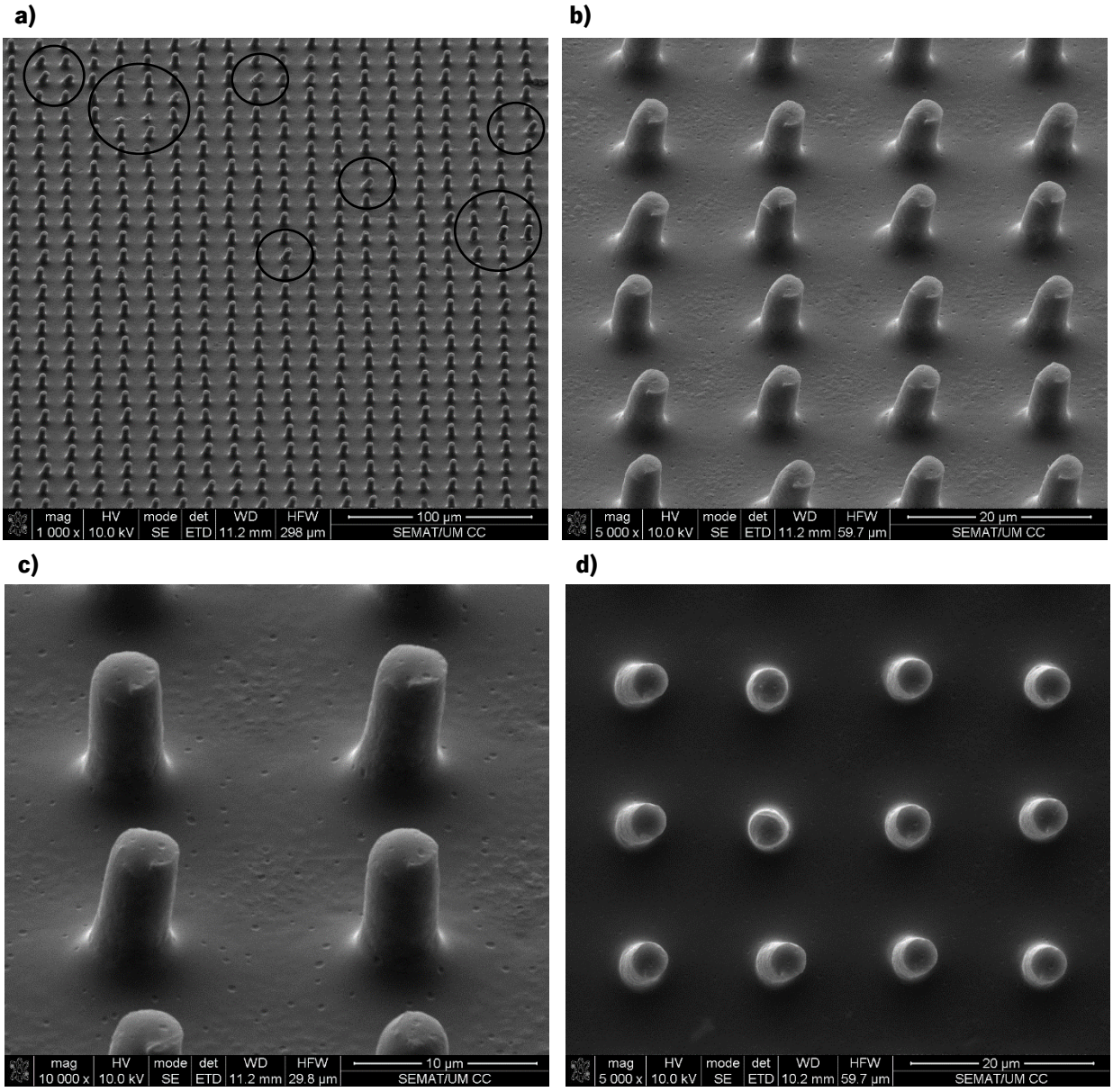

Figure 73 - SEM images of a microstructured sample with the coating application. a) 1000x magnification of the surface showing some defects related to demolding, such as distorted pillars, broken features and pulled out structures. b) 5000x magnification of the surface demonstrating slightly tilted structures and an evenly spread coating. c) 10000x magnification of the surface where apart from some distorted features it also possible to see a good uniformity of the coating over the sample are. d) 5000x magnification of the top of the surfaces, also making possible to observe some distortion of the features.

For understanding the effect of the coating on the water contact angle, first a PC non-microstructured sample with the coating deposition was analyzed in order to perceive the effect of the coating alone on the WCA. The sample presented a mean water contact angle of 106,92 ° ±1,97. This proved that the application of the coating alone could enhance the hydrophobicity of a surface, with the WCA presenting an increase of almost 31 ° (Figure 74).

Figure 74 - Water droplet placed on top of a non-microstructured PC surface with the coating application (WCA = 109,2°).

When measuring the microstructured samples with the coating, in the majority of the surface the water droplet would not adhere to the substrate, showing water repellency (Figure 75).

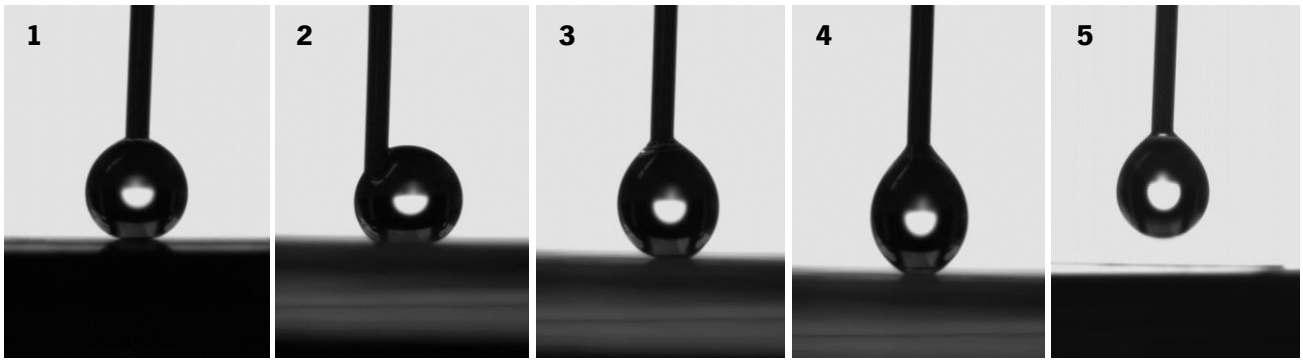

Figure 75 - Sequence of images showing the water droplet not adhering to the substrate.

After a few try's and exposing the droplets to external pressure by pressing the water droplets on to the surface, which could have caused a wetting state transition from Cassie-Bexter to Wenzel or even to the midterm wetting regime (due to the presence of high WCA) (Bormashenko, 2015), it was possible to put some droplets on the substrate and measured the water contact angles. The coating application boosted the WCA by about 31,48 °, corresponding to an increase of 27,66 %, with on average a WCA very close to the superhydrophobic regime (Figure 76), and taking into account that the first reaction of the substrate to the water droplet was water repellency, it could be stated that this strategy is really effective in obtaining superhydrophobic surfaces with good uniformity over the sample area.

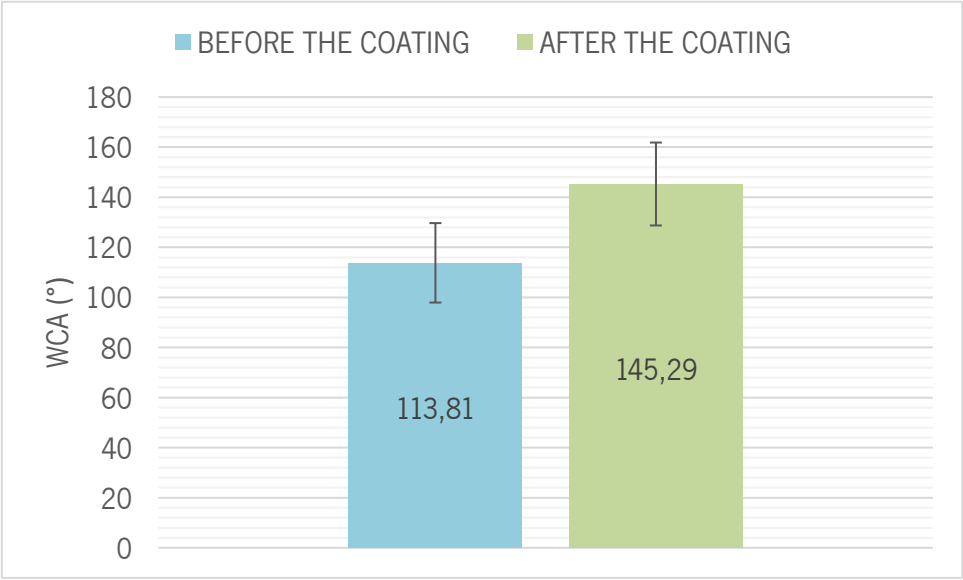

Figure 76 - Water contact angles before and after the coating application.

After observing that the combination of a microstructured patter and a coating could offer superhydrophobicity, it is necessary to understand how the coating can affect the optical transmittance.

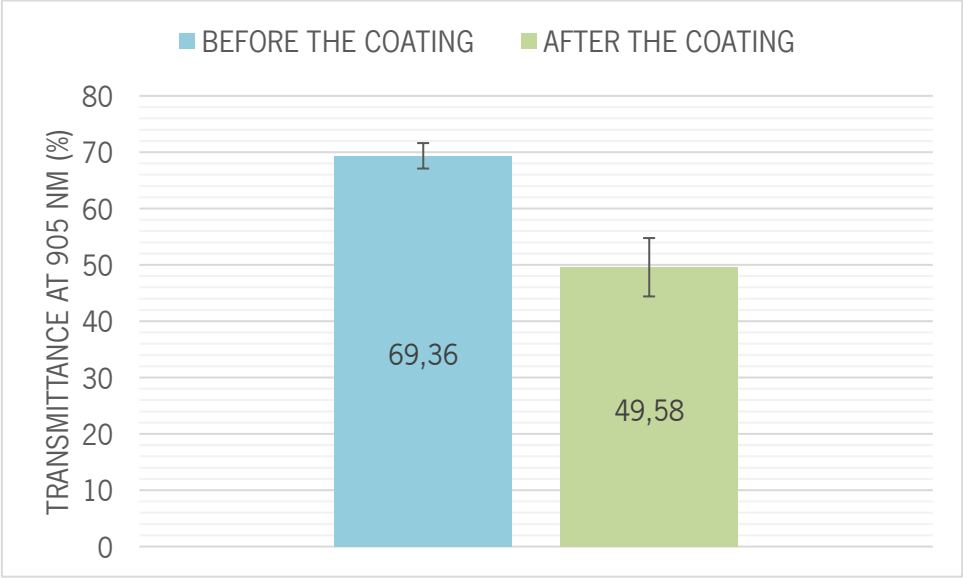

Figure 77 - Optical transmittance values at 905 nm before and after the coating application on the samples.

The application of a coating on the microstructured samples caused an average decrease of about 19,78 % of the optical transmittance at 905 nm (Figure 77) and at 1550 nm, the sample measured at Bosch offered an optical transmittance of 50,37 %, which represents a decrease of 12,38 % due to the coating presence (Figure 78). This reduction was already expected as the addition of an additional barrier to the light pathway will have a negative influence on the optical transmittance of the product as it becomes a source of scattering.

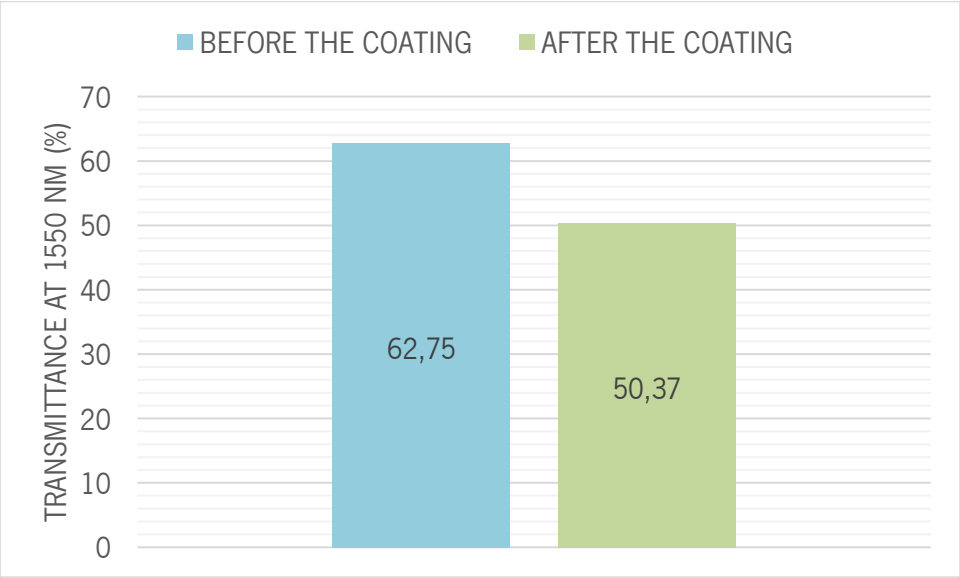

Figure 78 - Optical transmittance values at 1550 nm before and after the coating application on the sample.

It was also noticed that the spin coating process marked the part on the non-microstructured side due to the vacuum system that keeps the sample in place. The marks caused by the vacuum could not be eliminated through cleaning and contributed to worsening the optical transmittance of the samples (Figure 79).

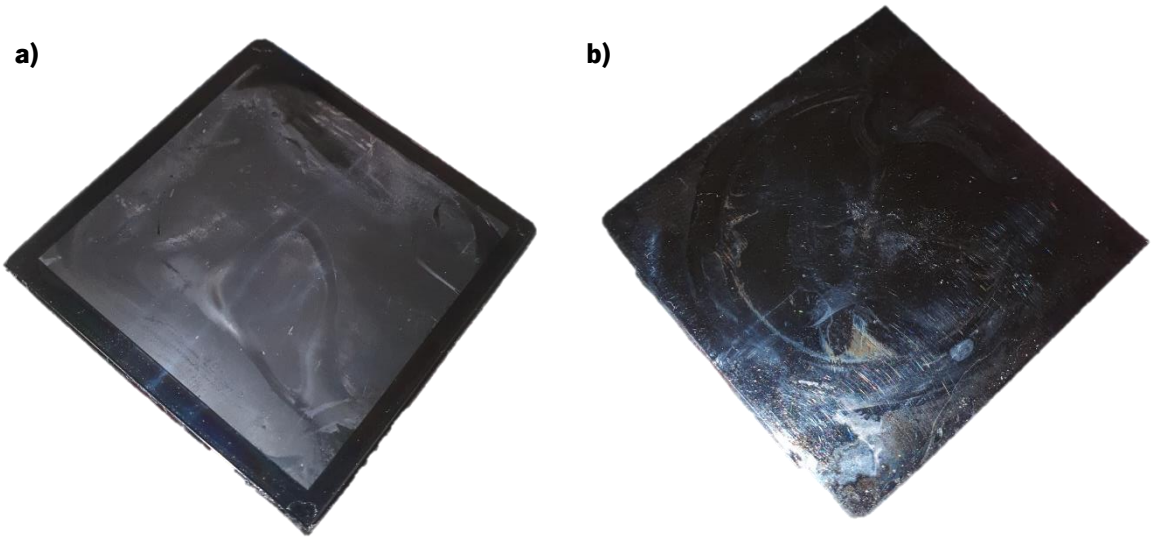

Figure 79 - Microstructured sample with the coating application. a) Microstructured zone. b) Non-microstructured or flat zone showing the marks caused by the vaccum.

These results show that applying a coating on a microstructured sample allows the achievement of superhydrophobicity, however, it becomes a problem in terms of light transmission and aesthetics. Furthermore, as it involves two different steps to produce the final part, the hot embossing process and the spin coating process, it increases the lead time of the productive process, not being suitable for high production rates.

5.3. Study 3 – Production of PMMA Samples through Hot Embossing

This study had the goal of determining the optimal conditions for the processing of PMMA through hot embossing, and the influence of the replicated pattern above the optical and hydrophobic conditions of the produced samples.

Although the results using polycarbonate were satisfactory in terms of replication of the mold pattern, the optical transmittance of PMMA is superior compared with PC. Likewise, it is of interest to study its processing through hot embossing and how the same replication pattern will affect its surface wettability and optical transmittance, and its consequent viability in the production of protective optical window for LiDAR sensors.

5.3.1. Processing Conditions and Plan of Experiments

The determination of the values of the processing parameters for PMMA (T_g = 117 °C). was made taking into account the results with the processing conditions of PC, in particular the replication pressure and replication time, and the existing reports in literature (Hashiura et al., 2001; Shamsi et al., 2014). In addition, the number of factors and levels that could be studied was limited by the number of non-microstructured samples available for using in the replication process.

Table 15 - Processing parameters applied in the embossing of PMMA samples.

Pre-heating time (min.)	Top Plate Temperature (˚C)	Replication Temperature (˚C) (bottom plate)	Replication Time (min.)	Replication Pressure (Ton.)	Demolding temperature (˚C)
5	80	125	10	4	90
		135		6	

In the study with polycarbonate, the replication pressure was set according to Becker *et al.* suggestions for the embossing of micro-sized features, mentioned in Chapter 2 (section 2.9), where the embossing pressure should be around 0,5 to 2 kN/cm^2. Likewise, taking into account that the embossing area remains the same, the pressure used in the previous study can be applied in the processing of PMMA. However, with the results obtained in study 1, it was possible to perceive that a replication pressure of 2 tonnes did not produce any significative result, therefore it was decided to study only a pressure of 4 tonnes and 6 tonnes for the replication of PMMA.

Study 1 also showed that a complete filling of the cavities can be achieved within 10 minutes of replication time, and this time is much more interesting to study for the processing due to its great influence on the cycle time, which is important to be as optimized as possible.

The replication temperatures studied were defined taking into account the glass transition temperature of the material (T_g = 117 °C) and the literature review about the embossing of PMMA (Hashiura et al., 2001; Shamsi et al., 2014). The top plate temperature also followed the same principles of the temperature applied for PC, it had to be below the glass transition temperature of the material and in accordance with the advised mold temperature of the technical datasheet. Lastly, the demolding temperature was defined in order to try to minimize the thermally induced stresses on the parts.

In this experiment, as mentioned previously, the factors taken into consideration are only the replication temperature and pressure, i.e., 2 factors. As observed in Table 16, this experiment presents both factors with 2 levels. By using the software Minitab, it was possible to create a 2-level Taguchi experiment, producing an L_4 orthogonal array. Therefore, for the study of the embossing of PMMA, it is needed to perform four different experiments (runs). For each run, it was produced three samples to be analyzed.

Table 16 - The experimental factors of the PMMA study and their levels.

Experimental Factors	Experimental Level	
	1	2
A: Replication Temperature (˚C)	125	135
B: Replication Pressure (Ton.)	4	6

Table 17 illustrates the experience plan to be performed during the study. The level 1 corresponds to the lower level and level 2 corresponds to the highest level.

Table 17 - Experiences plan of the PMMA study.

Exp.	A: Replication Temperature (˚C)	B: Replication Pressure (Ton.)
1	Level 1	Level 1
2	Level 1	Level 2
3	Level 2	Level 1
4	Level 2	Level 2

The conditions or runs performed in order to evaluate the effect of the process parameters in the replication quality are available in Table 18.

Table 18 - Conditions performed in PMMA samples.

Condition	Replication Temperature (˚C)	Replication Pressure (Ton.)
1	125	4
2	125	6
3	135	4
4	135	6

5.3.2. Surface Topography

The profile roughness values and the height maps showed that all of the conditions were able to cause changes on the surface of the samples, however, only condition 1 and condition 2 showed acceptable results in terms of surface quality and replication, with the condition 3 showing a significative number of degradation spots on the samples and condition 4 demonstrating samples with a surface completely degraded, as it will be observed below.

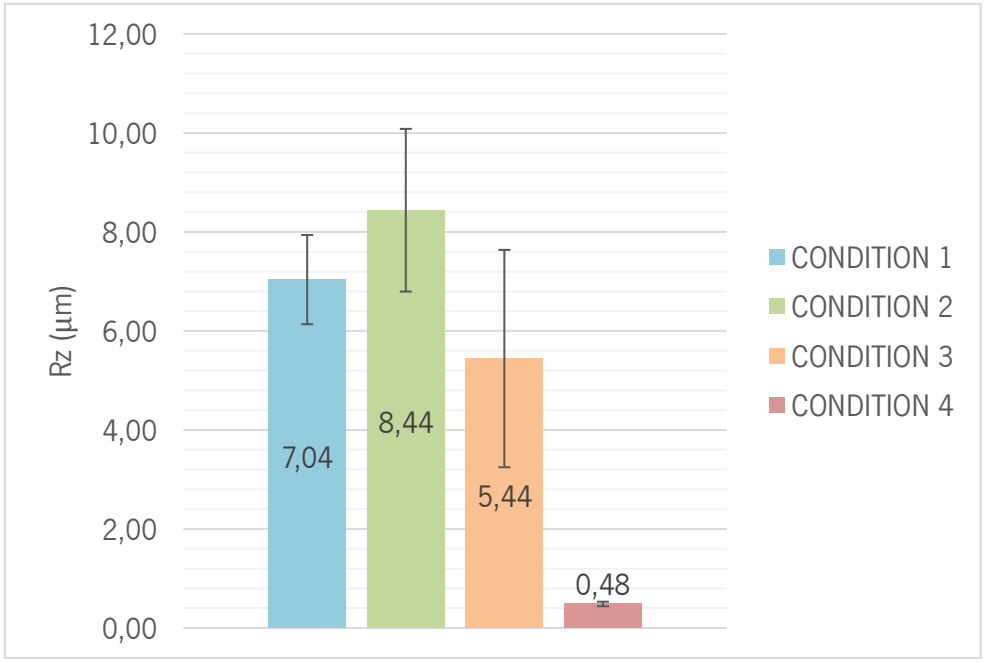

Figure 80 - Values of Rz obtained through the profile roughness measurement.

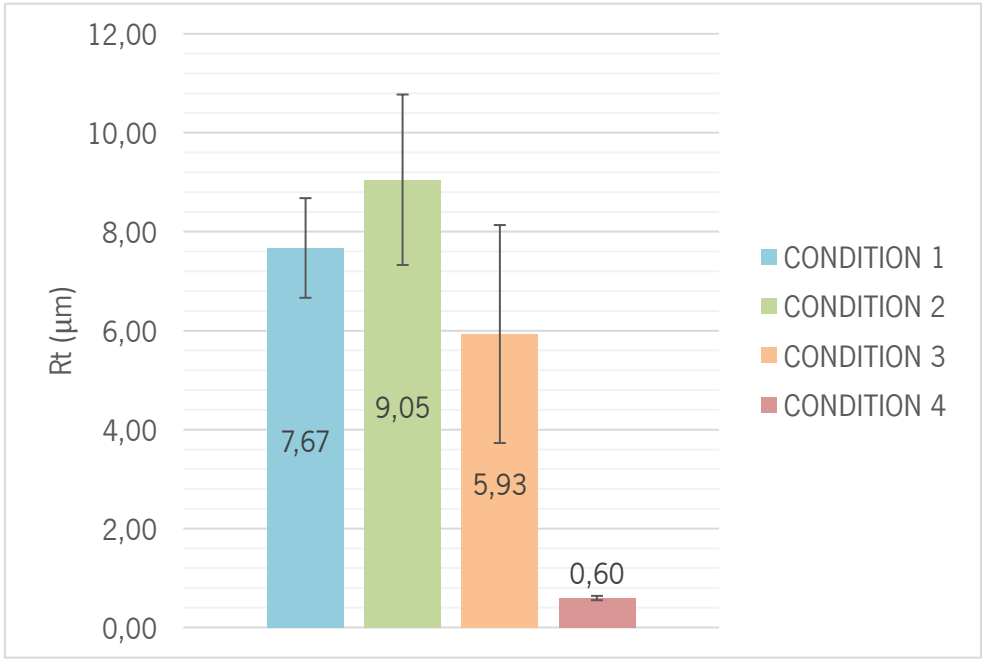

Figure 81 - Values of Rt obtained through the profile roughness measurement.

This set of conditions made it possible to achieve a maximum average up to 84 % of the desired replicated height, with average heights superior to 8 μm (Figure 80) and the highest pillars found on its surface with average heights of 9 μm (Figure 81). The complete filling of all the cavities by the PMMA was not achieved, but this was already expected to be more challenging than with PC, as the melt volume rate (MVR) of the PMMA is much smaller than the MVR of the PC used previously (PMMA presented an MVR of 3 cm^3/10 min. and PC had an MVR of 19 cm^3/10 min.) Likewise, the PMMA would offer less flow capacity in the filling of cavities in comparison with PC. However, this was not the only reason that could justify the structures not reaching the desired height, defects related with demolding and the thermal degradation of the structures also affected the replicated mean height.

The samples produced with condition 1, which presented an average height for the structures of 7,04 μm ± 0,90, presented defects related with demolding (Figure 82). The appearance of distorted features was constant throughout the surface, as well as the appearance of some pulled out structures (Figure 83). A great part of the analyzed microstructures of the samples produced with this condition presented these defects related to demolding, which negatively influenced the replication height. However, the highest microstructures found on the surface were well below 10 μm in height (Figure 81), which indicates that the complete filling of the cavities with this condition could not be achieved, a higher pressure is needed for the polymer to fill the mold cavities entirely.

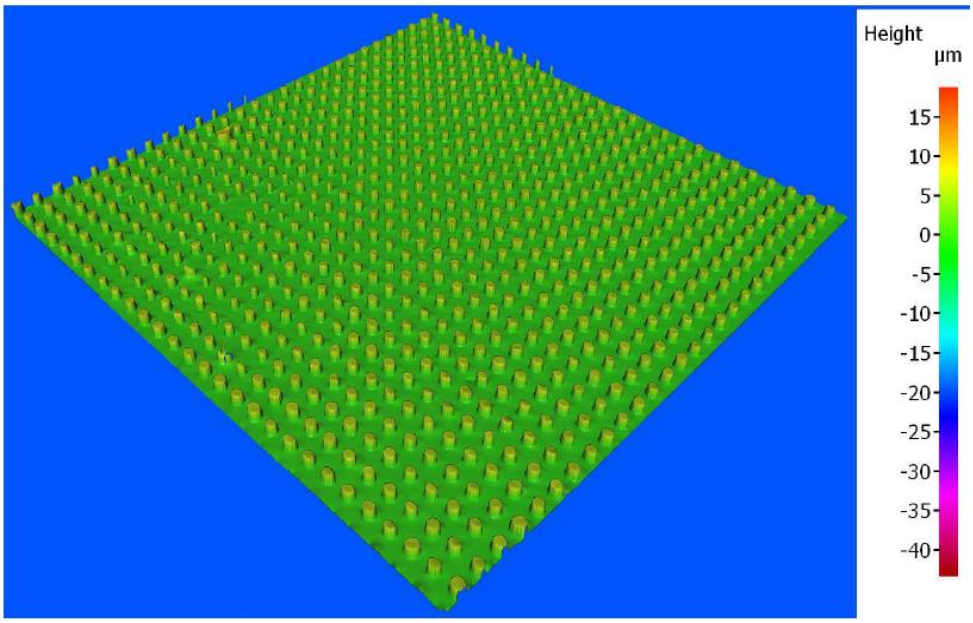

Figure 82 - Representative height map of a sample produced with condition 1, showing incomplete filling of the cavities.

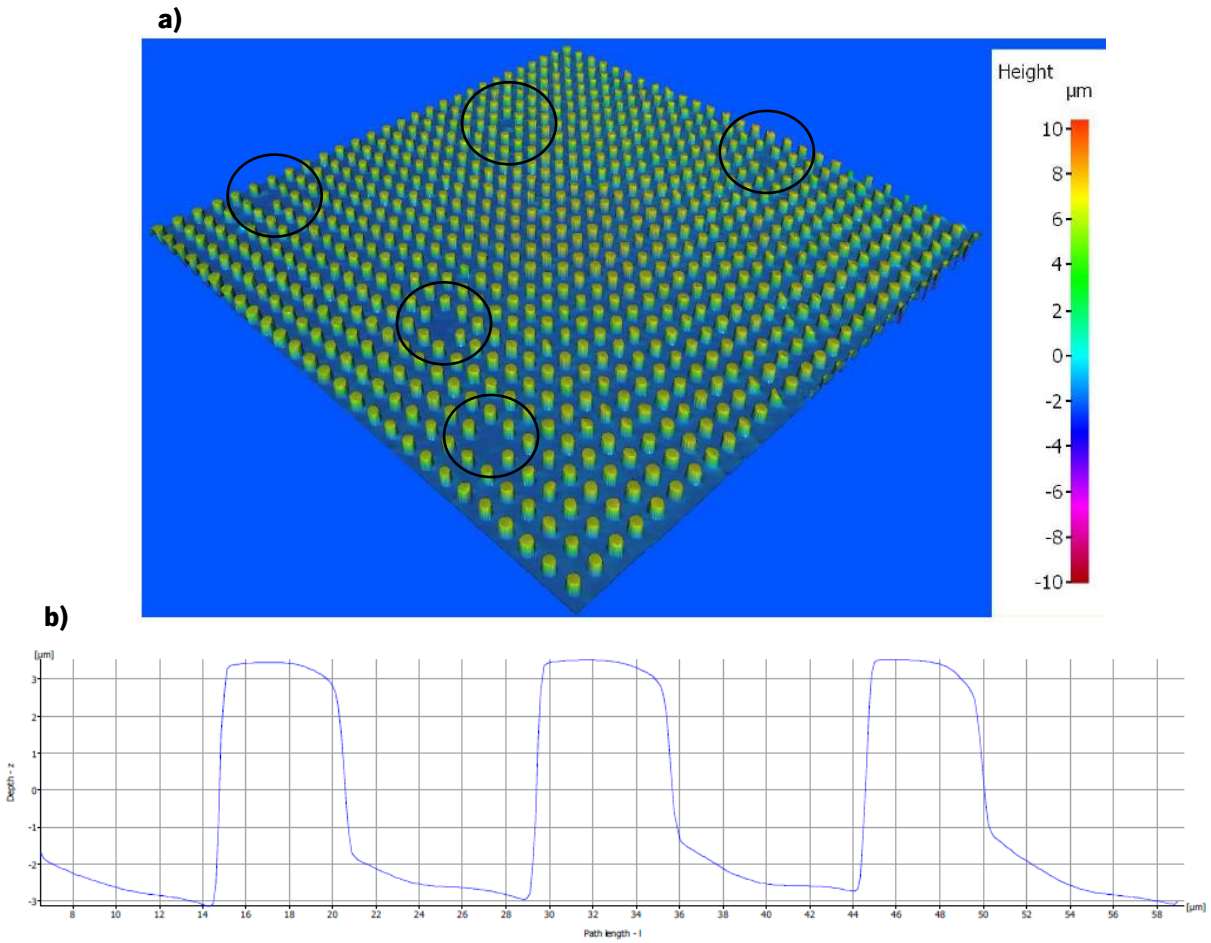

Figure 83 - Common defects observed in the samples produced with condition 1. a) Pulled out structures. b) Distorted structures.

The samples performed with the condition 2, which offered the best result for the average height, 8,44 µm ± 1,64 (Figure 84), also presented some defects such as distorted features and pulled out structures, which also affected the final average height of the pillars and uniformity of the surface (Figure 85). Although being the set of the parameters that led to a higher height for the microstructures, a great part of the features analyzed did not reach the 10 µm, and based on standard deviations obtained for both Rz and Rt, a good uniformity over the sample area was also not attained. This could be due to the defects mentioned previously and/or lack of uniformity of the temperature or pressure distribution over the sample during the replication process. However, the highest structures found on the surface had an average height of 9,05 µm ± 1,72, demonstrating that heights of around 10 µm were achieved in some of them. Furthermore, in spots of the samples where the structures did not present any of the defects mentioned previously, the structures had heights very close to 10 µm, even demonstrating a slight overstretch in some of the structures (Figure 86). This could mean that if the distortion of features could be avoided and if the process could be more controlled, micropillars with 10 µm, the desired height, could be achieved in this set of parameters.

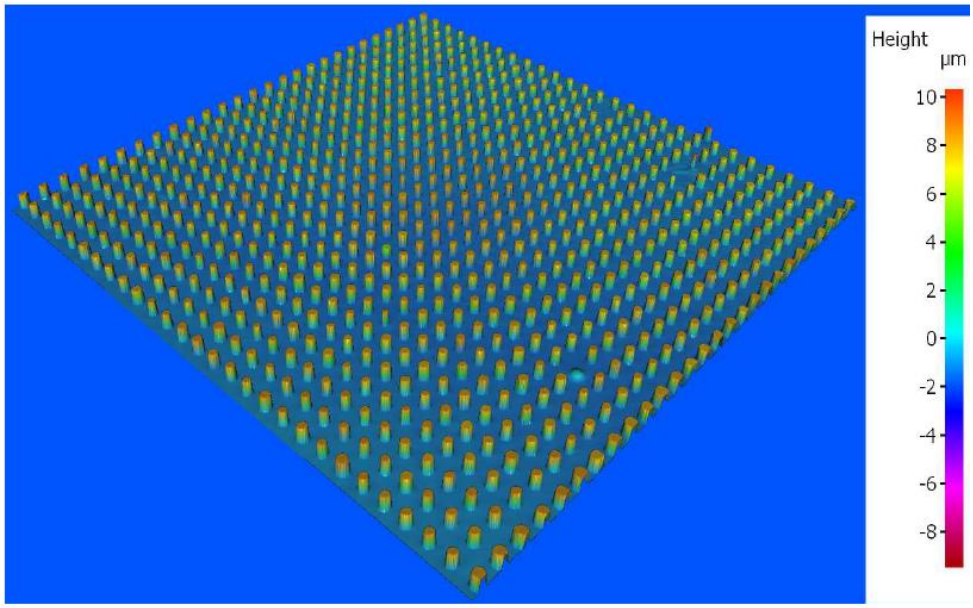

Figure 84 - Representative height map of a sample produced with condition 2.

a)

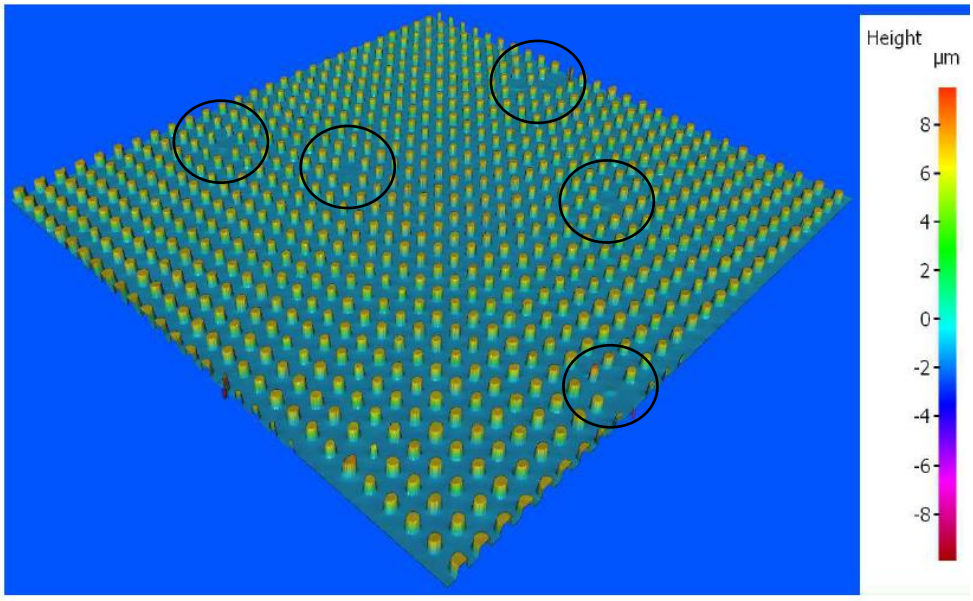

b)

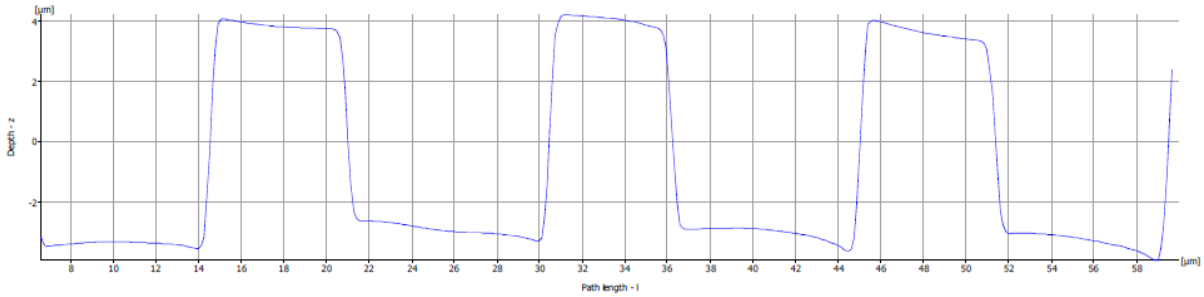

Figure 85 - Defects associated with demolding observed in the samples produced with condition 2. a) Pulled out microstructures. b) Distortion of the features, causing its dislocation and a larger appearance (larger diameter) to the structures.

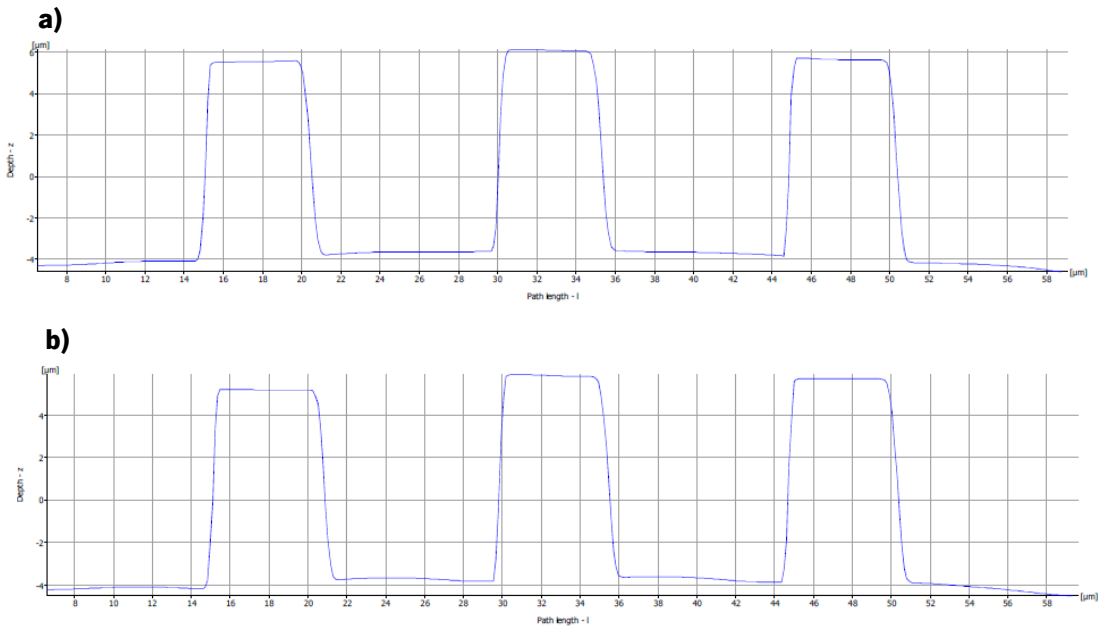

Figure 86 - Presence of structures with average heights very close to 10 µm. a) Rz = 9,74 µm, Rt = 10,21 µm. b) Rz = 9,58 µm, Rt = 10,41 µm.

Samples produced with the condition 3 showed clear signs of degradation on its surface, with most of the surface topography being unmeasurable due to the degradation of the micropillars caused by the temperature applied being too high (Figure 88). However, in some spots of the samples it was still possible to measured structures who presented average heights of 5,44 µm ± 2,20 (Figure 88a-c). The samples manufactured with condition 4, where in addition to the high temperature was also applied a bigger pressure, were completely degraded, being almost completely unmeasurable (Figure 89). Both conditions also caused a melting and unwanted deformation of the part (Figure 87). These results clearly show that a replication temperature of 135 °C was excessive for the material causing the thermal degradation and damage of its surface.

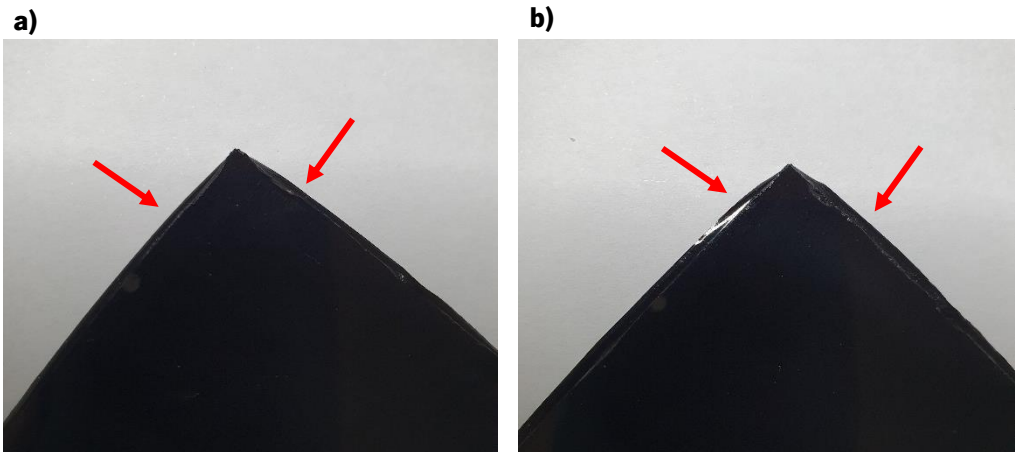

Figure 87 – Melting and unwanted deformation of the samples. a) Deformation on a sample produced with condition 3. b) Deformation more proeminent on a sample produced with condition 4.

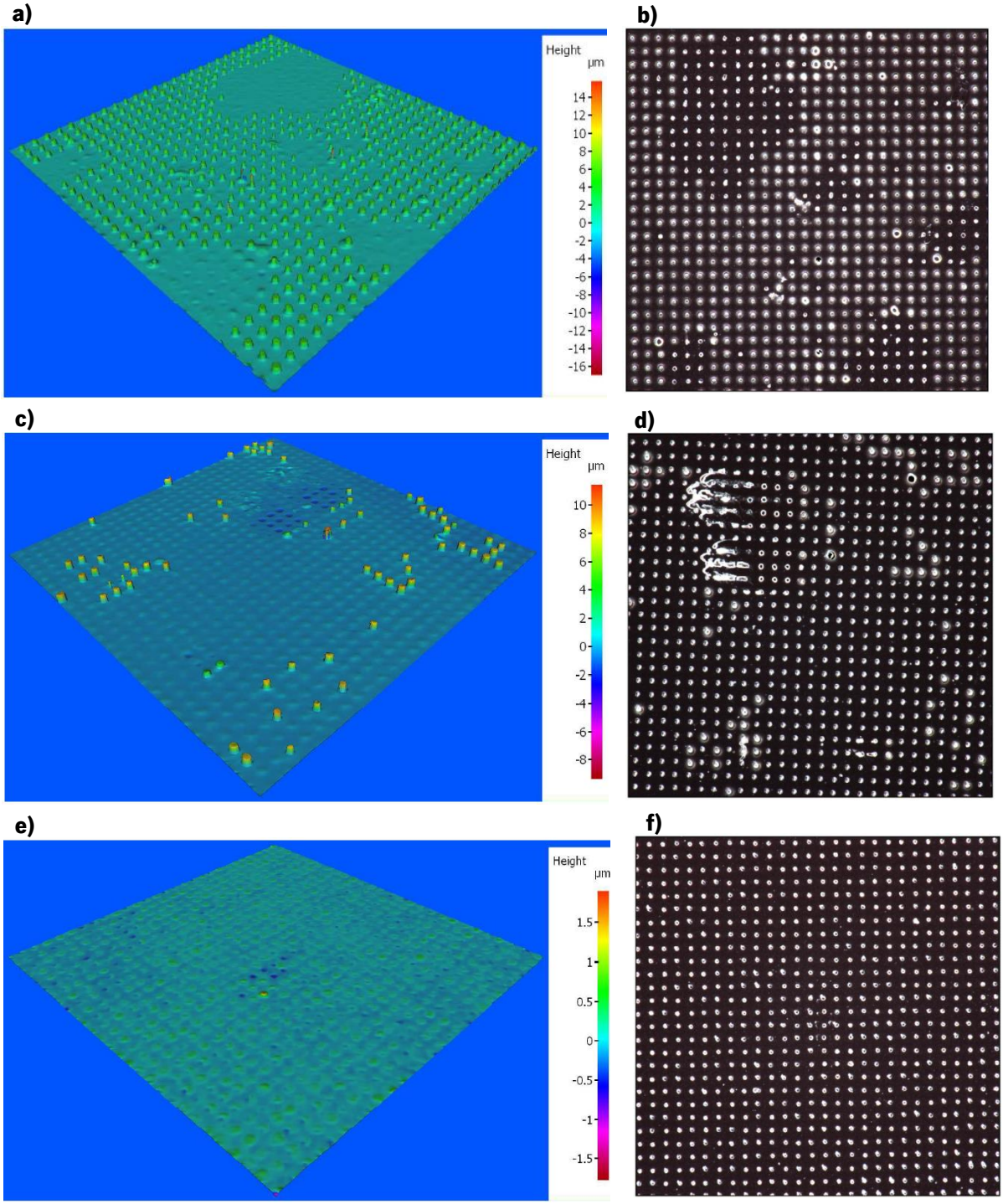

Figure 88 – Representative height maps and respective microscopical images of samples produced with condition 3. a-b) Height map and microscopical image showing microstructures on the surface, and the lack of some structures that could be due to pulled out during demolding or thermal degradation. c-d) Height map and microscopical image demonstrating the degradation of the majority of the surface. e-d) Height map and microscopical image showing a complete degraded surface due to the high temperature applied.

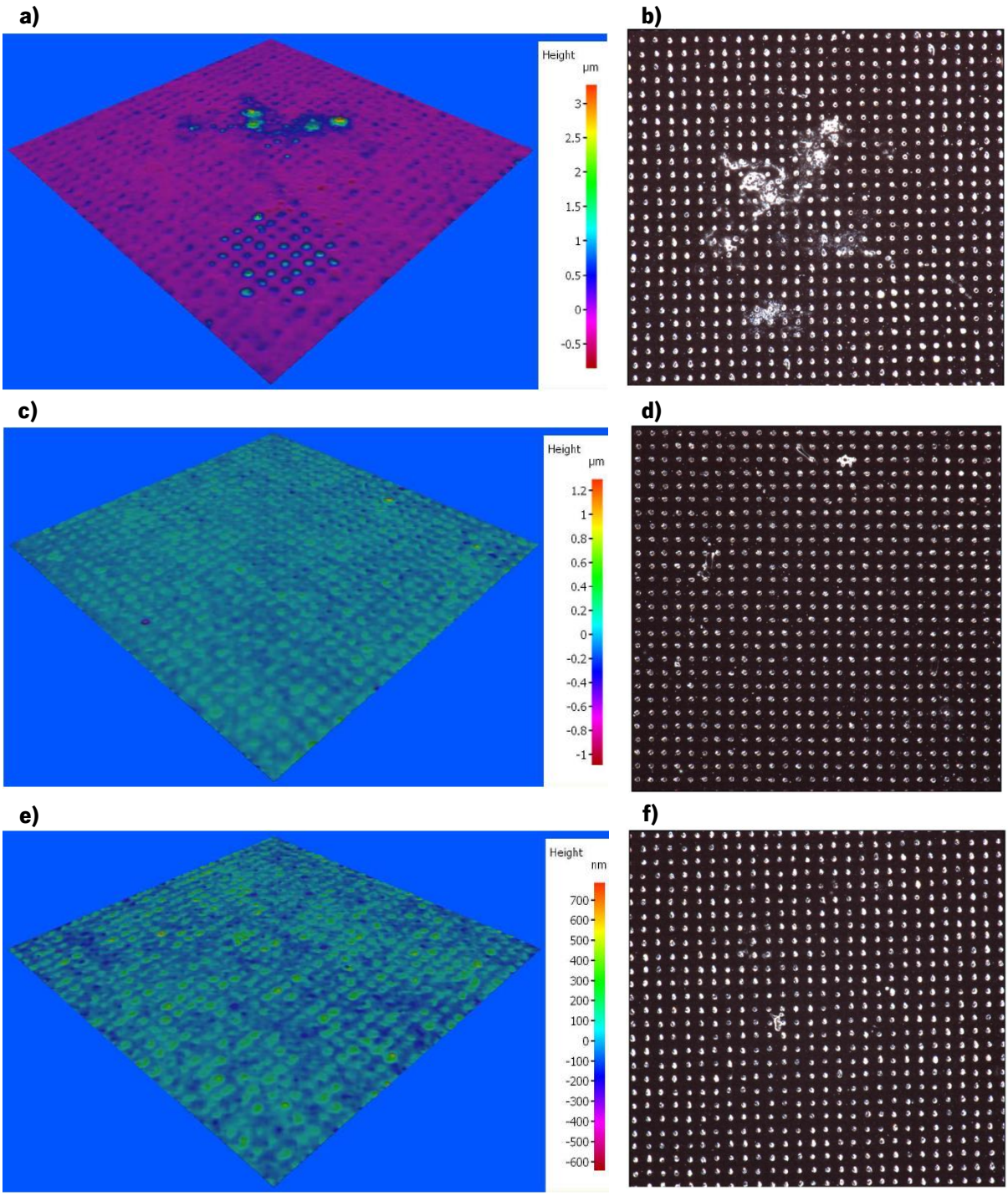

Figure 89 - Representative height maps and respective microscopical images of samples produced with condition 4. a-f) Height maps and microscopical images showing that the surface of the samples produced with this condition was completely degraded due to the use of a high temperature and high pressure during the replication process.

Based on the experimental results, an analysis of variance (ANOVA) was performed in order to assess the contribution of each processing parameter to the resulting mean replicated height (Rz).

Table 19 helps to understand the significance of each parameter and interaction for the relationship between the factors and the response. In this case, the determinant factors are the replication temperature, the replication pressure and the interaction between the replication temperature and pressure since they all present p-values below 0,05.

Table 19 - Analysis of variance for Rz.

Source	DF	Sum of Squares	Mean Square	F-value	P-value
Replication Temperature	1	47,9236	47,9236	639,38	0,000
Replication Pressure	1	7,2104	7,2104	96,20	0,001
Replication Temperature*Replication Pressure	1	21,7889	21,7889	290,70	0,000
Error	4	0,2998	0,0750		
Total	7	77,2228			

It is observed from Figure 90 that an increase of the temperature and an increase of pressure created a decrease in the height of the structures. Although these results are contradictory to the literature, in this case, its essentially related to the high replication temperature used. It was evident that, in this study, the highest temperature was not beneficial for obtaining a good replication, as it caused the degradation of the surface. The main plot effect for Rz also suggests that a lower pressure is beneficial for the height of the pillars, and this is most likely caused by the results obtained in condition 4, where the use of the highest pressure and temperature value completely damaged the replication of the samples.

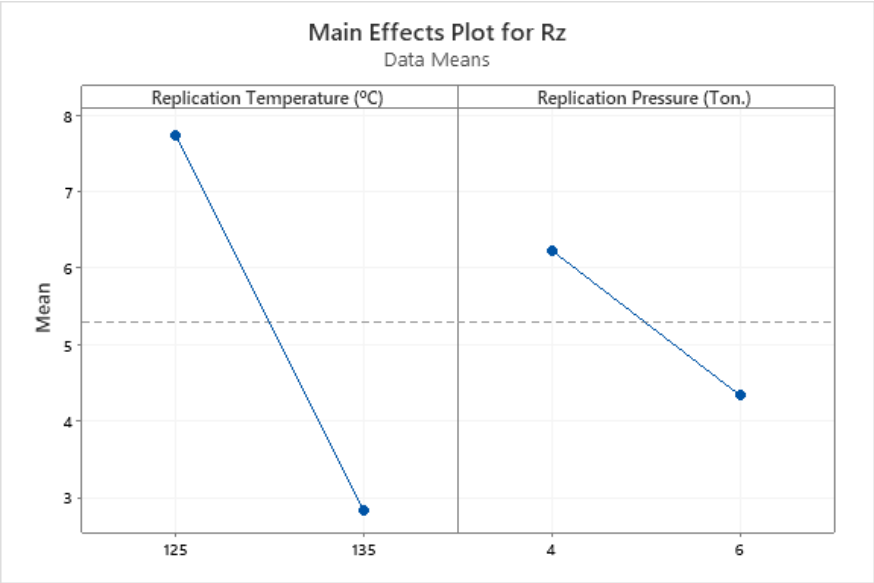

Figure 90 - Main effects plot for Rz.

The interaction effect observed in Figure 91 indicates that the relationship between the replication pressure and Rz depends on the value of the replication temperature. If a pressure of 4 tonnes is applied, a temperature of 125 °C will produce better results for the replicated mean height, and if the pressure used is 6 tonnes, a temperature of 125 °C is also associated with the highest mean height. This plot actually suggests that the best result would be obtained with the combination of 125 °C of temperature and 6 tonnes of pressure, opposing what was suggested by the main plot effects who showed that a smaller value of pressure was more beneficial for the height of the structures.

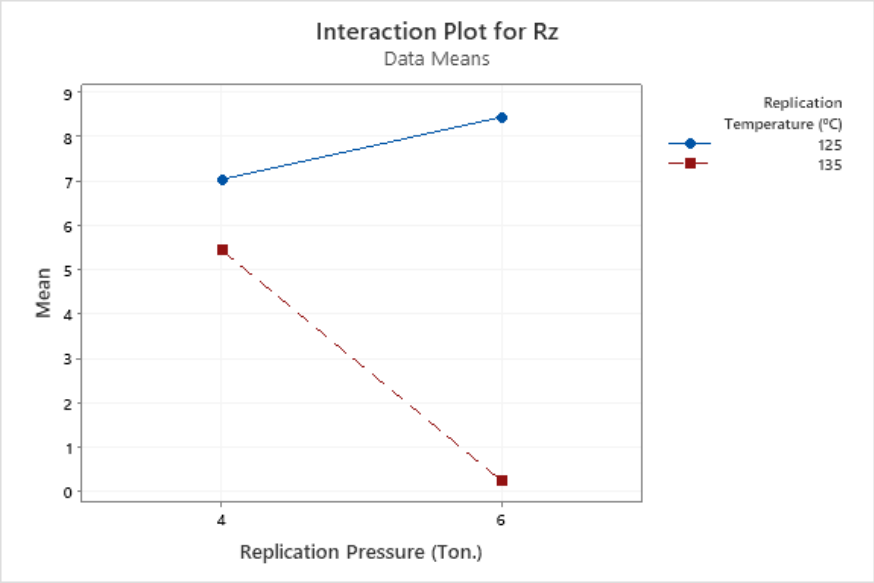

Figure 91 - Interaction plot between the replication pressure and replication temperature for Rz.

The response table suggests that the most influential parameter in this study for the replication height was the replication temperature and the least important parameter was the replication pressure. The increase of the temperature from 125 °C to 135 °C created the biggest influence on the response due to the degradation that affected the samples in a very negative way.

Table 20 - Response Table for Means of Rz.

Level	Replication Temperature	Replication Pressure
1	34,65	31,83
2	10,71	13,54
Delta	23,94	18,29
Rank	1	2

Therefore, for the replication of the PMMA it was evident through the experimental results and the ANOVA analysis that the set of parameters which led to higher microstructures was the condition 2. However, it was also visible that the complete filling of all the cavities and a uniform replication was not achieved. This could be due to different causes or even its combinations, such as the defects associated with demolding which affected the structures, the temperature and/or pressure distribution not being uniform on the sample area during the process and/or the pressure applied not being sufficient. Although the replication pressure used seemed to be enough to being able to fill the cavities, as some structures presented values near the desired height, as the PMMA is a material that offers more resistance to fill the cavities, in comparison with PC, the appliance of a higher pressure under a more controlled process could also be studied in further work to understand if gives the material a bigger capacity to fill the cavities.

5.3.3. Water Contact Angle

In order to evaluate what was the influence of the replicated structure pattern on the surface wettability, it was necessary to measure the water contact angle of the samples.

Initially, the water contact angle of a non-microstructured PMMA sample must be measured, so conclusions can be made about the actual influence of the replicated structure on the surface wetting property. The measurement of a control sample of PMMA Plexiglas 8N showed an average WCA of 67,71° ± 2,81, demonstrating that the sample was in the hydrophilic state, as expected (Figure 92).

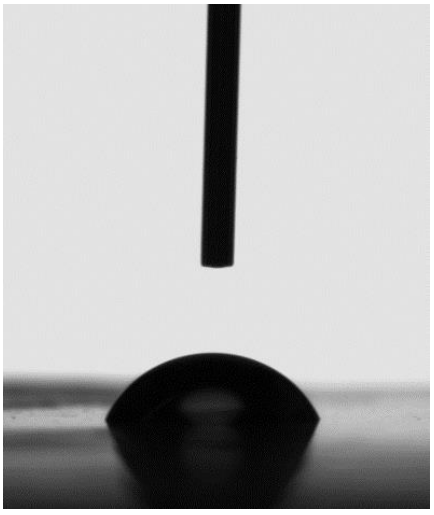

Figure 92 - Water droplet deposited on a non-microstructured PMMA sample (WCA = 67,3°).

Figure 93 presents the averages water contact angles measured in the PMMA microstructured samples produced with the various conditions studied.

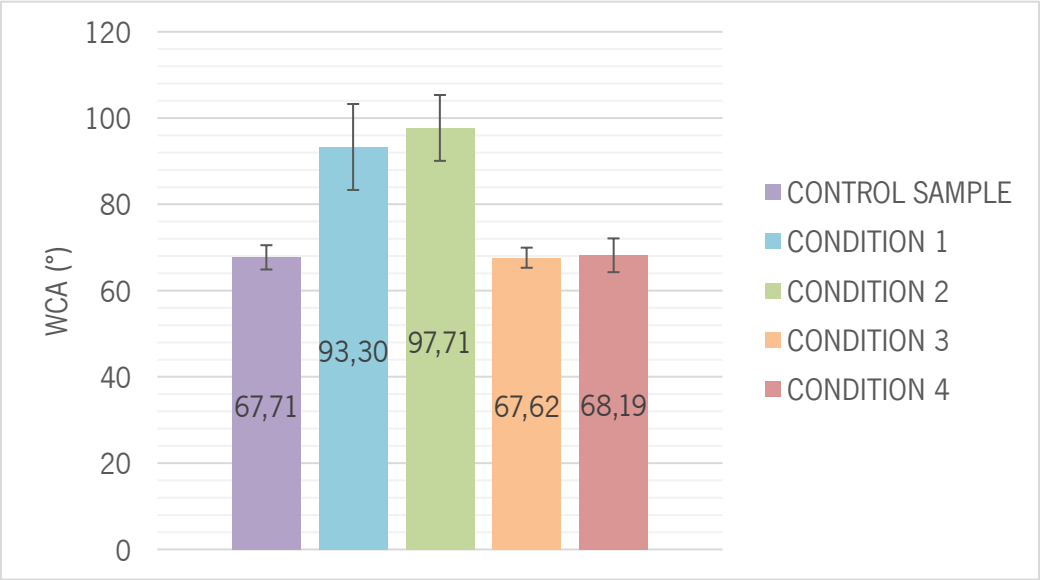

Figure 93 - Water contact angles measured in the samples with the various conditions.

The results obtained in the measurement of the PMMA microstructured samples suggested an enhancement of the hydrophobic property in condition 1 and 2, with all the samples produced with these conditions presenting water contact angles in the hydrophobic regime.

The presence of microstructures on the PMMA samples, even though the maximum average height obtained with condition 2 was only 84 % of the desired replication height for the micropillars, it still allowed an average increment of the WCA in 30 ° (97,71 ° ± 7,63), corresponding to an increase of almost 45 % on the water contact angle values in comparison with a non-microstructured sample. The highest WCA found on the produced samples with condition 2 was of 115,2 ° (Figure 94).

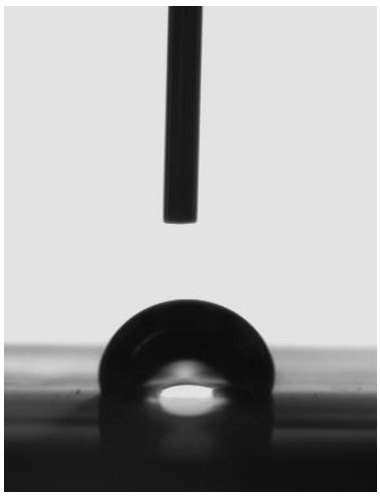

Figure 94 - Highest water contact angle found on a sample produced with condition 2.

The lack of increase in the WCA of the samples produced with condition 3 and 4 could be explained by the thermal degradation of the surface, as observed previously. The degradation of the structures did not allow the presence of the microstructured pattern, and, consequently, did not allow that the samples suffered an enhancement of its hydrophobic properties, remaining in the hydrophilic regime (Figure 95).

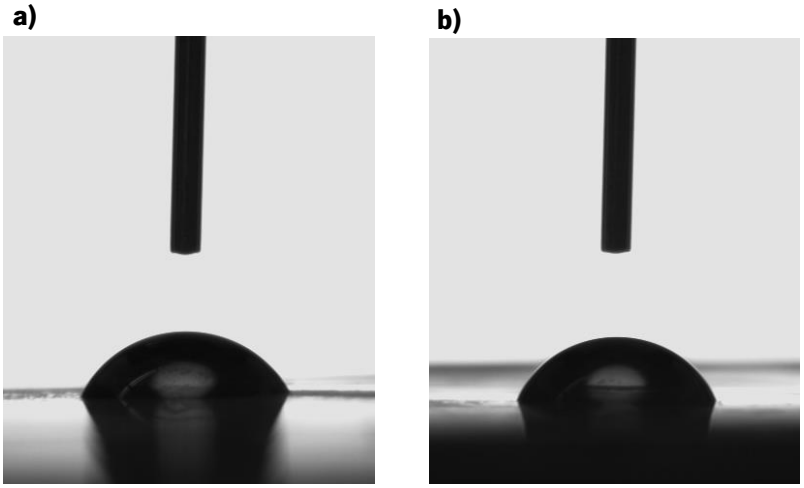

Figure 95 - Water droplet placed on samples that suffered degradation. a) Sample produced with condition 3 (WCA = 66,6°). b) Sample produced with condition 4 (WCA = 69,3°).

The results confirm that the microstructured pattern in study can enhance the hydrophobicity of the PMMA samples. Although the complete filling and uniformity of the structures was not achieved, it still caused the samples to fall into the hydrophobic regime.

5.3.4. Optical Transmittance

The final characterization of the samples consisted in the measurement of the optical transmittance in order to understand the effect of the replicated pillars on the optical transmittance performance of the PMMA samples in the main wavelength required for the sensor to operate, the 905 nm.

A non-microstructured and optical smooth sample of PMMA Plexiglas 8N offer a transmittance of 87,91 % ± 0,04 at 905 nm. As seen in Figure 96, the transmitted light values suffer a decrease across all samples. The decrease on the samples of condition 1 and condition 2 was influenced greatly by the increase of the surface roughness, due to the light scattering promoted by the microstructures. In the case of the condition 3 and 4, the samples suffered a smaller decrease of the optical transmittance in comparison with the samples of the conditions mentioned previously. These decreases of the transmittance on these samples were most likely due to the existence of some light scattering caused by the degradation of the surface of the samples and/or some optical damage that the sample surface could have suffered during the handling or the processing.

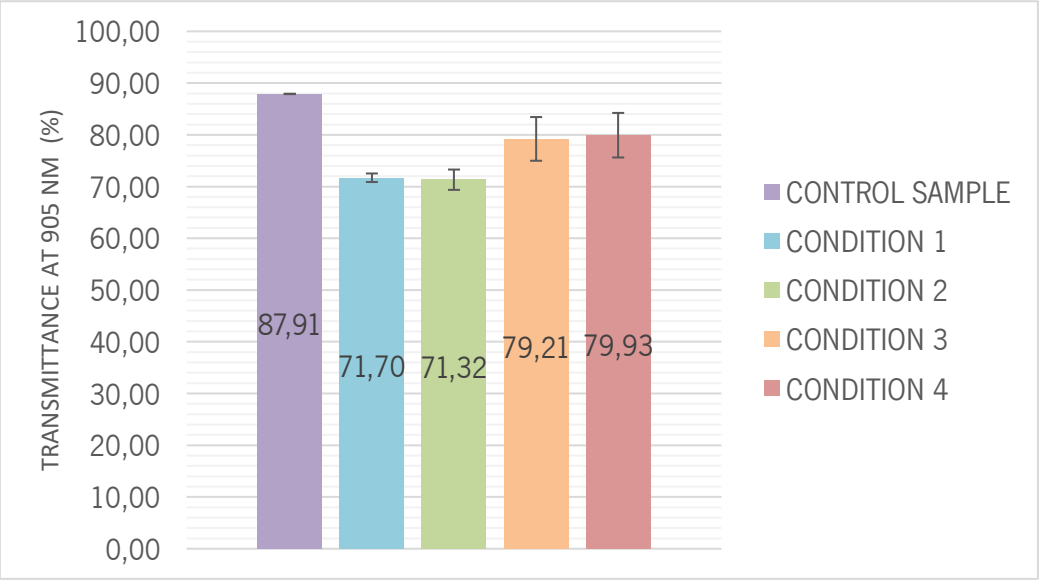

Figure 96 - Optical transmittance average values at 905 nm obtained in the samples produced with the various conditions.

In the samples of condition 2, which presented a satisfactory microstructured pattern on its surface, although a complete replication was not achieved, it still caused a decrease of 16,59 % on its optical transmittance (71,32 % ± 1,96). The decrease of the optical transmittance with this microstructured pattern was already expected, due to the results obtained with the PC, which also suffered a percentage reduction on its optical transmittance. These results once again confirm that this microstructured configuration has a negative influence on the optical transmittance, being the source of significant light scattering.

CHAPTER 6 – CONCLUSIONS

In the last decades several studies have been dedicated to understanding how to artificially achieve the self-cleaning property on a surface, through the evaluation of different structure patterns inspired by nature and its influence on the surface wettability, as well as other properties. The research carried out in this work had as main objective the study of the influence of a microstructure configuration previously developed in the wettability and optical transmittance of samples produced through an improvised hot embossing for the development of an optical protective window for a LiDAR sensor with self-cleaning ability and excellent optical performance.

The damage of both of the molds available was a major throwback in this study, as it obligated to rationalize their application in order to obtain the most accurate results possible. However, it was still possible to replicate the microstructured pattern on the samples and study its influence on the relevant properties for the study, the wettability and optical transmittance of the surface.

The microstructured PC Makrolon 2407 samples, produced with the best set of parameters determined in the preliminary study, demonstrated that a complete filling of the cavities could be achieved with these conditions. The surface replicated pattern caused an increase of almost 50% of the WCA, demonstrating that this microstructured pattern affects the wettability of a surface leading to hydrophobic properties. Moreover, some spots of the samples presented angles in the superhydrophobic regime giving positive signs that superhydrophobicity could be achieved in a more controlled environment of processing. It was also observed an average decrease of 12,89 % in the optical transmittance at 905 nm, demonstrating that the replicated configuration negatively affected the optical performance.

The second study tested the most widely applied approach for the production of superhydrophobic surfaces. The application of a hydrophobic coating on PC microstructured samples caused the repellency of the water droplets, however, it also caused a loss of 19,78 % and 12,38 % in the optical performance at 905 nm and 1550 nm, respectively. The results show that applying a coating on a microstructured sample is a really effective strategy in achieving superhydrophobicity, however, it becomes a problem in terms of light transmission and aesthetics.

After obtaining acceptable results with the PC samples, the third study concerned the evaluation of the application of PMMA Plexiglas 8N, which presents a higher optical transmittance than polycarbonate. With the various set of conditions tested, it was possible to achieve a maximum average up to 84% of the desired replicated height. The presence of microstructures on the PMMA samples, even though the desired replication height for the micropillars was not achieved, still allowed an increase of the WCA in 30°, corresponding to a percentage increase of almost 45% on the WCA values in comparison with a non-

microstructured sample. As expected, it was observed a decrease of 16,59 % on the optical performance of the samples that presented a satisfactory microstructured pattern on its surface.

These results, even though they were not obtained under perfect conditions and presenting fragilities, due to the lack of a proper machine and damage present on both of the molds used, gives some light about the path to be taken to achieve the self-cleaning behavior on a surface.

The goal of this project was not completely achieved, although beneficial developments were made. Through all the studies performed, it was possible to state that the microstructured pattern of the mold led to hydrophobic behavior in both PC and PMMA samples, however, it failed to achieve superhydrophobicity. The results obtained with PC samples, which presented WCA above 150° in some spots, suggests that in a more controlled environment and with a proper embossing machine, superhydrophobicity could be achieved, however, it would need to be tested in order to understand if it is a possibility. Furthermore, taken into account that the optical transmittance should be at least 85% in both required wavelengths, the results obtained with the PC and PMMA samples invalidate the application of this pattern in a protective optical window for a LiDAR sensor, as it causes a significative decrease of the optical transmittance value. It was also possible to determine that the application of a hydrophobic coating on the microstructured samples was not a suitable approach for the project, as it significantly affected the optical performance of the produced parts.

The improvised hot embossing process demonstrated to have good ability to replicate the mold pattern, especially in comparison with the injection molding results obtained in previous research and despite the difficulties. For PC, it was possible to obtain an acceptable replication quality with the complete filling of the cavities, and for PMMA, the parameters must continue to be studied in order to achieve the complete filling, with the appliance of a higher pressure or even a higher time.

CHAPTER 7 – FUTURE WORK

The main focus for future works must be the development of a new structured pattern that could lead to the superhydrophobic behavior as well as maintaining the transparency of the material in the required wavelength.

As it was stated in the literature review (section 2.6), designing and fabricating superhydrophobic and transparent materials can be achieved through the control of the structure's dimensions. According to Liu *et al.* (2019), the structures diameter should be lower than ¼ of the wavelength of light in order to prevent scatter and loss of transmission. Likewise, considering that the major wavelengths for the application are 905 nm and 1550 nm, the ideal diameter of the structures should be lower than ≈ 226 nm (905 × ¼). However, studies also showed that it was possible to achieve a good transmittance in similar wavelengths with structure diameters in the micrometer range, demonstrating that this is not a linear issue, and its dependent of other aspects, such as the material, the pitch, beyond others (Ngo et al., 2015).

The aspect ratio of the structures also has to be considered for achieving the desirable superhydrophobicity. The aspect ratio of the studied structures led to achieving hydrophobicity at least. Likewise, the application of a higher aspect ratio could be an option to be studied in order to achieve superhydrophobicity, especially if a single-scale roughness is applied. However, as the wetting regime of the surfaces studied seemed unstable, a hierarchical roughness should be considered in order to, in the future, achieve a stable self-cleaning ability. Furthermore, the application of a hierarchical structures would also allow the application of a lower aspect ratio, which would benefit the manufacturing process.

Other aspects such as the pitch between the structures should also be studied in order to find the critical step size that enables both superhydrophobicity and transparency, and further structures designs could also be studied. In the study made by Ngo *et al.* (2015), cone-shaped structures in the micrometer range allowed both superhydrophobicity and good optical transmittance in the 300-1000 nm spectral region, for example.

Both materials applied in this work should continue to be studied, as PC offers better mechanical properties and enables the achievement of higher WCA, as observed in this work, and PMMA offers a higher optical performance. Studies must be made with new replication patterns in order to understand which material is more beneficial for the project.

Apart from the characterization tests already made in this work, it would be important to evaluate the hysteresis of the water droplets placed on the structured surfaces by measurements performed in tilted platforms in order to properly characterize the self-cleaning ability. The characterization of optical

transmittance should also be measured at different incident angles in order to understand if it affects or maintains the optical performance. Mechanical characterization, such as impact and abrasion testes should also be performed to evaluate the resistance of the surfaces produced.

After obtaining a favorable configuration that allows the commitment between the self-cleaning ability and optical performance, the processing techniques for replicating the pattern must be studied again, in order to understand which is more beneficial for mass production as well as quality of the parts. In case of the hot embossing, the samples must be produced in a more controlled environment and with a proper embossing machine in order to obtain the optimal processing conditions and results as well as studying options that could optimize the process in order to be adapted to mass producing.

REFERENCES

Andersen, N. K., & Taboryski, R. (2015). Multi-height structures in injection molded polymer. *Microelectronic Engineering*, *141*, 211–214. https://doi.org/10.1016/j.mee.2015.03.017

Anderson, M. J., & Whitcomb, P. J. (2000). Design of Experiments. *Kirk-Othmer Encyclopedia of Chemical Technology*, 1–22.

Asghar, A., Abdul Raman, A. A., & Daud, W. M. A. W. (2014). A Comparison of Central Composite Design and Taguchi Method for Optimizing Fenton Process. *The Scientific World Journal*, *2014*, 869120. https://doi.org/10.1155/2014/869120

Barthlott, W., & Neinhuis, C. (1997). Purity of the sacred lotus, or escape from contamination in biological surfaces. *Planta*, *202*(1), 1–8. https://doi.org/10.1007/s004250050096

Becker, H., & Heim, U. (2000). Hot embossing as a method for the fabrication of polymer high aspect ratio structures. *Sensors and Actuators, A: Physical*, *83*(1), 130–135. https://doi.org/10.1016/S0924-4247(00)00296-X

Bhagat, S. D., & Gupta, M. C. (2015). Superhydrophobic microtextured polycarbonate surfaces. *Surface and Coatings Technology*, *270*, 117–122. https://doi.org/10.1016/j.surfcoat.2015.03.013

Bhushan, B., Koch, K., & Jung, Y. C. (2009). Fabrication and characterization of the hierarchical structure for superhydrophobicity and self-cleaning. *Ultramicroscopy*, *109*(8), 1029–1034. https://doi.org/10.1016/j.ultramic.2009.03.030

Bormashenko, E. (2015). Progress in understanding wetting transitions on rough surfaces. *Advances in Colloid and Interface Science*, *222*, 92–103. https://doi.org/10.1016/j.cis.2014.02.009

Cassie, A., & Bexter, S. . (1944). Wettability of porous surfaces. *Trans Faraday Soc*, *40*, 546–551.

Celia, E., Darmanin, T., Taffin de Givenchy, E., Amigoni, S., & Guittard, F. (2013). Recent advances in designing superhydrophobic surfaces. *Journal of Colloid and Interface Science*, *402*, 1–18. https://doi.org/10.1016/j.jcis.2013.03.041

Chen, Y., Zhang, Y., Shi, L., Li, J., Xin, Y., Yang, T., & Guo, Z. (2012). Transparent superhydrophobic/superhydrophilic coatings for self-cleaning and anti-fogging. *Applied Physics Letters*, *101*(3), 1–6. https://doi.org/10.1063/1.4737167

Chou, S. Y., Krauss, P. R., & Renstrom, P. J. (1995). Imprint of sub-25 nm vias and trenches in polymers. *Applied Physics Letters*, *67*(June), 3114. https://doi.org/10.1063/1.114851

Darmanin, T. (2015). *Superhydrophobic and superoleophobic properties in nature*. *August*. https://doi.org/10.1016/j.mattod.2015.01.001

Deshmukh, S., & Goswami, A. (2020). Hot Embossing of polymers – A review. *Materials Today: Proceedings*, *26*. https://doi.org/10.1016/j.matpr.2019.12.067

Farshchian, B., Ok, J. T., Hurst, S. M., & Park, S. (2010). Simple fabrication of hierarchical structures on a polymer surface. *Nanotechnology 2010: Advanced Materials, CNTs, Particles, Films and Composites - Technical Proceedings of the 2010 NSTI Nanotechnology Conference and Expo, NSTI-Nanotech 2010*, *1*(June 2010), 665–668.

Fei, L., He, Z., LaCoste, J. D., Nguyen, T. H., & Sun, Y. (2020). A Mini Review on Superhydrophobic and Transparent Surfaces. *Chemical Record*, *20*(11), 1257–1268. https://doi.org/10.1002/tcr.202000075

Feng, B. L., Li, S., & Li, Y. (2002). Super-Hydrophobic Surfaces : From Natural to Artificial Super-Hydrophobic Surfaces : From Natural to Artificial **. *Adv. Mater.*, *October*, 1857–1860.

Feng, L., Sun, X., Yao, S., Liu, C., Xing, W., & Zhang, J. (2014). Electrocatalysts and Catalyst Layers for Oxygen Reduction Reaction. In *Rotating Electrode Methods and Oxygen Reduction Electrocatalysts* (Issue January). https://doi.org/10.1016/B978-0-444-63278-4.00003-3

Forbes, P. (2008). Self-Cleaning Materials. In *Scientific American* (Vol. 299, Issue 2). https://doi.org/10.1038/scientificamerican0808-88

Furmidge, C. G. L. (1962). Studies at phase interfaces. I. The sliding of liquid drops on solid surfaces and a theory for spray retention. *Colloid Science*, *17*(4), 309–324.

Garbassi, F., Morra, M., & Occhiello, E. (1994). *Polymer Surfaces: From Physics to Technology*. John Wiley and Sons Ltd.

Guan, W. S., Huang, H. X., & Wang, B. (2013). Topographic design and application of hierarchical polymer surfaces replicated by micro-injection compression molding. *Journal of Micromechanics and Microengineering*, *23*(10), 105010.

Hashiura, Y., Ikehara, T., Kitajima, A., Goto, H., & Maeda, R. (2001). Optical switch array based on microforming process. *Device and Process Technologies for MEMS and Microelectronics II*, *4592*, 414. https://doi.org/10.1117/12.448996

Hejazi, V., Moghadam, A. D., Rohatgi, P., & Nosonovsky, M. (2014). Beyond Wenzel and Cassie-Baxter: Second-order effects on the wetting of rough surfaces. *Langmuir*, *30*(31), 9423–9429. https://doi.org/10.1021/la502143v

Her, E. K., Ko, T. J., Shin, B., Roh, H., Dai, W., Seong, W. K., Kim, H. Y., Lee, K. R., Oh, K. H., & Moon, M. W. (2013). Superhydrophobic transparent surface of nanostructured poly(methyl methacrylate) enhanced by a hydrolysis reaction. *Plasma Processes and Polymers*, *10*(5), 481–488. https://doi.org/10.1002/ppap.201200131

Hong, D., Ryu, I., Kwon, H., Lee, J.-J., & Yim, S. (2013). Preparation of superhydrophobic, long-neck vase-like polymer surfaces. *Physical Chemistry Chemical Physics*, *15*(28), 11862–11867.

Juang, Y. J., Lee James, L., & Koelling, K. W. (2002). Hot embossing in microfabrication. Part I: Experimental. *Polymer Engineering and Science*, *42*(3), 551–566. https://doi.org/10.1002/pen.10971

Karunakaran, R. G., Lu, C. H., Zhang, Z. H., & Yang, S. (2011). Highly Transparent Superhydrophobic Surfaces from the Coassembly of Nanoparticles (<=100 nm). *Langmuir*, *27*(8), 4594–4602.

Khare, T., Oak, U., Shriram, V., Verma, S. K., & Kumar, V. (2019). Biologically synthesized nanomaterials and their antimicrobial potentials. *Comprehensive Analytical Chemistry*, *87*, 263–289. https://doi.org/10.1016/BS.COAC.2019.09.002

Kiew, C. M., Lin, W. J., Teo, T. J., Tan, J. L., Lin, W., & Yang, G. (2009). Finite element analysis of PMMA pattern formation during hot embossing process. *IEEE/ASME International Conference on Advanced Intelligent Mechatronics, AIM*, 314–319. https://doi.org/10.1109/AIM.2009.5229996

Koch, K., & Barthlott, W. (2009). Superhydrophobic and superhydrophilic plant surfaces: An inspiration for biomimetic materials. *Philosophical Transactions of the Royal Society A: Mathematical, Physical and Engineering Sciences*, *367*(1893), 1487–1509. https://doi.org/10.1098/rsta.2009.0022

Kutila, M., Pyykönen, P., Ritter, W., Sawade, O., & Schäufele, B. (2016). Automotive LIDAR sensor development scenarios for harsh weather conditions. *IEEE Conference on Intelligent Transportation*

Systems, Proceedings, ITSC, 265–270. https://doi.org/10.1109/ITSC.2016.7795565

Lampamn, S., Sanders, B., Hrivnak, N., Kinson, J., Polakowski, C., & Henry, S. (2003). Surface Analysis. In S. Lampman (Ed.), *Characterization and failure analysis of plastics* (1st ed., pp. 383–403). ASM International.

Lee, C. H., Jung, P. G., Lee, S. M., Park, S. H., Shin, B. S., Kim, J. H., Hwang, K. Y., Kim, K. M., & Ko, J. S. (2010). Replication of polyethylene nano-micro hierarchical structures using ultrasonic forming. *Journal of Micromechanics and Microengineering*, *20*(3). https://doi.org/10.1088/0960-1317/20/3/035018

Lee, S., Lee, K. W., Kim, J.-H., Lee, K., Lee, S. S., & Hong, S. (2011). Mass-producible superhydrophobic surfaces. *Chemical Communications*, *47*(43), 12005–12007.

Lee, Y., Park, S. H., Kim, K. B., & Lee, J. K. (2007). Fabrication of Hierarchical Structures on a Polymer Surface to Mimic Natural Superhydrophobic Surfaces. *Adv. Mater.*, *19*(17), 2330–2335.

Li, J. M., Liu, C., & Peng, J. (2008). Effect of hot embossing process parameters on polymer flow and microchannel accuracy produced without vacuum. *Journal of Materials Processing Technology*, *207*(1–3), 163–171. https://doi.org/10.1016/j.jmatprotec.2007.12.062

Li, J., Yu, W., Zheng, D., Zhao, X., Choi, C. H., & Sun, G. (2018). Hot embossing for whole Teflon superhydrophobic surfaces. *Coatings*, *8*(7), 1–13. https://doi.org/10.3390/coatings8070227

Li, K., Hernandez-Castro, J. A., Turcotte, K., Morton, K., & Veres, T. (2020). Superhydrophobic thermoplastic surfaces with hierarchical micro-nanostructures fabricated by hot-embossing. *Proceedings of the IEEE Conference on Nanotechnology*, *2020-July*, 81–84. https://doi.org/10.1109/NANO47656.2020.9183514

Li, X. M., Reinhoudt, D., & Crego-Calama, M. (2007). What do we need for a superhydrophobic surface? A review on the recent progress in the preparation of superhydrophobic surfaces. *Chemical Society Reviews*, *36*(8), 1350–1368. https://doi.org/10.1039/b602486f

Li, Y., & Ibanez-Guzman, J. (2020). LiDAR for Autonomous Driving. *Ieee Signal Processing Magazine*, *37*(4), 50–61. http://www.hesaitech.com/en/autonomous_driving.html

Li, Yinyong, Dai, S., John, J., & Carter, K. R. (2013). Superhydrophobic surfaces from hierarchically structured wrinkled polymers. *ACS Applied Materials and Interfaces*, *5*(21), 11066–11073. https://doi.org/10.1021/am403209r

Lin, M. C., Yeh, J. P., Chen, S. C., Chien, R. Der, & Hsu, C. L. (2013). Study on the replication accuracy of polymer hot embossed microchannels. *International Communications in Heat and Mass Transfer*, *42*, 55–61. https://doi.org/10.1016/j.icheatmasstransfer.2012.12.008

Liu, C., Li, J. M., Liu, J. S., & Wang, L. D. (2010). Deformation behaviar of solid polymer during hot embossing process. *Microelectronic Engineering*, *87*(2), 200–207.

Liu, K., Tian, Y., & Jiang, L. (2013). Bio-inspired superoleophobic and smart materials: Design, fabrication, and application. *Progress in Materials Science*, *58*(4), 503–564. https://doi.org/10.1016/j.pmatsci.2012.11.001

Liu, Y., Xu, Q. F., & Lyons, A. M. (2019). Durable, optically transparent, superhydrophobic polymer films. *Applied Surface Science*, *470*(November 2018), 187–195. https://doi.org/10.1016/j.apsusc.2018.11.113

Ma, J., Ai, Y., Kang, L., Liu, W., Ma, Z., Song, P., Zhao, Y., Yang, F., & Wang, X. (2018). A Novel Nanocone Cluster Microstructure with Anti-reflection and Superhydrophobic Properties for Photovoltaic

Devices. *Nanoscale Research Letters*, *13*, 0–5. https://doi.org/10.1186/s11671-018-2754-4

Ma, M., & Hill, R. M. (2006). Superhydrophobic surfaces. *Current Opinion in Colloid and Interface Science*, *11*(4), 193–202. https://doi.org/10.1016/j.cocis.2006.06.002

Maghsoudi, K., Jafari, R., Momen, G., & Farzaneh, M. (2017). Micro-nanostructured polymer surfaces using injection molding: A review. *Materials Today Communications*, *13*, 126–143. https://doi.org/10.1016/j.mtcomm.2017.09.013

Maghsoudi, Khosrow, Vazirinasab, E., Momen, G., & Jafari, R. (2020). Advances in the Fabrication of Superhydrophobic Polymeric Surfaces by Polymer Molding Processes. *Industrial and Engineering Chemistry Research*, *59*(20), 9343–9363. https://doi.org/10.1021/acs.iecr.0c00508

Malshe, A., Rajurkar, K., Samant, A., Bapat, S., & Jiang, W. (2013). Bio-inspired functional surfaces for advanced applications. *CIRP Annals - Manufacturing Technology*, *62*(2), 607–628.

Martins, C. (2020). *Study of microstructures replication for self- cleaning applications*. University of Minho.

Matschuk, M., & Larsen, N. B. (2013). Injection molding of high aspect ratio sub-100 nm nanostructures. *Journal of Micromechanics and Microengineering*, *23*(2). https://doi.org/10.1088/0960-1317/23/2/025003

McHale, G., Shirtcliffe, N. J., & Newton, M. I. (2004). Contact-angle hysteresis on super-hydrophobic surfaces. *Langmuir*, *20*(23), 10146–10149. https://doi.org/10.1021/la0486584

Michael, N., & Bhushan, B. (2007). Hierarchical roughness makes superhydrophobic states stable. *Microelectronic Engineering*, *84*(3), 382–386. https://doi.org/10.1016/J.MEE.2006.10.054

Montgomery, D. C., & Runger, G. C. (1994). Applied Statistics and Probability for Engineers. In *European Journal of Engineering Education* (3rd ed., Vol. 19, Issue 3). John Wiley & Sons. https://doi.org/10.1080/03043799408928333

Morra, M., Occhiello, E., & Garbassi, F. (1989). Contact angle hysteresis in oxygen plasma treated poly(tetrafluoroethylene). *Langmuir*, *5*(3), 872–876. https://doi.org/RETURN TO ISSUEPREVARTICLENEXT Contact angle hysteresis in oxygen plasma treated poly(tetrafluoroethylene) M. Morra, E. Occhiello, and F. Garbassi Cite this: Langmuir 1989, 5, 3, 872–876 Publication Date:May 1, 1989 https://doi.org/10.1021/la00087a050

Nakajima, A., Hashimoto, K., & Watanabe, T. (2001). Recent studies on super-hydrophobic films. *Monatshefte Fur Chemie*, *132*(1), 31–41. https://doi.org/10.1007/s007060170142

Nakajima, Akira, Abe, K., Hashimoto, K., & Watanabe, T. (2000). Preparation of hard super-hydrophobic films with visible light transmission. *Thin Solid Films*, *376*(1–2), 140–143. https://doi.org/10.1016/S0040-6090(00)01417-6

Ngo, C. V., Davaasuren, G., Oh, H. S., & Chun, D. M. (2015). Transparency and superhydrophobicity of cone-shaped micropillar array textured polydimethylsiloxane. *International Journal of Precision Engineering and Manufacturing*, *16*(7), 1347–1353. https://doi.org/10.1007/s12541-015-0177-z

Øgendal, L. (2019). Light Scattering a brief introduction. *University of Copenhagen*, *May*, 45.

Omar, F. (2013). *Hot Embossing Process Parameters : Simulation and Experimental Studies*. i–189. http://orca.cf.ac.uk/id/eprint/51655

Pareek, R., & Bhamniya, J. (2013). Optimization of Injection Moulding Process using Taguchi and ANOVA. *International Journal of Scientific & Engineering Research*, *4*(1), 1–6.

Park, C. I., Jeong, H. E., Lee, S. H., Cho, H. S., & Suh, K. Y. (2009). Wetting transition and optimal design for microstructured surfaces with hydrophobic and hydrophilic materials. *Journal of Colloid and Interface Science*, *336*(1), 298–303. https://doi.org/10.1016/j.jcis.2009.04.022

Park, J. K., Ryu, J., Koo, B. C., & Lee, S. (2012). How the change of contact angle occurs for an evaporating droplet: Effect of impurity and attached water films. *Soft Matter*, *8*(47), 11889–11896.

Peng, L., Deng, Y., Yi, P., & Lai, X. (2014). Micro hot embossing of thermoplastic polymers: A review. *Journal of Micromechanics and Microengineering*, *24*(1). https://doi.org/10.1088/0960-1317/24/1/013001

Pereira, J. (2018). *"Development of a self-cleaning surface of a glass cover by replication processes."* University of Minho.

Pinto, A. M. F. R., Oliveira, V. B., & Falcão, D. S. (2018). Miniaturization of direct alcohol fuel cells: Microfabrication techniques and microfluidic architectures. *Direct Alcohol Fuel Cells for Portable Applications*, 245–264. https://doi.org/10.1016/B978-0-12-811849-8.00007-3

Roach, P., Shirtcliffe, N. J., & Newton, M. I. (2008). Progess in superhydrophobic surface development. *Soft Matter*, *4*(2), 224. https://doi.org/10.1039/b712575p

Röhrig, M., Schneider, M., Etienne, G., Oulhadj, F., Pfannes, F., Kolew, A., Worgull, M., & Hölscher, H. (2013). Hot pulling and embossing of hierarchical nano- and micro-structures. *Journal of Micromechanics and Microengineering*, *23*(10). https://doi.org/10.1088/0960-1317/23/10/105014

Schulz, H., Wissen, M., & Bogdanski, N. (2005). *Choice of the molecular weight of an imprint polymer for hot embossing lithography*. *78*(1), 625–632. https://doi.org/10.1016/j.mee.2004.12.079

Shamsi, A., Amiri, A., Heydari, P., Hajghasem, H., Mohtashamifar, M., & Esfandiari, M. (2014). Low cost method for hot embossing of microstructures on PMMA by SU-8 masters. *Microsystem Technologies*, *20*(10–11), 1925–1931. https://doi.org/10.1007/s00542-013-2000-z

Singh, K., & Dupaix, R. B. (2012). Hot-Embossing Experiments of Polymethyl Methacrylate Across the Glass Transition Temperature With Variation in Temperature and Hold Times. *Polymer Engineering and Science*, *52*(6), 1284–1292.

Stormonth-Darling, J. M., Pedersen, R. H., How, C., & Gadegaard, N. (2014). Injection moulding of ultra high aspect ratio nanostructures using coated polymer tooling. *Journal of Micromechanics and Microengineering*, *24*(7). https://doi.org/10.1088/0960-1317/24/7/075019

Sun, J., Li, H., Huang, Y., Zheng, X., Liu, Y., Zhuang, J., & Wu, D. (2019a). Simple and A ff ordable Way To Achieve Polymeric Superhydrophobic Surfaces with Biomimetic Hierarchical Roughness. *ACS Omega*, *4*(2), 2750–2757. https://doi.org/10.1021/acsomega.8b03138

Sun, J., Li, H., Huang, Y., Zheng, X., Liu, Y., Zhuang, J., & Wu, D. (2019b). Simple and Affordable Way to Achieve Polymeric Superhydrophobic Surfaces with Biomimetic Hierarchical Roughness. *ACS Omega*, *4*(2), 2750–2757. https://doi.org/10.1021/acsomega.8b03138

Sun, J., Zhuang, J., Liu, Y., Xu, H., Horne, J., Wujcik, E. K., Liu, H., Ryu, J. E., Wu, D., & Guo, Z. (2019). Development and Application of Hot Embossing in Polymer Processing : A Review. *ES Materials & Manufacturing*, *6*, 3–17. https://doi.org/10.30919/esmm5f605

Teisala, H., Tuominen, M., & Kuusipalo, J. (2011). Adhesion mechanism of water droplets on hierarchically rough superhydrophobic rose petal surface. *Journal of Nanomaterials*, *2011*(June). https://doi.org/10.1155/2011/818707

Telgarsky, M., Simdikova, I., Sbarski, I., Harvey, E., & Kueper, A. (2004). Comparison of embossing properties of polycarbonate and polystyrene for deep microstructures. *Materials Forum*, *27*(October 2015), 100–103.

Tyona, M. D. (2013). A theoritical study on spin coating technique. *Advances in Materials Research*, *2*(4), 195–208. https://doi.org/10.12989/amr.2013.2.4.195

Verplanck, N., Coffinier, Y., Thomy, V., & Boukherroub, R. (2007). Wettability switching techniques on superhydrophobic surfaces. *Nanoscale Research Letters*, *2*(12), 577–596. https://doi.org/10.1007/s11671-007-9102-4

Wenzel, R. N. (1936). Resistance of solid surfaces to wetting by water. *Ind Eng Chem*, *28*(8), 988–994.

Worgull, M. (2009). *Hot Embossing: Theory and Technology of Microreplication* (First Edit). William Andrew.

Wu, D., Sun, J., Liu, Y., Yang, Z., Xu, H., Zheng, X., & Gou, P. (2016). Rapid Fabrication of Microstructure on PMMA Substrate by the Plate to Plate Transition-Spanning Isothermal Hot Embossing Method Nearby Glass Transition Temperature Daming. *Polymer Engineering and Science*, *57*(3), 268–274.

Xu, Q., Zhang, W., Dong, C., Sreepresad, T. S., & Xia, Z. (2016). Biomimetic self-cleaning surfaces : synthesis , mechanism and applications. *J. R. Soc. Interface*, *13*, 20160300. https://doi.org/http://dx.doi.org/10.1098/rsif.2016.0300

Yeong, Y. H., & Gupta, M. C. (2017). Hoy embossed micro-textured thin superhydrophobic Teflon FEP sheets for low ice adhesion. *Surf. Coat. Technol.*, *313*, 17–23.

Yılgör, I., Yılgör, E., & Söz, C. K. (2016). *Superhydrophobic polymer surfaces : preparation, properties and applications*. https://www.degruyter.com/document/isbn/9783110652987/html

Young, T. (1805). An essay on the cohesion of fluids. *Philos Trans Roy Soc Lond*, *95*, 65–87.

Yu, C., Sasic, S., Liu, K., Salameh, S., Ras, R. H. A., & van Ommen, J. R. (2020). Nature–Inspired self–cleaning surfaces: Mechanisms, modelling, and manufacturing. *Chemical Engineering Research and Design*, *155*(2002), 48–65. https://doi.org/10.1016/j.cherd.2019.11.038

Yu, S., Guo, Z., & Liu, W. (2015). Biomimetic transparent and superhydrophobic coatings: From nature and beyond nature. *Chemical Communications*, *51*(10), 1775–1794. https://doi.org/10.1039/c4cc06868h

Zheng, Y., Gao, X., & Jiang, L. (2007). Directional adhesion of superhydrophobic butterfly wings. *Soft Matter*, *3*(2), 178–182. https://doi.org/10.1039/b612667g

Zhou, M., Xiong, X., Jiang, B., & Weng, C. (2018). Fabrication of high aspect ratio nanopillars and micro/nano combined structures with hydrophobic surface characteristics by injection molding. *Applied Surface Science*, *427*, 854–860. https://doi.org/10.1016/j.apsusc.2017.08.003

APPENDICES

Appendix A – Polycarbonate Technical Data Sheet

Makrolon® 2407

General purpose grades / Low viscosity

MVR (300 °C/1.2 kg) 19 cm³/10 min; general purpose; low viscosity; UV stabilized; easy release; injection molding - melt temperature 280 - 320 °C; available in transparent, translucent and opaque colors

ISO Shortname

PC

	Property	Test Condition	Unit	Standard	typical Value
Rheological properties					
C	Melt volume-flow rate	300 °C/ 1.2 kg	cm³/10 min	ISO 1133	19
C	Molding shrinkage, parallel	60x60x2 mm/ 500 bar	%	ISO 294-4	0.65
C	Molding shrinkage, normal	60x60x2 mm/ 500 bar	%	ISO 294-4	0.7
	Molding shrinkage, parallel/normal	Value range based on general practical experience	%	b.o. ISO 2577	0.5 - 0.7
	Melt mass-flow rate	300 °C/ 1.2 kg	g/10 min	ISO 1133	20
Mechanical properties (23 °C/50 % r. h.)					
C	Tensile modulus	1 mm/min	MPa	ISO 527-1,-2	2400
C	Yield stress	50 mm/min	MPa	ISO 527-1,-2	66
C	Yield strain	50 mm/min	%	ISO 527-1,-2	6.0
C	Nominal strain at break	50 mm/min	%	ISO 527-1,-2	> 50
	Stress at break	50 mm/min	MPa	ISO 527-1,-2	65
	Strain at break	50 mm/min	%	b.o. ISO 527-1,-2	120
C	Tensile creep modulus	1 h	MPa	ISO 899-1	2200
C	Tensile creep modulus	1000 h	MPa	ISO 899-1	1900
	Flexural modulus	2 mm/min	MPa	ISO 178	2350
	Flexural strength	2 mm/min	MPa	ISO 178	98
	Flexural strain at flexural strength	2 mm/min	%	ISO 178	7.0
	Flexural stress at 3.5 % strain	2 mm/min	MPa	ISO 178	74
C	Charpy impact strength	23 °C	kJ/m²	ISO 179-1eU	N
C	Charpy impact strength	-30 °C	kJ/m²	ISO 179-1eU	N
	Charpy impact strength	-60 °C	kJ/m²	ISO 179-1eU	N
	Charpy notched impact strength	23 °C/ 3 mm	kJ/m²	ISO 7391/b.o. ISO 179-1eA	65P(C)
	Charpy notched impact strength	-30 °C/ 3 mm	kJ/m²	ISO 7391/b.o. ISO 179-1eA	14C
	Izod notched impact strength	23 °C/ 3 mm	kJ/m²	ISO 7391/b.o. ISO 180-A	65P
	Izod notched impact strength	-30 °C/ 3 mm	kJ/m²	ISO 7391/b.o. ISO 180-A	12C
C	Puncture maximum force	23 °C	N	ISO 6603-2	5100
C	Puncture maximum force	-30 °C	N	ISO 6603-2	6000
C	Puncture energy	23 °C	J	ISO 6603-2	55
C	Puncture energy	-30 °C	J	ISO 6603-2	65
	Ball indentation hardness		N/mm²	ISO 2039-1	116

Figure 97 - Polycarbonate Technical Data Sheet.

Makrolon® 2407

	Property	Test Condition	Unit	Standard	typical Value
Thermal properties					
C	Glass transition temperature	10 °C/min	°C	ISO 11357-1,-2	143
C	Temperature of deflection under load	1.80 MPa	°C	ISO 75-1,-2	124
C	Temperature of deflection under load	0.45 MPa	°C	ISO 75-1,-2	136
C	Vicat softening temperature	50 N; 50 °C/h	°C	ISO 306	143
	Vicat softening temperature	50 N; 120 °C/h	°C	ISO 306	145
C	Coefficient of linear thermal expansion, parallel	23 to 55 °C	10^{-4}/K	ISO 11359-1,-2	0.65
C	Coefficient of linear thermal expansion, transverse	23 to 55 °C	10^{-4}/K	ISO 11359-1,-2	0.65
C	Burning behavior UL 94 [UL recognition]	0.75 mm	Class	UL 94	V-2
	Burning behavior UL 94 [UL recognition]	2.7 mm	Class	UL 94	HB
C	Oxygen index	Method A	%	ISO 4589-2	27
	Thermal conductivity, cross-flow	23 °C; 50 % r. h.	W/(m·K)	ISO 8302	0.20
	Resistance to heat (ball pressure test)		°C	IEC 60695-10-2	135
	Relative temperature index (Tensile strength) [UL recognition]	1.5 mm	°C	UL 746B	125
	Relative temperature index (Tensile impact strength) [UL recognition]	1.5 mm	°C	UL 746B	115
	Relative temperature index (Electric strength) [UL recognition]	1.5 mm	°C	UL 746B	125
	Relative temperature index (Tensile impact strength) [UL recognition]	1.5 mm	°C	UL 746B	115
	Relative temperature index (Electric strength) [UL recognition]	1.5 mm	°C	UL 746B	125
	Glow wire test (GWFI)	0.75 mm	°C	IEC 60695-2-12	850
	Glow wire test (GWFI)	1.5 mm	°C	IEC 60695-2-12	875
	Glow wire test (GWFI)	3.0 mm	°C	IEC 60695-2-12	930
	Glow wire test (GWIT)	0.75 mm	°C	IEC 60695-2-13	875
	Glow wire test (GWIT)	1.0 mm	°C	IEC 60695-2-13	875
	Glow wire test (GWIT)	1.5 mm	°C	IEC 60695-2-13	875
	Glow wire test (GWIT)	3.0 mm	°C	IEC 60695-2-13	875
	Application of flame from small burner	Method K and F/ 2.0 mm	Class	DIN 53438-1,-3	K1, F1
	Needle flame test	Method K/ 1.5 mm	s	IEC 60695-11-5	5
	Needle flame test	Method K/ 2.0 mm	s	IEC 60695-11-5	5
	Needle flame test	Method K/ 3.0 mm	s	IEC 60695-11-5	10
	Needle flame test	Method F/ 1.5 mm	s	IEC 60695-11-5	60
	Needle flame test	Method F/ 2.0 mm	s	IEC 60695-11-5	120
	Needle flame test	Method F/ 3.0 mm	s	IEC 60695-11-5	120
	Burning rate (US-FMVSS)	>=1.0 mm	mm/min	ISO 3795	passed
	Flash ignition temperature		°C	ASTM D1929	480
	Self ignition temperature		°C	ASTM D1929	550
Electrical properties (23 °C/50 % r. h.)					
C	Relative permittivity	100 Hz	-	IEC 60250	3.1
C	Relative permittivity	1 MHz	-	IEC 60250	3.0
C	Dissipation factor	100 Hz	10^{-4}	IEC 60250	5
C	Dissipation factor	1 MHz	10^{-4}	IEC 60250	90
C	Volume resistivity		Ohm·m	IEC 60093	1E14
C	Surface resistivity		Ohm	IEC 60093	1E16
C	Electrical strength	1 mm	kV/mm	IEC 60243-1	34
C	Comparative tracking index CTI	Solution A	Rating	IEC 60112	250
	Comparative tracking index CTI M	Solution B	Rating	IEC 60112	125M
	Electrolytic corrosion		Rating	IEC 60426	A1

Figure 98 - Polycarbonate Technical Data Sheet.

Makrolon® 2407

	Property	Test Condition	Unit	Standard	typical Value
Other properties (23 °C)					
C	Water absorption (saturation value)	Water at 23 °C	%	ISO 62	0.30
C	Water absorption (equilibrium value)	23 °C; 50 % r. h.	%	ISO 62	0.12
C	Density		kg/m³	ISO 1183-1	1200
	Water vapor permeability	23 °C; 85 % RH/ 100 µm film	g/(m²·24 h)	ISO 15106-1	15
	Gas permeation	Oxygen/ 100 µm film	cm³/(m²·24 h·bar)	b.o. ISO 2556	800
	Gas permeation	Oxygen/ 25.4 µm (1 mil) film	cm³/(m²·24 h·bar)	b.o. ISO 2556	3150
	Gas permeation	Nitrogen/ 100 µm film	cm³/(m²·24 h·bar)	b.o. ISO 2556	160
	Gas permeation	Nitrogen/ 25.4 µm (1 mil) film	cm³/(m²·24 h·bar)	b.o. ISO 2556	630
	Gas permeation	Carbon dioxide/ 100 µm film	cm³/(m²·24 h·bar)	b.o. ISO 2556	4800
	Gas permeation	Carbon dioxide/ 25.4 µm (1 mil) film	cm³/(m²·24 h·bar)	b.o. ISO 2556	18900
	Bulk density	Pellets	kg/m³	ISO 60	660
Material specific properties					
	Refractive index	Procedure A	-	ISO 489	1.584
	Haze for transparent materials	3 mm	%	ISO 14782	< 0.8
	Luminous transmittance (clear transparent materials)	1 mm	%	ISO 13468-2	89
C	Luminous transmittance (clear transparent materials)	2 mm	%	ISO 13468-2	89
	Luminous transmittance (clear transparent materials)	3 mm	%	ISO 13468-2	88
	Luminous transmittance (clear transparent materials)	4 mm	%	ISO 13468-2	87
Processing conditions for test specimens					
C	Injection molding-Melt temperature		°C	ISO 294	280
C	Injection molding-Mold temperature		°C	ISO 294	80
C	Injection molding-Injection velocity		mm/s	ISO 294	200
Recommended Processing and Drying Conditions					
	Melt Temperatures		°C	-	280 - 320
	Standard Melt Temperature		°C	-	300
	Barrel Temperatures - Rear		°C	-	250 - 260
	Barrel Temperatures - Middle		°C	-	270 - 280
	Barrel Temperatures - Front		°C	-	280 - 290
	Barrel Temperatures - Nozzle		°C	-	290 - 300
	Mold Temperatures		°C	-	80 - 120
	Hold Pressure (% of injection pressure)		%	-	50 - 75
	Plastic Back Pressure (specific)		bar	-	50 - 150
	Peripheral Screw Speed		m/s	-	0.05 - 0.2
	Shot-to-Cylinder Size		%	-	30 - 70
	Dry Air Drying Temperature		°C	-	120
	Dry Air Drying Time		h	-	2-3
	Moisture Content max. (%)		%	-	<= 0,02
	Vent Depth		mm	-	0.025 - 0.075

Figure 99 - Polycarbonate Technical Data Sheet.

Appendix B – PMMA Technical Data Sheet

PLEXIGLAS®

Product Information

PLEXIGLAS® 8N

Properties:

	Parameter	Unit	Standard	PLEXIGLAS® 8N
Mechanical Properties				
Tensile Modulus	1 mm/min	MPa	ISO 527	3300
Stress @ Break	5 mm/min	MPa	ISO 527	77
Strain @ Break	5 mm/min	%	ISO 527	5.5
Charpy Impact Strength	23°C	kJ/m²	ISO 179/1eU	20
Thermal Properties				
Vicat Softening Temperature	B / 50	°C	ISO 306	108
Glass Transition Temperature		°C	ISO 11357	117
Temp. of Deflection under Load	0.45 MPa	°C	ISO 75	103
Temp. of Deflection under Load	1.8 MPa	°C	ISO 75	98
Coeff. of Linear Therm. Expansion	0 – 50°C	E-5 /°K	ISO 11359	8
Classes of construction product			DIN EN 13501-1	E
Flammability UL 94	1.6 mm	Class	IEC 60695-11-10	HB
Rheological Properties				
Melt Volume Rate, MVR	230°C / 3.8kg	cm³/10min	ISO 1133	3
Optical Properties	d=3 mm			
Luminous transmittance	D65	%	ISO 13468-2	92
Haze			ASTM D1003	< 0.5
Refractive Index	589nm/23°C		ISO 489	1.49
Other Properties				
Density		g/cm³	ISO 1183	1.19
Recommended Processing Conditions				
Predrying Temperature		°C		max. 98
Predrying Time in Desiccant-Type Drier		h		2 – 3
Melt Temperature		°C		220 – 260
Mold Temperature (Injection Molding)		°C		60 – 90

Figure 100 - PMMA Technical Data Sheet.